WL-TR-94-2036

ELECTRON INTERACTIONS WITH NON-LINEAR POLYATOMIC MOLECULES AND THEIR RADICALS AND IONS

Ashok Kumar Jain
Charles A. Weatherford

Florida A & M University
Physics Department
Tallahassee, Florida 32307

DECEMBER 1993

FINAL REPORT FOR 06/07/90 — 06/06/93

APPROVED FOR PUBLIC RELEASE; DISTRIBUTION IS UNLIMITED.

AERO PROPULSION AND POWER DIRECTORATE
WRIGHT LABORATORY
AIR FORCE MATERIEL COMMAND
WRIGHT PATTERSON AFB OH 45433-7251

NOTICE

When Government drawings, specifications, or other data are used for any purpose other than in connection with a definitely Government-related procurement, the United States Government incurs no responsibility or any obligation whatsoever. The fact that the government may have formulated or in any way supplied the said drawings, specifications, or other data, is not to be regarded by implication, or otherwise in any manner construed, as licensing the holder, or any other person or corporation; or as conveying any rights or permission to manufacture, use, or sell any patented invention that may in any way be related thereto.

This report is releasable to the National Technical Information Service (NTIS). At NTIS, it will be available to the general public, including foreign nations.

This technical report has been reviewed and is approved for publication.

ALAN GARSCADDEN
Research Physicist
Advanced Plasma Research Section
Power Components Branch
Aerospace Power Division
Aero Propulsion and Power Directorate

JERRELL M. TURNER
Chief, Advanced Plasma Research Section
Power Components Branch
Aerospace Power Division
Aero Propulsion and Power Directorate

MICHAEL D. BRAYDICH, Lt Col, USAF
Deputy Chief
Aerospace Power Division

If your address has changed, if you wish to be removed from our mailing list, or if the addressee is no longer employed by your organization please notify WL/POOC-3, WPAFB, OH 45433-7919 to help us maintain a current mailing list.

Copies of this report should not be returned unless return is required by security considerations, contractual obligations, or notice on a specific document.

REPORT DOCUMENTATION PAGE

Form Approved
OMB No. 0704-0188

1. AGENCY USE ONLY (Leave blank)	2. REPORT DATE	3. REPORT TYPE AND DATES COVERED
	December 1993	FINAL 06/07/90—06/06/93

4. TITLE AND SUBTITLE
ELECTRON INTERACTIONS WITH NON-LINEAR POLYATOMIC MOLECULES AND THEIR RADICALS AND IONS

5. FUNDING NUMBERS
C F33615-90-C-2032
PE 62203
PR 2003
TA 12
WU 03

6. AUTHOR(S)
ASHOK KUMAR JAIN
CHARLES A. WEATHERFORD

7. PERFORMING ORGANIZATION NAME(S) AND ADDRESS(ES)
PHYSICS DEPARTMENT
FLORIDA A&M UNIVERSITY
TALLAHASSEE, FL 32307

8. PERFORMING ORGANIZATION REPORT NUMBER

9. SPONSORING/MONITORING AGENCY NAME(S) AND ADDRESS(ES)
AERO PROPULSION AND POWER DIRECTORATE
WRIGHT LABORATORY
AIR FORCE MATERIAL COMMAND
WRIGHT PATTERSON AFB, OH 45433-7251

10. SPONSORING/MONITORING AGENCY REPORT NUMBER
WL-TR-94-2036

11. SUPPLEMENTARY NOTES

12a. DISTRIBUTION/AVAILABILITY STATEMENT
APPROVED FOR PUBLIC RELEASE;
DISTRIBUTION IS UNLIMITED

12b. DISTRIBUTION CODE

13. ABSTRACT *(Maximum 200 words)*

This is the final report for work accomplished during the period of June 1990 through 1993 under Air Force Contract F33615-90-C-2032.

The work involved the computation of collision cross sections for electron collisions with non-linear polyatomic molecules and their radicals and ions. A reliable set of cross section data for elastic and inelastic processes in these systems has been produced without resorting to a fitting procedure. The computational model employed the adiabatic-nuclei-approximation for electron scattering from molecules in the gas phase.

In addition, a method for calculating the required cross sections by solving the Schrödinger equation as a partial differential equation using a finite difference discretization has been developed.

14. SUBJECT TERMS	15. NUMBER OF PAGES 172
	16. PRICE CODE

17. SECURITY CLASSIFICATION OF REPORT	18. SECURITY CLASSIFICATION OF THIS PAGE	19. SECURITY CLASSIFICATION OF ABSTRACT	20. LIMITATION OF ABSTRACT
UNCLASSIFIED	UNCLASSIFIED	UNCLASSIFIED	UL

TABLE OF CONTENTS

List of Figures

PREFACE AND ACKNOWLEDGEMENTS

This work was accomplished during the period June 1990 through 1993 under the Air Force Contract F33615–90–C–2032. The Air Force contract manager was Lt Patrick D. Kee and the contract officer was Rebecca B O'Kelley. This technical report entitled "*Electron Interaction with Non–Linear Polyatomic Molecules and their Radicals and Ions*" was prepared at the Physics Department, Florida A& M University, Tallahassee, Florida.

We would like to thank the Florida State University Supercomputer Research Institute (SCRI) for providing supercomputer time on the CRAY-YMP machine. In addition supercomputer time on the NMFECC CRAY–2 machine at Livermore was also made available to us through SCRI, which is partially funded by the US Department of Energy through contract no. DE-FC05-85ER250000. We extend our thanks to SCRI staff for their help throughout the execution of this work. We would like to take this opportunity to thank especially Joe Lannutti (Director, SCRI), Chris Lacher (Chairman, Resource Allocation Committee), Robert Holden (Manager, Supercomputing group), and many others at the SCRI and innovation park facilities.

A part of the present research work was performed in collaboration with Professor F. A. Gianturco (Department of Chemistry, University of Rome, Italy) and Dr. D.G. Thompson (Department of Applied Mathematics and Theoretical Physics, The Queen's University of Belfast, N Ireland). A travel grant from NATO (CRG 890470) is thankfully acknowledged. A research collaboration with Dr. V. Di Martino (Italy) and Nico Sanna Italy) is thankfully acknowledged here. It is also a pleasure to thank our colleagues at the Physics Department, FAMU. We are grateful to Drs. L. Boesten, T. W. Shyn, O. Sueoka, H. Tanaka, M. Hayashi, Steve Buckman, M A Khakoo and C. Szmytkowski for sending their experimental data prior to publication. I am also thankful to Avesh Jain for helping in preparing some tables and figures of the present research data .

1. INTRODUCTION

This final report describes the work done on the project entitled " **Electron Interactions with Non–Linear Polyatomic Molecules and their Radicals and Ions** " during the entire period of June 1990 to June 1993. The present theoretical research was carried out under the auspices of Air Force contract No. F33615-90-C-2032. The work was performed at the Physics Department, Florida A&M University, Tallahassee, Florida with the direct supervision and participation of Dr. Ashok K. Jain, Principal Investigator (PI), and Dr. Charles A. Weatherford (Co-PI). A part of this project was performed in collaboration with Professor F. A. Gianturco (Department of Chemistry, University of Rome, Italy) and Dr. D. G. Thompson (Department of Applied Mathematics, The Queen's University of Belfast, N. Ireland), and Dr. Aaron Temkin (NASA-Goddard, Greenbelt, MD). The collaboration with the University of Rome was partially funded by the NATO (under contract No CRG 890470) in terms of a renewed 2–year travel grant. The work with Dr. Aaron Temkin was performed with partial support of NASA grants NAG-5307 and NAGW-2930. The computational work was fully supported by the FSU Supercomputer Research Institute (SCRI) in terms of supercomputer time on the CRAY-YMP (at Tallahassee) and on the NMFECC CRAY-2 machine (at Livermore).

The overall goal of this project was to develop state–of–the–art computer programs and to perform calculations on various elastic and inelastic cross sections for low energy electron collisions with non–linear polyatomic molecules and their ions and radicals. It is a well known fact that such a project involves a large amount of computing because of complexities involved in the dynamics of the collision system. Our main purpose has been to produce a reliable set of useful cross–section data for elastic as well as inelastic processes without involving any fitting procedure. When electrons interact with neutral molecular targets, time considerations of the electronic and nuclear motions allow us to treat rotational, vibrational, and electronic processes rather independently. This is the so–called adiabatic–nuclei–approximation (ANA) which has made *ab initio* electron–molecule

calculations a dream come true. Even under the great simplifications introduced by the ANA formulation, the treatment of electron–polyatomics is still a very difficult problem owing to, for example, the multicenter nature of the interaction, the presence of non–local electron exchange, charge correlation and polarization effects and the opening of several other rearrangement channels .

For the simple case of elastic (including rotational excitation processes) scattering at the static–exchange level (neglecting short range correlation and long range polarization effects), the solution of inhomogenous integro-differential coupled equations *iteratively* is an arduous task for the case of non–linear targets. Consequently, it is not surprising that just a few years ago, most of the electron–polyatomic calculations were carried out by employing model potentials for exchange and polarization effects [1]. For the first time, our group developed scattering codes [2–7] which solve electron–polyatomic scattering equation iteratively to treat electron exchange effects exactly. To implement short range correlation and long range polarization effects correctly is still an open problem. We, however, include these charge distortion effects non–empirically using the perturbative techniques.

In brief, the electron–molecule problem is set up in the single–center–expansion (SCE) scheme under the body–fixed (BF) coordinate system in the ANA close–coupling formulation. The continuum electron function is obtained numerically for each irreducible representation of the molecule point group. The convergence of bound and continuum functions with respect to SCE size is tested properly to make this approach meaningful. We have recently developed SCE orbitals from multicenter molecular wavefunctions [8]. Thus, given a molecule of any symmetry, we should be able to investigate low energy electron scattering at the *ab initio* level.

In Section 2, we provide a summary of work completed so far, and Section 3 gives a list of published (or accepted) and submitted papers during the entire period of the contract. The theory of the present calculations is presented in Section 4 and Section 5 provides the corresponding numerical details and a list of computer programs employed for this work.

In Section 4, we also discuss our recent method [6] on a most efficient use of an iterative scheme in terms of comp. ter time without sacrificing any numerical accuracy.

In Section 6, w summarise our main calculations on the rotationally elastic, inelastic and summed cross sections for electron collisions from several molecules such as the CH_4, SiH_4, GeH_4, NH_3, H_2O, and H_2S molecules in the energy range of 0–20 eV. A detailed set of cross sections values (Figures and Tables) has already been provided in previous progress reports [9–10]. For all these species, experimental data on the differential (DCS), integral and momentum transfer cross sections are available for comparison. For the e–H_2O case, there are experimental data on the rotational excitation process as well. In Section 7, we present our low energy electron scattering study with C_2H_2 molecules by employing a similar (as mentioned above) technique but using a different set of computer codes for linear molecules. The present e–C_2H_2 cross sections are parameter–free and compare very well with recent measurements.

In Section 8, we discuss our main findings on the effect of gas temperature on the cross sections in connection with several theorems by Shimamura [11–17]. Section 9 summarises our present results on the total cross sections for a large variety of diatomic and polyatomic molecules from about 20 eV to up to several thousand eV.

Finally, the concluding remarks are made in Section 10. The last section is presented as an Appendix. In this Appendix, Dr. Charles A Weatherford reports his work on the PDE technique in electron–molecule scattering.

2. SUMMARY OF WORK PERFORMED (June 1990 – June 1993)

1. The electron – SiH_4 scattering at 0.01–20 eV was investigated [5]. The exchange (exactly) and polarization (approximately but parameter–free) effects were included to make a direct comparison with the experimental data. This is a detailed study on the low–energy behaviour of electrons in silane gas. Our *ab initio*, parameter–free calculations clearly exihibit the cross section minimum below 1 eV and a shape–resonance feature around 2–4 eV; this is in agreement with measured data. No any other *ab initio* calculation (with polarization effects) on the e–SiH_4 low–energy cross sections with such details and amount of cross section data is available in the literature.

2. We have suggested and tested a new optimized *iterative* scheme to solve the integro–differential equations more economically In order to treat exchange effects exactly in an efficient way. The new scheme is more suitable for the case of polar molecules where convergence problems are severe. In the optimized scheme, the continuum wavefunction of the electron with full iterative procedure is calculated only once at a selected energy, say E, i.e., $f_{\ell\ell'}(r;E)$. The $f_{\ell\ell'}(r;E)$ is employed as a starting point for iterative scheme at other energies. We found for the H_2O case (and very rcently for the NH_3 case also) that the number of iterations required in the optimised scheme is smaller, by a factor of two to three, than the usual one [6]. Further, we noticed that the exact–exchange treatment is necessary for low partial waves only. The non–penetrating higher partial waves can be described by a simple model exchange potential under the density functional theory. Thus, the new scheme, which is very economical and essential to treat polar molecules, can be described as follows. For low partial waves (say $\ell = \ell_E$), we consider full exact–exchange calculation; for $\ell \geq \ell_E$, say up to $\ell = \ell_M$, we employ a model exchange (for example the free–electron–gas exchange) approximation; and finally for very high partial waves $\ell \geq \ell_M$, say $\ell = \ell_{UB}$, we use unitarised Born approximation. A paper on the optimized iterative scheme

with test calculations on the e–H_2O system has been published recently [6].

3. The effects of gas temperature were investigated on the rotational excitations in a molecule (CH_4 and SiH_4) by slow electron impact. We have found that the rotational excitation process is sensitive to gas temperature in an experimental situation and one should be careful in comparing theoretical rotational excitation cross sections with measurements. In particular, for example, the theory predicts zero cross sections at zero angle for the $0 \rightarrow 3$ rotational transition in a spherical top molecule, while measurements (on the CH_4 molecule) give non–zero DCS in the forward direction [18].

4. We studied [7] various approximations to include polarization effects in the e–SiH_4 collisions at low energies. In this calculation, we have employed two types of parameter–free model polarization potentials alongwith exact–exchange effects. Our conclusion is that a polarization potential determined from polarised–orbital type approach is a better model than the one from the target density functional theory.

5. The low–energy electron scattering with H_2O, H_2S and NH_3 gases was investigated under the same theory as mentioned above. We tested convergence of the differential and total cross sections for these polar gases, for which the ANA theory fails in the forward direction. The final detailed results on the rotationally elastic, inelastic and summed cross sections (differential, integral, momentum transfer and energy loss) for both the polar gases (H_2O and H_2S) were completed. This work is being written up in separate papers.

6. We also developed a single–center computer program [8] to expand molecular quantities (orbitals, density, static potential etc.) around the center–of–mass (COM) of the target from the calculations of Quantum Chemistry codes such as the HONDO or GAUSSIAN. This work was done in collaboration with the group at Chemistry Department, University of Rome, Italy. We made attempts to study some big molecules such as the GeH_4, CF_4, SF_6, etc.. The first calculations on the e–GeH_4 collisions were

carried out and results were published [19]. We have also finished some calculations on the electron–SF_6 scattering at low energies.

7. In order to see the behavior of electron–molecule cross sections at higher energies (from about 20 eV to up to several thousand eV), we have adopted a simple but accurate scheme to determine total (elastic plus all inelastic channels) cross sections for a large class of molecules. A comparison is made with experimental data for all the gases [20].

8. We carried out extensive calculations on the low energy behaviour of electrons in C_2H_2 molecule. The cross sections (differential as well as integral) compare very well with experimental data, particularly, the shape resonance phenomenon. Two papers were published on this work [21–22].

9. Finally, our state–of–the–art computer codes, some modified during this period of contract, are in a situation to carry out low energy electron scattering calculations for any molecule of reasonable size and symmetry. There are a large number of molecules for which no theoretical study exists, while the cross sections are needed in many applied sciences.

The computing facilities, provided by the FSU SuperComputer Research Institute (SCRI), have been excellent in order to carry out the above programs effectively. We have made use of supercomputers (CRAY-2 at the NMFECC, Livermore and CRAY-YMP at the SCRI, Tallahassee) through the FSUCC allocation committee. Most of the graphical work and small calculations were carried out at the FSU and SCRI VAX machines which serve as front–end system for the supercomputers.

3. LIST OF PUBLICATIONS (June 1990 – 1993)

Papers Published:

[1]. " Theoretical Study of Low–energy Electron–SiH_4 Collisions using Exact Exchange plus Parameter–Free Polarization Potential, " by **Ashok Jain** and **D G Thompson.** J. Phys. **B24**, 1087 (1991).

[2]. " Effect of the Gas Temperature on the Rotational Excitation of Spherical Top Molecules by Low Energy Electrons: CH_4 and SiH_4.," by **Ashok Jain.** (Z. Phys. D, Atoms, Molecules and Clusters, Vol. 21, 153 (1991).

[3]. " Exact–Exchange Treatment in Electron–Polyatomic Molecules in a Computationally Optimised Iterative Scheme, " by **Ashok Jain, F A Gianturco** and **D G Thompson**, J. Phys. **B24**, 255 (1991).

[4]. " Polarization Effects in Low–Energy Electron Scattering from Silane Molecules Treating Electron Exchange Correlation Exactly, " by **Ashok Jain**, Phys. Rev. **A44**, 772 (1991)

[5]. " Differential, Integral and Momentum Transfer Cross Sections for Electron Scattering with Germane (GeH_4) Molecules at 1–100 eV, " by **Ashok Jain, K L Baluja, V Di Martino** and **F A Gianturco.** (Chem. Phys. Lett., **183**, 34 (1991).

[6]. " Differential, Integral and Momentum Transfer Cross Sections for Electron Scattering with Germane (GeH_4) Molecules at 1–100 eV, " by **Ashok Jain, K. L. Baluja, V. Di Martino** and **F. A. Gianturco**, Chem. Phys. Lett. **183**, 34–39 (1991).

[7]. " Slow Electron Collisions with CO Molecules in an Exact Exchange plus Parameter–free Polarisation Model, " by **Ashok Jain** and **D. W. Norcross**, Phys. Rev. **A45**, 1644–1656 (1991).

[8]. " Total (Elastic plus Inelastic) Cross Sections for Electron Scattering with CF_4 and GeH_4 Molecules at 10–5000 eV, " by **K. L. Baluja, Ashok Jain, V. Di Martino**

and **F. A. Gianturco**, Europhysics Lett., **17**, 139–144 (1992).

[9]. " Total (Elastic plus Inelastic) Cross sections for electron Collisions with Molecules at 10–5000 eV: H_2, Li_2, HF, CH_4, CO, N_2, HCN, C_2H_2, O_2, SiH_4, PH_3, H_2S, HCL and CO_2, " by **Ashok Jain** and **K. L. Baluja**, Phys. Rev. **A45**, 202 (1992).

[10]. "Electron Scattering from Non–Linear Molecules using Multicenter Wavefunction Expansions, " by **F. A. Gianturco, Ashok Jain** and **V. Di Martino**, Nuovo Cimento, **14**, 411 (1992).

[11]. " On the $^2\Pi_g$ Shape Resonance in Electron–C_2H_2 Scattering," by **Ashok Jain**, J. Phys. **B25**, L439, (1992).

[12]. " Low Energy (0.01 – 20 eV) Electron Scattering with C_2H_2 Molecules", by **Ashok Jain** J. Phys. **B26**, 4833 (1993).

Papers under preparation

[13]. " Slow Electron Collisions with H_2O Molecules in an Exact–Exchange plus Parameter–free Polarization Potential Model, " by Ashok Jain and D. G. Thompson. (to be submitted to J. Phys. B).

[14]. " A Theoretical Study of Slow Electron Impact from Ammonia (NH_3) Gas: Rotationally Elastic, Inelastic and Summed Cross Sections, " by Ashok Jain and D. G. Thompson (to be submitted in Phys. Rev. A).

[15]. "Elastic and Rotational Excitation Cross Sections for Low Energy Electron Scattering with H_2S Molecules in a Parameter–Free Exact–Static–Exchange plus Polarization Model," , by Ashok Jain (to be submitted in Phys. Rev. A).

4. REVIEW OF THEORETICAL APPROACH

When low–energy electrons interact with molecular targets, several processes, elastic and inelastic, can take place in the present energy region (E $\leq$ 20 eV):

$$e^- + A_nB_m \rightarrow e^- + A_nB_m \qquad (elastic)$$
$$\rightarrow e^- + (A_nB_m)^* \quad (inelastic; \quad vibrational\ and/or\ rotational)$$

(There are also other inelastic processes such as the electronic excitation, dissociative, associative, or ionization channels.) The basic Schrödinger equation involves an interaction Hamiltonian and the corresponding wave function of the total system:

$$(H_{int} - E)\Psi_T(\mathbf{r}, \mathbf{r}_i, \mathbf{R}) = 0, \tag{4.1}$$

where the electron–molecule Hamiltonian is given by:

$$H_{int} = H_{elec}(\mathbf{r}_i; \mathbf{R}) + V_{int}(\mathbf{r}, \mathbf{r}_i, \mathbf{R}) + H_{nuc}(\mathbf{R}). \tag{4.2}$$

Here $\mathbf{r}$ represents the projectile electron coordinate and $\mathbf{r}_i$ and $\mathbf{R}$ collectively represent the target electronic and nuclear coordinates, respectively. It is not possible to solve equation (1) exactly for any of the channels or collision systems. We first describe the iterative techniques to solve integro–differential (see below) equation under the SCE formalism.

4.1. Single-Center-Expansion (SCE) Iterative Method

In order to obtain various elastic and inelastic cross sections (differential as well as integral), we make use of the adiabatic–nuclei–approximation (ANA) [23] and set up our scattering equations in the SCE scheme under the close–coupling formalism. The FNA is generally a very good approximation except in certain cases: for example, near threshold and sharp shape–resonance energy regions, for polar molecules, etc.

In the body–fixed (BF) frame of reference, the time–independent Schrödinger equation of the electron–molecule system reads as (omitting the parametric dependence on internuclear coordinates $\mathbf{R}$):

$$[-\frac{1}{2}\vec{\nabla}_r^2 + H_{\rm elec}(\mathbf{r}) + V_{\rm int} - E]\Psi_{\rm T}(\mathbf{r}, \mathbf{r}_i) = 0, \tag{4.1.1}$$

where the operators in the bracket are respectively the kinetic energy operator of the scattered electron, the unperturbed molecular target Hamiltonian, the interaction potential of the electron–molecule complex and the total energy of the system. The total wave function $\Psi_{\rm T}$ can be expanded such that:

$$\Psi_{\rm T} = A \sum_{i=1}^{n} \Phi_i(\mathbf{r_1}, \mathbf{r_2}, \ldots \mathbf{r_Z}) F_i(\mathbf{r}), \tag{4.1.2}$$

where Φ_i are the target electronic states and any other suitable pseudostates that can represent the target response function to the polarization of the molecule because of the incoming electron. The continuum function $F_i(\mathbf{r})$ describes the projectile motion in molecular state i and A is the usual antisymmetrization operator to ensure Pauli principle. In the expansion (4.1.2), we have neglected the correlation functions of the $(N+1)$–electron–molecule complex.

We can assume that the center of the electron–molecule system is at the center–of–mass (COM) of the target. The spin of the scattered electron is coupled with the total spin of the molecule to form the eigenstate of $\mathbf{S}^2$ and its projection along the symmetry axis (say $\mathbf{S}_z$) corresponding to the total spin quantum number S and its substate M_S which are ***constants of motion*** during the collision. Each of these eigenstates can be expanded over the set of angular functions according to the prescriptions of a BF frame of reference which provides the basis of an irreducible representation (IR) $p\mu$ of the molecular symmetry point group. Thus we can write the total wave function as:

$$\Psi_T^{p\mu SM_S} = \sum_{i=1}^{n} \sum_{\ell h} \Phi_{i\ell h}^{p\mu SM_S}(\mathbf{r}_1, \mathbf{r}_2 \ldots \mathbf{r}_Z, \hat{\mathbf{r}}, \sigma)(r)^{-1} F_{i\ell h}^{p\mu SM_S}(\mathbf{r}), \tag{4.1.3}$$

where σ is the spin variable of the scattered electron. The functions Φ in equation (4.1.3) are defined as:

$$\Phi_{i\ell h}^{p\mu SM_S} = \sum_{M_{S_i} m_{s_i}} \phi_i^{p_i \mu_i S_i M_{S_i}}(\mathbf{r}_1, \mathbf{r}_2, \ldots \mathbf{r}_Z) X_{\ell h}^{p\mu}(\hat{\mathbf{r}}') \eta(\frac{1}{2}, m_{s_i}) C_{M_{S_i} m_{s_i} M_S}^{S_i \; \frac{1}{2} \; S}, \tag{4.1.4}$$

where η's are electron spin functions for the scattered electron and C's are the Clebsch–Gordon coefficients. The bound orbitals ϕ_i describe Z–electron target wave function used in expansion (4.1.4), each transforming like a particular IR of the molecular point group and with a specific total spin eigenstate. The main molecular symmetry axis defines the M_S direction.

As a standard technique, we now project the scattering equation onto the channel functions and obtain the well known coupled integro–differential equations for each scattered electron channel function ($p\mu S$):

$$[\frac{d^2}{dr^2} - \frac{\ell_i(\ell_i+1)}{r^2} + k_i^2] F_{i\ell h}^{p\mu S}(r) = 2 \sum_{i'=1}^{n} \sum_{\ell' h'} [V_{i\ell h, i'\ell' h'}^{p\mu S}(r) + W_{i\ell h, i'\ell' h'}^{p\mu S}(r)], \tag{4.1.5}$$

4.2 Static and Exchange Interactions

The direct potential matrix $V^{p\mu S}$ defines the coupling between two channel functions through the Coulomb operator (for details see Ref. 1). The exchange interaction is represented by the non–local term, $W^{p\mu S}$, which gives rise to the integro–differential nature of the coupled scattering equations. We do not give all the details here for obvious reasons (see Ref. 1 for full details). For a closed–shell molecule, belonging to the totally symmetric $^1A_1$ IR of the molecular point group, equation (4.1.5) does not depend on the spin

quantum numbers. The equation (4.1.5) is known as the static–exchange interaction of the electron–molecule system if we retain only the ground state ($i = 1$) of the target. From a numerical point of view, it is convenient to include the target distortion (polarization) effects via a model potential added to the direct potential matrix in equation (4.1.5). At short distances, the correlation effects can be treated in a similar fashion. The exchange term in equation (4.1.5) is basically of the following type:

$$W^{p\mu} = \sum_{\alpha} \int \phi_{\alpha}^{*}(\mathbf{x}) |\mathbf{r} - \mathbf{x}|^{-1} F^{p\mu}(\mathbf{x})\, d\mathbf{x} \phi_{\alpha}(\mathbf{r}), \tag{4.2.1}$$

Recently a program has been developed to treat $W^{p\mu}$ exactly under the iterative procedure [2]. Under the static–exchange plus (model) polarization (SEP) model, the integro–differential coupled equation to be solved for a closed–shell system for each symmetry $p\mu$ is rewritten from Eq. (4.1.5) as (suppressing the $p\mu$ symbol for simplicity):

$$[\frac{d^2}{dr^2} - \frac{\ell(\ell+1)}{r^2} + k^2] F_{\ell h}(r) = 2 \sum_{\ell' h'} [V^{\mathrm{st}}_{\ell h, \ell' h'}(r) + V^{\mathrm{pol}}_{\ell h, \ell' h'} + W_{\ell h, \ell' h'}(r)], \tag{4.2.2}$$

The potential matrix $V^{\mathrm{st}}_{\ell h, \ell' h'}$ in Eq. (4.2.2) is determined from the following expression for the static potential:

$$V_{\mathrm{st}}(\mathbf{r}) = \int |\Phi_0|^2 \{ \sum_{j=1}^{Z} |\mathbf{r} - \mathbf{r_j}|^{-1} d\mathbf{r_1} d\mathbf{r_2} \cdots d\mathbf{r_Z} \} - \sum_{i=1}^{M} Z_i |\mathbf{r} - \mathbf{R_i}|^{-1}. \tag{4.2.3}$$

where Φ_0 is the target ground state wavefunction given as a single Slater determinant of one–electron Z spin orbitals $\phi_i(\mathbf{r})$ and M the number of nuclei in the molecule.

In a model exchange problem, the non–local exchange term in the right–hand side of Eq. (4.2.2) can be replaced by a local potential, say $V^{\mathrm{ex}}_{\ell h, \ell' h'}(r)$. A very popular form of $V^{\mathrm{ex}}(r)$ has been the free–electron–gas–exchange(FEGE) approximation which was modified by Hara [24] (to be denoted by HFEGE) for electron-molecule collisions. In the HFEGE, the V^{ex} reads as:

$$V^{\rm ex}(\mathbf{r}) = \frac{2}{\pi} k_F(\mathbf{r}) \{ \frac{1}{2} + \frac{1-\eta^2}{4\eta} \ln |\frac{1+\eta}{1-\eta}| \}, \qquad (4.2.4)$$

where, $k_F(\mathbf{r}) = (3\pi^2 \rho_0(\mathbf{r}))^{\frac{1}{3}}$ and $\eta = (k^2 + 2I + k_F^2)^{\frac{1}{2}}/k_F$. Here I is the ionization potential of the target and $\rho_0(\mathbf{r})$ is the unperturbed charge density of the molecule. Several versions of HFEGE are available by varying the value of I [25]. Thus, writing the integro–differential equation (4.2.2) in a convenient matrix form, $\mathbf{LF} = \mathbf{WF}$ where $\mathbf{WF}$ is the exchange term, the iterative scheme is $\mathbf{LF^i} = \mathbf{WF^{i-1}}$, where $i = 0, 1, \ldots$. In order to start the solution, we chose $\mathbf{F^0}$ to be the solution obtained from the HFEGE potential (4.2.4). Our earlier scattering code (POLY, see Section 5.3) has been modified for the solution of Eq. (4.2.2). The new code (POLYEX) is now working successfully on the CRAY-2 and FSU's VAX and CRAY-YMP systems.

4.3 Polarization Interaction

It is very hard to include polarization effects accurately; however, the asymptotic form is known exactly, i.e.:

$$V_{\rm pol}(r,\theta,\phi) = \frac{-1}{2r^4} [\alpha_0 (4\pi)^{\frac{1}{2}} S_0^{01} + \alpha_2 (\frac{4}{5}\pi)^{\frac{1}{2}} S_2^{01} + \alpha_2^1 (\frac{4}{15}\pi)^{\frac{1}{2}} S_2^{21}], \qquad (4.3.1)$$

where the S_ℓ^{mq} is a real spherical harmonic (see Ref. 1 for its definition and various properties), (r,θ,ϕ) are the coordinates of the projectile referring to the center of the target and the spherical (α_0) and nonspherical (α_2 and α_2^1) polarizabilities are expressed in terms of the polarizability tensor α_{ii} of the target, namely:

$$\alpha_0 = \frac{1}{3}(\alpha_{11} + \alpha_{22} + \alpha_{33});\ \alpha_2 = \frac{2}{3}(\alpha_{33} - \frac{1}{2}\alpha_{11} - \frac{1}{2}\alpha_{22});\ \alpha_2^1 = \alpha_{11} - \alpha_{22}.$$

In order to represent the $V^{\rm pol}$ at short distances, one has to introduce some kind of adjustable parameter(s) in the cut–off function which is multiplied to the right–hand side

of equation (4.3.1). The value of the unknown parameter is determined by the fitting procedure. An important development was made by our group in evaluating an approximate parameter–free polarization potential [26] based on the second–order perturbation theory [27] and the criterion of Temkin [28]. In this method, the molecule is supposed to be in an electric field $\mathbf{E} = E\hat{\mathbf{r}}$ (produced by the incoming electron) at $\mathbf{r}(r\theta\phi)$, which results in an extra potential energy V, the leading term of which is given by:

$$\begin{aligned} V(\mathbf{r}_1, \mathbf{r}_2, \ldots \mathbf{r}_Z; \mathbf{E}) &= \mathbf{E} \cdot \sum_{i=1}^{Z} \mathbf{r}_i \\ &= E \sum_{i=1}^{Z} r_i \, \hat{\mathbf{r}} \cdot \hat{\mathbf{r}}_i \end{aligned} \tag{4.3.2}$$

The energy of the molecule in the electric field can be expanded as a Taylor series in $E_i (i = 1, 2, 3)$, the components of $\mathbf{E}$ along the axes of our coordinate system. The second order energy reads as:

$$W_2 = \frac{1}{2} \sum_{ij} E_i \alpha_{ij} E_j, \tag{4.3.3}$$

In the method of Pople and Schofield [27], the first order wave function Φ_1 is expanded in terms of ground–state Φ_0 functions as:

$$\Phi_1 = \Phi_0 \sum_{i=1}^{Z} f(\mathbf{r}_i) \cdot \mathbf{E}, \tag{4.3.4}$$

where unknown coefficients f's are determined variationally from the following expression of W_2, i.e.:

$$W_2 = \langle \Phi_1 | H_{mol} - W_0 | \Phi_1 \rangle + 2 \langle \Phi_0 | V | \Phi_1 \rangle. \tag{4.3.5}$$

The success of this parameter–free model for the polarization potential (to be denoted as the JT polarization approximation) along with an exact treatment of exchange has been exceptional in our recent investigation of the low–energy electron–CH_4 interactions [3].

4.4 Cross–Section Formulae

We now summarize our cross section formulae. As a special case, we will provide explicit expressions in the simple case of spherical molecules such as the CH_4, SiH_4 etc. For full details we refer to our review article [1]. In this project, we have investigated mainly the rotationally elastic, inelastic and summed channels for differential, integral, momentum transfer and energy–loss cross sections. As mentioned above, we solve our scattering problem in the fixed–nuclei approximation under the BF frame of reference. In order to obtain physical parameters, we transform the BF scattering amplitude, $f(\hat{\mathbf{k}} \cdot \hat{\mathbf{r}})$, ($\hat{\mathbf{k}}$ and $\hat{\mathbf{r}}$ are respectively the initial and final directions of the projectile) into the space–fixed amplitude $f(\hat{\mathbf{k}} \cdot \hat{\mathbf{r}}'; \alpha\beta\gamma)$ (where $\hat{\mathbf{r}}'$ now refers the direction of scattered electron with respect to SF coordinate system and $(\alpha\beta\gamma)$ are the three Euler angles) by making use of rotation matrices. The SF scattering amplitude is given by:

$$f(\hat{\mathbf{k}}.\hat{\mathbf{r}}'; \alpha\beta\gamma) = \sum_{\ell h m \ell' h' m' \lambda p \mu} \frac{1}{ik} \pi (2\ell+1)^{\frac{1}{2}} i^{\ell - \ell'} b^{p\mu}_{\ell h m} b^{p\mu}_{\ell' h' m'} Y^{\lambda}_{\ell'}(\hat{\mathbf{r}}') \times \mathbf{D}^{\ell'}_{\lambda m}(\alpha\beta\gamma) \mathbf{D}^{\ell}_{0m}(\alpha\beta\gamma) (\mathbf{S}^{p\mu}_{\ell h, \ell' h'} - \delta_{\ell\ell'}\delta_{hh'}), \tag{4.4.1}$$

where b's are defined earlier[1], $\mathbf{D}$'s are the rotation D–matrices and $\mathbf{S}$ is the scattering S–matrix. In the impulse approximation [29], the scattering amplitude for a particular rotational transition $JKM \rightarrow J'K'M'$ is written as:

$$f(JKM \rightarrow J'K'M') = \langle \psi_{JKM} | f(\hat{\mathbf{k}}.\hat{\mathbf{r}}'; \alpha\beta\gamma) | \psi_{J'K'M'} \rangle, \tag{4.4.2}$$

where $|\psi_{JKM}\rangle$ is the rotational eigenfunctions of a molecule (asymmetric, symmetric or spherical tops) which are given in standard texts. Expressions for a general asymmetric top are discussed in Ref. 1. Here we discuss formulae for spherical tops only. The differential cross section for the $J \rightarrow J'$ transition is obtained by summing over all final magnetic substates $K'M'$ and averaging over all initial substates KM, i.e.:

$$\frac{d\sigma}{d\Omega}(J \to J') = \frac{k'}{k}\frac{1}{(2J+1)^2}\sum_{KMK'M'}|f(JKM \to J'K'M')|^2, \qquad (4.4.3)$$

where k' is the wavenumber of the scattered electron given by the relation:

$$2k'^2 = 2k^2 + E_J - E_{J'} \quad . \qquad (4.4.4)$$

For a spherical top molecule, the energy of the Jth level is given by $E_J = BJ(J+1)$, where B is the rotational constant of the molecule in question. It is convenient to express the DCS in terms of Legendre polynomials:

$$\frac{d\sigma}{d\Omega}(J \to J') = \frac{k'}{k}\sum_{L}^{2\ell_{max}+1} A_L(J \to J')P_L(\cos\theta). \qquad (4.4.5)$$

Here θ is the scattering angle between the vectors $\hat{\mathbf{k}}$ and $\hat{\mathbf{r}}'$. The expansion A_L coefficients are found to be [30]:

$$A_L(J \to J') = \frac{(2J'+1)(2L+1)(-1)^L}{4k^2(2J+1)}\sum_{ll'\bar{l}\bar{l}'}[(2l+1)(2l'+1)(2\bar{l}+1)(2\bar{l}'+1)]^{\frac{1}{2}} i^{l-l'}(-i)^{\bar{l}-\bar{l}'}$$
$$\begin{pmatrix}\bar{l} & l & L\\ 0 & 0 & 0\end{pmatrix}\begin{pmatrix}l' & \bar{l}' & L\\ 0 & 0 & 0\end{pmatrix}\sum_{j=|J-J'|}^{J+J'}(-1)^j W(ll'\bar{l}\bar{l}';jL)M_{ll'}^{jm_j}M_{\bar{l}\bar{l}'}^{jm_j\,*} \qquad (4.4.6)$$

where the M–matrix is defined as:

$$M_{ll'}^{jm_j} = \sum_{mm'hh'p\mu}(-1)^m\, \bar{b}_{lhm}^{p\mu}\begin{pmatrix}l & l' & j\\ m & m' & -m_j\end{pmatrix}\bar{b}_{l'h'm'}^{p\mu}\,\mathbf{T}_{lh,l'h'}^{p\mu} \quad . \qquad (4.4.7)$$

Here, as usual, the $\mathbf{T}$–matrix is defined in terms of the $\mathbf{S}$–matrix as $\mathbf{T} = (\mathbf{S} - \mathbf{1})$ where $\mathbf{S} = (\mathbf{1} + \mathbf{iK})(\mathbf{1} - \mathbf{iK})^{-1}$. The scattering $\mathbf{K}$ matrix for each symmetry $(p\mu)$. In equation (4.4.7) $\begin{pmatrix}a & b & c\\ d & e & f\end{pmatrix}$ is a $3-j$ symbol, $W(abcd;ef)$ is the well known Racah coefficient and the $b_{lhm}^{p\mu}$ coefficients are the expansion terms in the definition of symmetry–adapted basis functions in terms of real spherical harmonics [1]. From equation (4.4.5), it is easy to find

simple forms of the total (σ_t) and momentum transfer (σ_m) cross sections in terms of A_L coefficients, namely:

$$\sigma_t^{JJ'} = 4\pi A_0(J \rightarrow J') \quad ; \quad \sigma_m^{JJ'} = 4\pi[A_0(J \rightarrow J') - \frac{1}{3}A_1(J \rightarrow J')]. \tag{4.4.8}$$

It is easy to determine A_0 and A_1 coefficients for σ_t and σ_m rather than the full expansion (4.4.6) for the DCS. For example, the A_0 and A_1 are given by the following simpler expressions:

$$A_0 = \frac{1}{4k^2} g(JJ') \sum_{\ell\ell' j m_j} (-1)^{\ell+\ell'} |M_{\ell\ell'}^{j m_j}|^2, \tag{4.4.9}$$

and:

$$\begin{aligned} A_1 = \frac{3}{4k^2} g(JJ') \sum_{\ell\ell' j m_j} (-1)^{\ell+\ell'+j} [& \{(\ell+1)(\ell'+1)\}^{\frac{1}{2}} W(\ell\ell'\ell+1\ell'+1; j1) M_{\ell\ell'}^{j m_j} M_{\ell+1\ell'+1}^{j m_j^*} \\ & + \{\ell(\ell'+1)\}^{\frac{1}{2}} W(\ell\ell'\ell-1\ell'+1; j1) M_{\ell\ell'}^{j m_j} M_{\ell-1\ell'+1}^{j m_j^*} \\ & + \{(\ell+1)\ell'\}^{\frac{1}{2}} W(\ell\ell'\ell+1\ell'-1; j1) M_{\ell\ell'}^{j m_j} M_{\ell+1\ell'-1}^{j m_j^*} \\ & + (\ell\ell')^{\frac{1}{2}} W(\ell\ell'\ell-1\ell'-1; j1) M_{\ell\ell'}^{j m_j} M_{\ell-1\ell'-1}^{j m_j^*}] \end{aligned} \tag{4.4.10}$$

where $g(JJ')$ represents the statistical $(2J'+1)/(2J+1)$ factor. The vibrationally elastic (rotationally summed) cross sections are obtained by summing over J' for $J = 0$. The selection rule for the transition $J \rightarrow J'$ can easily be worked out from the asymptotic form of the static potential (4.2.3) which transforms as ${}^1A_1$ symmetry of the molecular point group. For any specified values of J and J', the angular momentum transfer j (Eq. 4.4.6) takes the following values:

$$|J - J'| \leq j \leq J + J' \quad ; \quad |l - l'| \leq j \leq l + l', \tag{4.4.11}$$

In addition, calculations on the polar polyatomic molecules (H_2O and NH_3) need further attention in order to remove the defficiencies of the ANA formalism towards convergence of the differential and total integral cross sections [see Refs. 31–32]. We employ the

multipole–extracted–adiabatic–nuclei (MEAN) approximation [32]. In the MEAN methodology, a maximum use has been made of the first–Born–approximation (FBA) for the higher symmetries and partial waves. So far, such a program exists only for the linear molecules and we have modified our previous code [see Section 5.3]. Finally, in the MEAN approximation, the differential cross sections (DCS) for a rotational transition $J \rightarrow J'$ are written as [32]:

$$\frac{d\sigma}{d\Omega}^{JJ'} = \frac{d\sigma^{\rm FBA}}{d\Omega}(J \rightarrow J') + \frac{k_{J'}}{4k_J}\sum_{l_t}[C(Jl_tJ';00)]^2\frac{1}{k^2}\sum_{\lambda=0}^{\lambda_{\rm max}}(B_{\lambda,l_t} - B^{\rm FBA}_{\lambda,l_t})P_\lambda(\cos\theta), \tag{4.4.12}$$

where the first term is the usual closed form for the rotational excitation ($J \rightarrow J'$) DCS in the space–fixed FBA; k_J and $k_{J'}$ are respectively the wave vectors in the initial and final channels; C(.....) is a Clebsch–Gordan coefficient; l_t is the angular momentum transfer during the collision; B_{λ,l_t} are the DCS expansion coefficients , expressed in terms of scattering matrix, and $B^{\rm FBA}_{\lambda,l_t}$ are the corresponding quantities in the FBA evaluated in the BF coordinate system

The expression for the space–fixed FBA quantities are given in Ref. 1. The important quantity is the FBA differential and integral cross sections to be employed in equation (4.4.12). Here we give these expressions explicitly:

$$\frac{d\sigma}{d\Omega}(J \rightarrow J' = \frac{k'}{\pi k}\frac{(2J'+1)}{(2J+1)}\sum_{\ell m}(2\ell+1)^{-1}\left|\int_0^\infty dr\, r^2 v_{\ell m}(r) j_\ell(qr)\right|^2. \tag{4.4.13}$$

and the integrated quantity is expressed as:

$$\sigma_{0\rightarrow J'} = \frac{2(2J'+1)}{k^2}\sum_{\ell m}(2\ell+1)^{-1}\int_{|k-k'|}^{k+k'} dq\, q\left|\int_0^\infty dr\, r^2 v_{\ell m}(r) j_\ell(qr)\right|^2. \tag{4.4.14}$$

where dipole and quadrupole terms correspond respectively from $J = 0$ to $J' = 1$ and 2. It is to be noted here that except at very low energy (below 0.1 eV) the short–range form of $v_{\ell m}(r)$ coefficients is very important. We have included these coefficients exactly at all radial distances, rather than employing the asymptotic form in terms of dipole, quadrupole, etc., moments.

5. REVIEW OF NUMERICAL DETAILS

Here, we provide a brief review of numerical and computational aspects of the present approach employed for electron scattering from molecules. The basic ingredients are the molecular wavefunction and the Coulomb interaction to describe bound and bound–free quantities. A near–Hartree–Fock description of the target is sufficient for the present purpose. For full details we refer our earlier work [1, 9-10]. For completeness purpose, here we summarize the target bound functions, iterative procedure, and finally a list of computer programs employed for the present calculations.

5.1 Molecular Wavefunctions

For any polyatomic molecule, the multi–center target wavefunctions are easy to determine using standard Quantum Chemistry codes. In a single–center–expansion approach, however, determining actual electronic densities around the bound nuclei still rquires a large computational effort in order to represent correctly or with high precision the total charge distribution. Relativistic effects are neglected in our present work and the separation of electronic and nuclear motions is assumed under the usual Born–Oppenheimer approximation (BOA). To understand the nature of polyatomic electrons, it is necessary to consider the symmetry properties in terms of symmetry–adapted wave functions (SAWF).

For our purpose to study molecular species like CH_4, SiH_4, GeH_4, SF_6, CF_4, H_2O, H_2S, NH_3, etc., the SCE approach is very successful. We employed a computer code MOLMON (see Section 5.4) to generate bound orbitals at the fixed equilibrium geometry of the target. In general, the molecular orbitals are written in terms of LCAO (linear combination of atomic orbitals) centered at the COM of the molecule. In order to represent molecular states, we follow the nomenclature of Herzberg [33]. In brief, the capital letter A is used to represent one–dimensional IR with character $+1$, while for character -1, the letter B is used. For a two–dimensional IR, the letter E is used, while a three–dimensional IR is denoted by letter T. Suffixes $1, 2, 3..$ are used to distinguish different

IR's with the same dimensions. The subscripts g or u differentiate between even (gerade) or odd (ungerade) representations of the same class if *inversion* symmetry also exists (for example in the case of SF_6 molecule). Lower case letters (a, b, e, t etc.) are used to denote individual orbitals. For example the ground state of the H_2O molecule is written as follows: $1a_1^2\, 2a_1^2\, 3a_1^2\, 1b_1^2\, 1b_2^2\ (^1A_1)$.

For the present set of molecules, we have included up to $\ell_{\max} = 7$ in the SCE expansion of bound and continuum orbitals. The molecular quantities (such as the total energy, various multipole moments, etc.) obtained with the present SCE basis compare reasonably well with the experimental and other sophisticated calculations (see Ref. 9).

5.2 SCE Parameters from Multicenter Target Wavefunctions

Recently our group [8] has developed an interface computer code to generate SCE orbitals from multicenter target wavefunctions. First, the bound and continuum orbitals around the COM of the target are written as follows:

$$\phi_\alpha(\mathbf{r}_i) = \sum_{hl} r^{-1} u_{hl}^{\alpha}(r) X_{hl}^{p_\alpha \mu_\alpha}(\hat{\mathbf{r}}), \tag{5.2.1}$$

and:

$$F^{p\mu}(\mathbf{r}_i) = \sum_{hl} r^{-1} f_{hl}^{p\mu}(r) X_{hl}^{p\mu}(\hat{\mathbf{r}}), \tag{5.2.2}$$

Here α labels a specific multicenter MO. In order to perform expansion (5.2.1–2), we need to start from the multicenter wavefunction which describes the molecule and then generate the $u_{hl}(r)$ coefficients by quadrature. from these coefficients we can determine the corresponding total density in its expansion form:

$$\rho(\mathbf{r}) = \sum_{hl\alpha} r^{-1} \rho_{hl}^{\alpha}(r) X_{hl}^{\alpha}(\hat{\mathbf{r}}), \tag{5.2.2}$$

In the present work we started with four molecular systems, belonging to T_d symmetry. These are the SiH_4, GeH_4, SF_6 and CF_4 molecules. The SF_6 molecule has extra inversion symmetry also. The presence of the large electronic density away from the COM in CF_4, makes the study of numerical convergence of the expansion particularly interesting. The initial HF–SCF calculations were carried out using the HONDO package [34] and the general features of the relevant optimized geometries and basis set expansions were listed in Ref. 8. We see that the triple–zeta plus polarization (TZ+P) functions were employed for SiH_4 and CF_4, thus yielding a fairly accurate description of the ground state electronic charge density, while the GeH_4 target was treated at the split–valence level of accuracy and involved 66 contracted functions. Each total charge density was then employed in a quadrature scheme that produced the symmetry adapted coefficients of Eq. (5.2.2) and each of the MO contributions of Eq. (5.2.1). The numerical procedure starts from a set of points in the space $\mathbf{r} = (x, y, z)$ which is the one generated by the HONDO algorithm, and uses them to perform a transformation to polar coordinates (r, θ, ϕ). It is the number of latter points which is employed to construct the integration grids for Eqs. (5.2.1) and (5.2.2) that yields the required coefficients. The Gauss–Laguerre integration, for each coefficient in both equations, was carried out over a range of 500 r values, from 0.001 a_0, up to about 15 a_0, with a variable grid that became denser around the origin and around the outer nuclear positions. In the radial region with $r < 1.0a_0$, and for $\ell \leq 12$, the θ–integration and ϕ–integration were carried out on a grid of $20 \times 20 = 400$ pivots. As the r–value increased, the grid size went up to its maximum value of 9216 pivots (96×96). The test on the original values of either the orbitals or of the densities showed agreement of $\sim 0.1\%$ for the expansion with $\ell \leq 20$ in the multipolar coefficients, at typical distances either around the mid–bond or at the outer molecular nuclei.

A comparison of the behavior of the radial density coefficients for the three systems examined were shown in Fig. 5.2.1 of Ref. 10, where the radial region around the outer–atom position was shown in each case. Our conclusions are the following :

1. The lightest molecule, silane, exhibits quite fast convergence, even over the rather difficult region of the hydrogen cusps around the outer nucleus position at $\sim 2.787a_0$. This is due to the fairly compact, nearly spherical structure of a system in which a rather low electron density is involved in the bonding and around the H atoms away from central Silicon atom.
2. The feature of rapid convergence is also exhibited by the germane molecule (bottom part of the figure 5.2.1) where, being at even larger distance ($R = 2.905a_0$) than silane, the location of the hydrogen atoms affects little the essentially spherical structure of the central atom, where more than 90% of the charge density is located.
3. The situation, on the other hand, is quite different in the case of CF_4 molecule: large electron density portions exist around the outer Florine atoms and, therefore, the convergence in ℓ is much slower. We see that at distances corresponding to the F atom positions ($2.45a_0$), that all coefficients are much stronger than their counterparts for silane (note the much larger scale for the CF_4 case) and values up to $\ell = 20$ are still contributing in a sizeable way around the F atoms.

The specific behavior of the electronic densities is obviously to influence the features of the different contributions to the electron molecule interaction (4.2.3), since they are going to depend rather closely on the electronic density of the target. In particular, the use of expansion (5.2.1–2) for the bound and continuum electrons allows us to write the CC equations as coupled, radial integro–differential equations for each FN configuration (see Eqs. 4.1.5 and 4.2.2). The coupling matrix of Eq. (4.1.5) is given by:

$$V^{p\mu}_{hl,h'l'}(\mathbf{r}) = \left\langle X^{p\mu}_{hl}(\hat{\mathbf{r}}) | V^{A_1}_{\rm st}(\mathbf{r}) | X^{p\mu}_{h'l'}(\hat{\mathbf{r}}) \right\rangle. \tag{5.2.3}$$

If we write the SCE expansion of interaction potential in terms of SAWF:

$$V^{A_1}_{\rm st}(\mathbf{r}) = \sum_{hl} v_{hl}(r) X^{A_1}_{hl}(\hat{\mathbf{r}}), \tag{5.2.4}$$

where we have assumed a closed–shell molecule with A_1 IR for its total density and interaction potential, we have to go through a numerical quadrature in order to evaluate the multipolar expansion of the potential. The results for SiH_4, GeH_4 and CF_4 targets were shown in Figs. 5.2.2, 5.2.3 and 5.2.4 of Ref. 10, respectively.

From Fig. 5.2.2 of Ref. 10, we see for the silane molecule that the radial region of the coefficients around the second nuclear cusp on the H atom. The Si cusp converges very rapidly, as expected, and the static potential at $r \sim 0$ has its largest contribution given by the $\ell = 0$ coefficient. It is clear from seeing the increasingly narrower cusps as ℓ increases, that several terms are, however, still needed to correctly describe quantitatively the localized anisotropy of interaction due to the four H atoms, placed at the four corners of the usual cube, describing tetrahedral molecules. On the other hand, the values of the various coefficients at $R \sim 2.787a_0$ (the position of the H atom) decreases rather rapidly with increasing ℓ and, therefore, one sees clearly in the bottom part of the Fig. 5.2.2 of Ref. 10 that by the time $\ell = 20$ the contribution to the static potential is less than 0.2 atomic units and it is so over rather limited radial region ($\Delta R \sim 0.3a_0$). As this value should be compared with the values of lower coeffcients over the whole range of action of the static potential, it is reasonable to expect that such high multipoles, in the present case, would contribute rather small to the scattering process.

The similar coefficients for GeH_4 molecule were depicted in Fig. 5.2.3 of Ref. 10. They show even more dramatically the effect of the compact charge distribution around the central Ge atom and the more removed position of the H atoms ($R = 2.905a_0$); the atomic charge at the COM of the system has increased here from 14 to 32 and, therefore, the corresponding static potential with an incoming electron is given almost totally by the $\ell = 0$ term. The coefficients for higher ℓ values are, therefore, nearly negligible both around $R \sim 0$ and all along the bond region until one reaches the H atom environment, where they contribute more or less the same amounts as in the silane case of Fig. 5.2.2 of Ref. 10. The higher order contributions with $\ell > 12$ as shown in Fig. 5.2.3 (see Ref.

10), indicate once more the fairly rapid convergence of the static potential expansion for the GeH_4 target; nearly all coefficients vanish within the examined radial region, except in the narrow area around $\sim 2.9a_0$, where they never contribute more than $\sim 1au$. All the higher contributions with $\ell > 20$ and up to $\ell \sim 30$ are markedly smaller and were not shown in the figure.

Thus we preliminarily concluded that both silane and germane are nearly spherical molecules with compact electronic charge distribution which are given quite realistically by the first few coefficients in the multipolar expansion of Eq. 5.2.4.

Finally, for the CF_4 case (Fig. 5.2.4 of Ref. 10), The $\ell = 0$ term is still the largest around the origin and higher order terms are markedly smaller near the origin. On the other hand, the radial region where the F atoms are located ($R = 2.45a_0$) show now much larger contributions from the higher multipolar terms: the scale used in Fig. 5.2.4 of Ref. 10 is one order of magnitude bigger than that of the previous cases and yet we see that $\ell = 10$ is still contributing rather substantially. The same is true for, say, $\ell = 19$ that is now about 10 times larger than its value for H atoms of the previous cases (silane and germane molecules) and still 20 % of the cusp value for the $\ell = 10$ contribution. One, therefore, sees here a nearly linear scaling of the strength of the static potential with Z value of the off-center atom that is being considered. Such a result could be used to estimate the rate of convergence of the coefficients and the ℓ_{max} value which should be included in (5.2.4) to reach any predetermined level of accuracy in the static potential. In the present example of CF_4 one clearly sees that higher order terms need to be included and ℓ values up to $\ell = 30$ had to be calculated in order to reach the same negligible cusp behavior around F atoms as those shown before by the other two molecules discussed above.

Thus with the above SCE codes, we have made preliminary attempts to develop SCE quantities for much heavier targets (SF_6, CCl_4 etc.) including the CF_4 one. We will show some of our cross section calculations for the electron-SF_6 system at low to high impact energies.

5.3 An Optimized Iterative Scheme

The full account of this section is already given in the previos progress reports [9–10]. At the static–exchange level [1], the Schrödinger equation for the continuum electron function $F^{p\mu}(\mathbf{r})$ for any irreducible representation $(p\mu)$ in the BF coordinate system can be written as (see also Section 4.1):

$$[-\frac{1}{2}\vec{\nabla}_r^2 + V_{\rm st}(\mathbf{r}) - \frac{1}{2}k^2]F^{(p\mu)}(\mathbf{r}) = \sum_\alpha \int \phi_\alpha^*(\mathbf{r}')|\mathbf{r}-\mathbf{r}'|^{-1}F^{(p\mu)}(\mathbf{r}')d\mathbf{r}'\phi_\alpha(\mathbf{r}), \qquad (5.3.1)$$

where k is the incident electron wavevector and the static potential $V_{\rm st}$ is given by Eq. (5.2.4). Here Φ_0 is the target ground state wavefunction given as a single Slater determinant of one–electron N spin orbitals $\phi_i(\mathbf{r})$ and M is the number of nuclei in the molecule. The right hand side of Eq. (5.3.1) is the non–local exchange–correlation term arising from antisymmetrization of the e–molecule wave function. In the SME approach, this term is replaced by a local exchange potential and the corresponding scattering calculation becomes quite easy computationally (see Ref. 1). The function $f_{ij}(r)$ in the following will represent the radial part of the continuum function with channel indices i and j.

Finally, after projecting the integro–differential equation (5.3.1) onto the symmetry–adapted angular basis functions of $F^{(p\mu)}(\mathbf{r})$ (5.2.2), we obtain a set of coupled integro–differential equations (4.2.2) which can be written in a convenient matrix form, $\mathbf{LF}^{(p\mu)} = \mathbf{WF}^{(p\mu)}$, where $\mathbf{WF}^{(p\mu)}$ is the exchange term. The iterative scheme is $\mathbf{LF}_i^{(p\mu)} = \mathbf{WF}_{i-1}^{(p\mu)}$, with $i = 1, 2, \ldots$. The optimized scheme is summarized as follows.

1. We need to solve the full integro–differentinal Eq. (4.2.2) only for a few low partial waves; We have earlier shown [6] this scheme of low–, intermediate– and high–ℓ values which implies that for low partial waves (say $\ell_{\rm max} = L_e$), we need the full SEE scheme, for $\ell \geq L_e$ (say $\ell_{\rm max} = L_m$), we can employ the SME model and finally for $\ell \geq L_m$ (say $\ell_{\rm max} = L_B$), the Unitarised–Born–Approximation (UBA) [35] will be a good approximation. This partition is similar to the angular–frame–transformation

(AFT) scheme of Norcross and Collins [31], but differs in implementation in an actual calculation.

2. Suppose we want to determine the SEE **K**–matrix at energy E_1. When $\mathbf{F}_0^{\mathrm{SME}}(E_1)$ is used to start the iterative scheme, it leads to the final $\tilde{\mathbf{F}}_n^{\mathrm{SEE}}(E_1)$ converged continuum function after n iterations. However, if we want to apply the same iterative scheme at another energy, say E_2, we can use either $\mathbf{F}_0^{\mathrm{SME}}(E_2)$ (requiring approximately the same number of n iterations) or $\tilde{\mathbf{F}}_n^{\mathrm{SEE}}(E_1)$ (requiring only $\bar{n}$ iterations) to obtain the final $\tilde{\mathbf{F}}_{\bar{n}}^{\mathrm{SEE}}(E_2)$ at energy E_2. We have shown [9] that $\bar{n}$ is much less than n and the final results converge to the same values, i.e., $\tilde{\mathbf{F}}_n^{\mathrm{SME}}(E_2) = \tilde{\mathbf{F}}_{\bar{n}}^{\mathrm{SEE}}(E_2)$. If $\tilde{\mathbf{F}}(E)$ is a slowly varying function with respect to the impact energy E, we can use a well converged scattering function at an energy E_1 to start the iteration at the next energy E_2. Thus, by using the criterion:

$$\mathbf{F}_0^{\mathrm{SEE}}(E_p) = \tilde{\mathbf{F}}_n^{\mathrm{SEE}}(E_{p-1}), \tag{5.3.2}$$

to start iteration at a given energy E_p, we can save a significant amount of computer time without losing any accuracy.

3. Also, the number of required iterations depends almost linearly on the size of the **K**–matrix. For example, for the electron–H_2O scattering in the A_1 symmetry, a 16–channel problem requires 34 iterations as compared to only 24 in a 12–channel calculation [9]. With the new optimized scheme (Eq. 5.2), as described above, only a much smaller number of iterations are required to obtain desired accuracy.

5.4 Computer Codes

In order to carry out the present calculations, we used the following computer codes developed by our group for more than the last 15 years. All these programs are now set up on the VAX, CRAY–YMP and CRAY–2 machines at the FSU supercomputer facilities.

1. **MOLMON** generates SCE target wavefunctions in terms of STO's. At present, this code can include $\ell_{max} = 7$ in the SCE of each orbital. This code is made available to us by Professor F. A. Gianturco.
2. **MOPE** calculates expansion coefficient of the single center expansion of static potential and electronic density from the orbitals generated by the MOLMON program. Dr. D. G. Thompson wrote this code.
3. **FEGE** determines expansion coefficients of the SCE of FEGE or correlation polarization potential. This code was written by S. S. Salvini.
4. **ASYMP** provides rotational eigenenergies and eigenfunctions of a symmetric top molecule. The code was written by Ashok Jain, the PI.
5. **POPLE** calculates the polarization potential (see Sec. 4.3) by employing the Pople–Schoffield method. The program was written by Ashok Jain, the PI.
6. **POLY** is the main scattering code written by N. Chandra, modified for polyatomic case by D G Thompson and later modified by Ashok Jain. This code calculates scattering K–matrix, eigenphase sums and partial cross sections for a particular scattering state.
7. **POLYEX** is a modified version of POLY to implement the iterative scheme. This code was developed by Paul McNaughten. Later, we modified this code to implement optimised iterative scheme and also interfacing it with the HONDO code.
8. **EROTVIB** was written by Ashok Jain. It evaluates various cross sections for asymmetric, symmetric and spherical top molecules from the K–matrix input of POLYEX code.

9. **RESON** is a small code which determines resonance parameters from the given eigenphase sums.
10. **INTERFACE** is an interfacing program between our POLYEX code and the Quantum Chemistry HONDO program. INTERFACE calculates SCE quantities from multicenter electronic density, orbital and static potential quantities. The program was written by Vi D. Martino and Ashok Jain.
11. **BORN** is a general program which determines FBA quantities in the body–fixed frame of references (Born K–matrices, Unitarised Born T–matrix etc.) and cross sections (differential, integral and momentum transfer) in the space–fixed coordinate system. This program has the provision to use numerical potential (rather than the asymptotic form only). This code is written by Ashok Jain.
12. **POLDEN** determines the polarized charge density of the target by employing the Pople and Shofeld method. This code was developed by Ashok Jain.
13. **VIBAVEG** calculates vibrational matrix element from the given R–dependent scattering parameter (amplitude, potential matrix, multipole moments etc.) and vibrational eigenfunctions.
14. **DERIV** is a small program which determines first or second derivative of a given R–dependent quantity (energy, multipole moments, cross sections etc.).

6. RESULTS AND DISCUSSION

6.1 Electron–CH_4 Cross Sections

The total elastic cross sections (DCS, σ_t, σ_m) on the e–CH_4 were published [3–4] before this contract. However, in this project, we presented results on the rotationally elastic, inelastic and summed DCS integral, momentum transfer, and *energy–loss cross sections* [see Tables 6.1–6.2 of Ref. 9]. These results were compared with recent measurements on the DCS, integral, and momentum transfer parameters. We also carried out calculations in the Ramsauer–Townsend (RT) minimum region, in the 7–8 shape–resonance regime and also at very low energies (below 0.1 eV). No any other *ab initio* calculation has been extended to such a wide range of energy and several types of cross sections.

A large set of differential, integral and momentum transfer cross sections for any $J \rightarrow J'$ transition (with any value of initial J value to a final allowed J' value) are available in tabular form from the PI. The energy range is 0.001–20 eV. In addition, we have generated single center target basis functions for a large value of $\ell_{max} = 20$. In the reported results (Tables 6.1 and 6.2 of Ref. 9), we employed our earlier SCE wave function with only $\ell_{max} = 7$. The corresponding surfaces for electronic density, static potential and individual bound orbitals are available on a radial mesh from the author of this report. The CH_4 molecule has always served a prototype molecule for testing a theoretical model for polyatomic targets. Our *ab initio* calculations with exact exchange and parameter–free correlation–polarization potential have shown that observed behavior of DCS can be described very well by theory even at very low energies.

The cross sections reported in Tables 6.1 and 6.2 of Ref. 9 were determined from the theory described in the previous sections. In brief, exchange correlation is implemented exactly and polarization effects are included approximately via a local real potential based on the method of Pople and Shofield [27] and the non–penetrating criterion of Temkin [28], in which the incoming electron is not allowed to penetrate the target charge cloud. In this

non–empirical calculation, our results at very low energies (RT minimum region) compare very well with experiment. In addition, our value of -2.9 au for the scattering length for the e–CH_4 system compares well with the experimental value of -2.48 [36].

6.2 Electron–SiH_4 Cross Sections

We determined the low energy electron collisional cross sections from silane molecules in the exact–static–exchange plus polarization (ESEP) model [9]. For comparison purpose, we also included static–model–exchange plus polarization (SMEP) results; this comparison gave us an idea of the importance of exchange effects in this low energy region. The results without polarization (ESE) were also included in the discussion [9].

The electron–silane cross sections are very important from the point of view of plasma physics [37]. There are several experimental [37–46] and theoretical studies [47-52] on the low energy electron interactions with SiH_4. Similar to CH_4 case, the e–SiH_4 low energy cross sections are characterised by RT minimum below 1 eV and a shape resonance feature around 2–4 eV. Very recently, low energy DCS have been measured by Tanaka *et al.* [46].

We discussed [9] the qualitative features of low energy e–SiH_4 cross sections such as the RT minimum below 1 eV and a 3–4 eV shape resonance phenomenon. Our ESEP model was found successful for (nearly) the correct position of the minimum (around 0.25 eV in a recent swarm study of Kurachi and Nakamura, Ref. 44) because of the A_1 scattering symmetry. Note that our earlier SMEP (static, FEGE and the JT polarisation potentials) results (Jain and Thompson, Ref. 47) or the present ESE (without polarization) curves are incorrect in this low energy region. The value of the position of this minimum as obtained by Yuan [51] in the spherical approximation is quite low (around 0.11 eV). Other calculations, where exchange is treated via a model local potential [48–49], do not give reliable results in this rather low energy region. The ESEP model clearly exihibited a shape resonance phenomenon around 3.75 eV; this structure is due to the d–wave of the

incoming electron's partial waves. Therefore, the E symmetry (which also have a d-wave component) also exihibits a weak shape resonance feature at about 4 eV.

We calculated [9] rotationally summed (vibrationally and electronically elastic) differential cross sections in the energy range from 1.8 to 20 eV, where recent absolute measured values were available [46]. This set of data and their discussion gave us the idea of the importance of polarization effects in this energy range for various angular regions. We found that the polarization interaction changes the shape (and magnitude too) of the DCS at all energies considered here. It was seen [9] that the ESEP model agrees much better with the experimental data as compared to the ESE model. We also noticed that the polarization effects are more important in the resonance region, where the structure in the DCS reflects the d–wave dominance. This is expected since polarization interaction influences the shape-resonance region considerably. In general, the agreement with experimental data was found reasonable. The dip at about 55^0 observed at 1.8 and 2.15 eV by Tanaka *et al.* is shifted in our results towards lower angle by about 10^0 difference. The second dip occuring in our DCS around 130^0 at 1.8 and 2.15 eV, seems to be shifted in the same fashion as the lower angle dip with respect to experimental data (however, the measured values are not available above 130^0 angle).

At somewhat higher energies ($E \geq 3$ eV), the two dips in the DCS are still visible, while such a structure in the measured angular functions is quite weak. It may be interesting to compare our DCS with another set of absolute experimental data (not available right now). The present predicted DCS values may be quite useful for normalizing purpose in future measurements. No other theoretical calculations were available on the DCS for the e-SiH_4 collisions in this energy range. We presented our ESEP DCS values in tabular form (see Tables 6.2.1 and 6.2.2 in ref. 9).

The integral cross sections (total, σ_t; momentum transfer, σ_m; viscosity, σ_v and energy–loss, σ_l) were calculated in the RT and resonance region. Our value of the cross section near the RT minimum is about 2.8×10^{-16} cm^2 for the σ_t and 0.4×10^{-16} cm^2 for

the σ_m. The swarm data of Kurachi and Nakamura [44] gives a minimum value of about 1.1×10^{-16} cm^2 in their σ_m curve, while Hayashi [45] estimates this minimum value to be 0.5×10^{-16} cm^2 . Finally, we concluded [9] that the agreement between present theory (ESEP model) and experimental results is rather encouraging keeping in mind that this low energy region is quite difficult to study both in theory and experiment.

We compared our σ_t and σ_m values in the 1–20 eV region with the experimental data [38, 42]. There is significant discrepancy between the two sets of measured values. Our present ESEP curve seems to be in fair agreement with recent measurements of Wan et al [38]. The position of the shape resonance in ESEP theory (around 3.75 eV) and experiment (around 3.1 eV) differs about 20%, while the magnitude of the cross sections in this energy region also has significant discrepancy; for example, the theoretical (ESEP) peak value of the σ_t is about 20% higher than the measured value of Wan *et al.*. Note that the inclusion of polarization effects shifts the shape resonance position from about 6.5 eV to about 3.75 eV and increases its magnitude by about 45%. Thus, the importance of polarization interaction in this energy region can not be overlooked.

For the σ_m values, we found significant discrepancy bewteen theory and experiment; however, there seems to be agreement in the general trend of the cross sections as a function of impact energy. In the resonance energy region, our calculations are much higher than the swarm data. The accuracy of the swarm analysis above 1 eV may be questionable. We also realized that a better polarization potential may be required in the present energy region. The momentum transfer cross sections are dominated by large angle scattering, therefore, there may be other reasons too for the observed discrepancy between present theory and swarm results.

At very low energies, the energy loss of the incoming projectile because of rotational channel, is a very important mechanism in e–molecule collisions. It is now possible to measure indirectly the rotational excitation cross sections for the electron-molecule system (Müller *et al.* [53]). With this possibility in mind, we discussed [9] rotationally elastic and

inelastic cross sections. The elastic $0 \rightarrow 0$ channel dominates all other inelastic processes at all angles except at those angles where a deep minimum occurs in the $0 \rightarrow 0$ DCS. From qualitative point of view, the general shape of rotationally inelastic DCS for the e-SiH_4 system is quite similar to the corresponding CH_4 curves [3]. The $0 \rightarrow 4$ transition depends weakly on the scattering angle, while the $0 \rightarrow 3$ one has considerable angular dependence. The $0 \rightarrow 6$ cross sections are generally smaller; however, as the energy is increased, they become larger than the other transitions at certain scattering angles. The total energy–loss DCS are almost flat with respect to angular variation. It is also clear from this work that a spherical approximation may not be an appropriate model for the total DCS in this energy range.

We found an effect of polarization potential on the rotational excitation process. Symmetry of the polarization term (there exists only the spherical, $\ell = 0$, term) for the T_d point group, the first Born approximation (FBA) will give zero cross section from the polarization potential term only. In the present calculation, we, however, saw a substantial difference in the DCS with and without polarisation effects. We demonstrated [9] that a polarised target is more efficient to excite its rotational modes through the angular momentum transfer from the projectile. We will see later the same comparison for integral cross sections at all energies considered here.

We also discussed the integral values of various rotational excitation cross sections. As expected, the pure elastic process has all the main features (RT minimum and the 3–4 eV shape–resonance) of the total scattering process. The rotational channels are small, but exihibit interesting features in the energy distribution of their cross sections. For example, the $0 \rightarrow 3$ curves have enhancement in the cross sections around 8 eV, while the 3–4 eV region shows a weak structure (remember there is a 3–4 eV shape resonance here in the elastic and total cross sections). The $0 \rightarrow 4$ cross sections are, however, enhanced in the 3–4 eV region. it is interesting to notice that this structure is produced mainly because of polarisation effect. The $0 \rightarrow 6$ cross sections were also characterised by an enhancement

around 10 eV. Here also, we see a significant change in the inelastic cross sections when polarisation effects are included.

Finally, we presented integrated energy–loss cross sections in all the three ($\Delta J = 3, 4, 6$) transitions with and without polarisation effects. We saw clearly that the inclusion of polarisation effect changes the behaviour of the energy–loss cross sections with respect to the projectile energy. At higher energies (E $\geq$ 15 eV), the $0 \rightarrow 6$ transition dominates over other lower order rotational excitations. The $0 \rightarrow 4$ cross sections are always higher than the $0 \rightarrow 3$ ones except at lower energies (below 2 eV), where the $0 \rightarrow 3$ transition dominates over all higher excitations. The total energy–loss or the stopping cross sections were found independent of initial J value of rotational state of the target. This agrees with a general theorem (per Shimamura [11–17]) that the stopping cross sections, when summed over all final rotational states, are independent of the initial rotational state of the molecule in a situation where the adiabatic–nuclei–rotation approximation is valid.

We also extended our calculations at further lower energies towards the zero–energy limit. For example, at 0.001, 0.0025, 0.005, 0.01, 0.025, and 0.05 eV energies the values of the $\sigma_t(\sigma_m)$ are (in units of 10^{-16} cm^2) 47.82 (46.45), 42.53 (40.4), 37.42 (34.64), 30.88 (27.63), 20.68 (16.63), and 12.83 (8.58) respectively. At 0.01 eV, the σ_m values given by various swarm studies are 56.0 (Hayashi [45]), 66.0 (Ohmori *et al.* [43]), and 32.0 (Kurachi and Nakamura [44]). It is rather frustating to see such a large discrepancy between these swarm values for the σ_m value at this low energy. The value of scattering length was estimated to be -4.2 au in our present ESEP calculation.

It is now a well established fact that in low energy regime, the use of model potentials for both the exchange and polarization forces is rather misleading because to make theory and experiment closer, these interactions do compensate for each other. In the situation where exchange is included exactly, In this sub section, we made a relative comparison with our SEP(JT) results (previous 6.2 Sections) with another model SEP(CP) calculation.

Finally, our SEP(JT) model appears to be better than the SEP(CP) one, in particular

in the RT minimum region. This conclusion is consistent with our similar investigation on the e–CH_4 system [3]. However, this conclusion will further be supported if differential measurements are available for the e–SiH_4 case. There is plenty of room to improve upon the JT potential by actually carrying out a full polarised–orbital calculation for the e–SiH_4 system.

6.3 Electron–GeH_4 Cross Sections

This is a rather too heavy spherical top molecule for which very recently DCS have been measured in the range of 2–100 eV [54]. No previous calculation exists for this collision system. Molecular wave functions and consequently the density and various interaction potentials were determined using the HONDO and INTERFACE programs (see Section 4.3). This part of the calculation was done at a simpler level than the one described above for other gases. A spherical approximation [19] was employed under the model exchange and polarization terms. The full results were reported [9].

We presented [9] low energy (at 2, 3, 5, 7.5, and 10 eV) DCS together with the experimental data [54]. The validity of the spherical model depends on the fact that the rotational excitation channel is very weak compared to the elastic process. This is not true below 10 eV, where rotationally inelastic DCS are significant. The importance of rotationally inelastic channel is increased when strong interference effects make the elastic DCS become either smaller or bigger at a specific angle for each energy. Hence the ensuing DCS are characterized by a dip in the angular distribution. We, therefore, expect some significant discrepancy to appear between our theoretical DCS and the measured ones below 10 eV whenever the above feature may be present. Another source of approximations below 10 eV DCS is the treatment of exchange and polarization effects within the present model. Nevertheless, we found a satisfactory agreement between theory and observation. However, the spherical model provides at times only a qualitative picture of the observed data since we see, for example, a very pronounced dip around 120^0 at 2 eV which is instead

very shallow in the experimental data.

Further, we found that at lower angles, the experimental DCS are very small as compared to computed values. As discussed by Boesten and Tanaka [55], the lowest angle DCS are rather too small in their measurements. It is also interesting to note that the background scattering is quite strong at 2 eV.

We also displayed results [9] at intermediate and high energies where our present model is likely to work markedly better [50]. We found that there is indeed very good agreement between theory and experiment and that, in particular, the structure observed in the experimental DCS is clearly reproduced in our calculations at all energies above 10 eV.

Finally, we displayed [9] the computed integral and momentum transfer cross sections. We saw a shape–resonance feature around 5 eV which is caused by the d–wave component of our potential scattering mechanism. Note that in CH_4 and SiH_4 molecules this enhancement in the total cross section occurs around 7–8 eV and 2–3 eV respectively. Thus the 5 eV structure seen here in the e–GeH_4 case becomes quite interesting in comparison with other T_d–symmetry targets. Below 1 eV, we have also evidence of a minimum around 0.2 eV, but such a structure is very sensitive to the approximations involved in including exchange and polarization effects and therefore we expect that it will need possible confirmation from more extensive calculations that are presently planned in our laboratory.

In order to further confirm the 5 eV feature in the e–GeH_4 elastic scattering, we plotted DCS as a function of energy [9]. The experimental DCS of Boesten and Tanaka [54] clearly exihibit this enhancement around 5 eV; this shape resonance phenomena was also present in our calculations. It is still to be seen if measured total cross sections and more accurate calculations reveal this structure.

It is still interesting to note, however, that the present calculations, which effectively decouple each contributing partial wave in the spatial region where the potential exists, are indeed presenting a fairly good description of the scattering process. Since the coherent

sum of angular momenta carried out to yield the DCS is a result of dynamical interference between trajectories, we are able to say that the present *spherical* potential is realistically treating such interference effects. The lack of angular anisotropy in the chosen interaction prevents us from correctly including, however, the potential coupling which causes additional interference in the multichannel S–matrix of the full problem [1]. However, it appears from the present results that, at least above 10 eV, such further effects are rather negligible and that the heavy GeH_4 target can be considered as being essentially still during the interaction ($\tau_{\rm coll} << \tau_{\rm rot}$) and is approximately spherical when probed by the impinging electron. Thus, the possible adiabatic convolution of the scattering amplitude over rotational eigenstates can be approximately treated via its spherical component only: i.e., we can write,

$$\begin{aligned} f_{\rm tot} &= \sum_{i,f} f(\Omega) \\ &\simeq \sum_{i,f} \langle \psi_i | f(\Omega; \hat{\mathbf{r}}_{N+1}) | \psi_f \rangle \\ &\simeq \sum_{i,f} \langle \psi_i \sum_{\lambda,m} f_{\lambda m}(\Omega) X_{\lambda m}(\hat{\mathbf{r}}_{N+1}) | \psi_f \rangle \\ &\simeq \sum_{i,f} \langle \psi_i | f_{00}^{i \rightarrow f}(\Omega) | \psi_f \rangle \\ &\simeq \sum_{i,f} f_{00}(\Omega) \delta_{if} \end{aligned} \tag{6.3.1}$$

where Ω is the space–fixed orientation, $\hat{\mathbf{r}}_{N+1}$ is the body–fixed electron–molecule orientation vector and the $|\psi_i\rangle$ is rotational eigenfunction of the molecule. Because of time scale considerations, vibrational excitations are even less likely to occur.

6.4 Electron–NH_3 Cross Sections

There are recent measurements on the e–NH_3 total [55-56] and differential [57] cross sections in the present energy region; however, no *ab initio* calculation (with exact exchange plus polarization effects) exists in order to make a proper comparison with the experiment.

The Schwinger multichannel variational (SMV) calculations of Pritchard *et al.* [58] are carried out only at the fixed-nuclei static–exchange level; consequently, in the absence of polarization effects, it may not be proper to compare these SMV results with experimental cross sections. More recently, Parker *et al.* [59] have employed complex Kohn variational principle to study e–NH_3 problem at the ***ab initio*** level. The only other fixed–nuclei close–coupling calculations employing model exchange and polarizations potentials are due to Jain and Thompson [60] and Gianturco [61].

Encouraged by the success of our present calculations on the CH_4, SiH_4, and GeH_4 molecules, we extended our ESEP theory (Section 4) for the e–NH_3 case where recent measured data are available. As is well known, for a polar molecule, the ANA theory predicts infinite cross section in the forward direction. Here we restricted ourselves only to the eigenphase sum, partial cross sections, and momentum transfer cross sections. We also present DCS and integral parameters, but these numbers can be considered only prelimenary at this time.

As mentioned above, the effects of polarization force is significant at all energies. We presented our $\sigma_t$and $\sigma_m$cross sections along with experimental data. We saw a qualitative agreement between our theory and measurements. The enhancement in both the integral and momentum transfer cross section around 10 eV is faithfully reproduced by our calculations [9].

Finally, we reported our preliminary angular functions at 8.5 and 15 eV along with measured points and the static–exchange (without polarization) SMV calculations of McKoy and coworkers [58]. Unfortunately, the experimental DCS on the low energy e–NH_3 scattering were not available properly. The measured values of Shyn [57] are only preliminary and definitive conclusion about the agreement between theory and experiment is very hard to draw at this moment.

6.5 Electron–H_2O Cross Sections

We calculated converged cross sections (DCS, σ_t, σ_m) for elastic and rotationally inelastic processes [10]. The H_2O molecule is polar molecule with above critical value of the dipole moment. Thus the dipole moment of water molecule is capable of supporting infinite number of bound states of the incoming electron. We have modified our existing codes in order to include full contribution of the higher partial waves which is important in the forward angle scattering. There are several recent measurements on the total [61–64] and the DCS [65–69] parameters for the e–H_2O system. We made a comparison between our theory and these measured data. In addition, other calculations [70–74] were also included in the present comparison.

First, we reported our values of eigenphase sums (Table 6.1.1 of Ref. 10) and partial cross sections (Table 6.1.2 of Ref. 10) for all the four symmetries A_1, A_2, B_1, and B_2. In these tables, we included our calculations with and without polarization effects. Again we found considerable effect of polarization force in the e–H_2O scattering. In this case, there is no resonance or RT effects. This is mainly due to the dominance of dipole scattering. The inclusion of polarization force in the ESE results is to decrease the cross sections. We saw a very weak hump structure in the ESEP A_1 symmetry results around 6 eV. The total DCS at various energies (1, 2, 3, 5, 6, 7.5, 10 and 15 eV) were presented along with several recent experimental data. We found a reasonable agreement between present theory and experiment at all energies [10]. There were no pronounced structures in all the DCS presented here for the electron–H_2O system.

Further we presented our integrated cross sections for the total (σ_t) and momentum transfer (σ_m) quantities. The experimental points were also included. Again the agreement between theory and experiment is fair considering the fact that the measured values [65–69] have been obtained by extrapolating their DCS at lower and higher angles; this procedure can introduce serious error in the integral cross sections. All these cross sections were tabulated [10].

6.6 Electron–H_2S Cross–Sections

The total cross sections for the electron–H_2S system have been measured by several groups [63, 75]. The low energy differential cross sections have also been investigated in the laboratory [76–77]. The theoretical calculations on the DCS and integral cross sections have been carried out by our group [78–79] using model potentials for exchange and polarization effects. The Khon complex method has also been applied to study low energy electron scattering with H_2S molecules [80]. The electron–H_2S collision system is known to have a shape resonance in the total cross section behavior [75–76]. It was shown by us [78] that this shape resonance is due to the B_2 symmetry of the collision system. The occurrence of a resonance in any electron molecule event is very sensitive to the exchange and polarization effects. In other words, the resonance parameters (width and position) have a strong dependence on the charge correlation effects. We found here that the B_2 symmetry scattering is quite sensitive with respect to the treatment of exchange effect.

The effect of polarization is dramatic in shifting the resonance position from about 5 eV to the correct position around 2 eV. The width is changed greatly too. The model (exchange) potential calculation [78] differes significantly with the present ESEP model. The exact values (in units of eV) of resonance parameters (E_r, Γ) in these model are as follows: ESEP (1.82, 0.838), ESE (4.2, 2.5) and MSEP (2.21, 1.3). The experimental values of the position of this shape resonance vary between 1.8 to 2.5 eV.

The total cross section for the electron–H_2S system exhibit two peaking regions around 2–3 eV and 6–10 eV [75]. The structure around 6–10 eV is definetely due to A_1 symmetry as is evident from the partial cross section of this symmetry. Our theoretical values for differential as well as integral quantities produce all the salient features in the cross section behavior. Very recently, Buckman and coworkers [77] have measured DCS at 15 and 20 eV. Our calculated DCS were found in fair agreement with the measurements of Buckamn's at 15 and 20 eV. The integral cross sections were reported [10] for total and momentum

transfer cross sections. For the total cross section, we found a fair agreement between our results and the measurements of Ref. 75. The first–Born–approximation (FBA) results totally fail in reproducing the shape and magnitude of the cross–section features. This proves the simple fact that first–order theories such as the FBA are incapable of describing low energy electron scattering with a polar molecule such as the H_2S.

In Ref. 10, we have given values the DCS and integral cross sections for rotationally elastic, inelastic and summed processes. We have given rotationally inelastic results only for the principal quantum numbers $(0J')$ (thus summing over the final τ' quantum numer). From these tables on the DCS, we immediately notice that the $0 \rightarrow 4$ is stronger than the $0 \rightarrow 3$ transition. The elastic cross sections exhibit a dip in the backward direction (around 120^0).

7. ELECTRON SCATTERING FROM C_2H_2 MOLECULES

7.1 On the $^2\Pi_g$ Shape Resonance

The electron (e) –C_2H_2 system is known to have a shape–resonance in its $^2\Pi_g$ symmetry ($\pi_u^4\pi_g$ configuration) in the 2 eV region. There is considerable discrepancy about the location of this resonance both in experimental and theoretical studies [81]. Total scattering [82-83] , electron transmission [84] and vibrational excitation [85–86] experiments have observed this resonance for the e–C_2H_2 scattering around 2.4–2.6 eV. Very recently, Krumbach *et al* [81] have employed Feshbach formalism to investigate the $^2\Pi_g$ state of $C_2H_2^-$ and found the position of this resonance around 2.9 eV. Tossel [87] has used MS-Xα method to investigate the e–C_2H_2 scattering. No other theoretical calculations are available in the literature in this low energy (below 5 eV) region for the e–C_2H_2 system.

In a shape–resonance phenomenon, the projectile electron, with non–zero angular momentum, is trapped by its own centrifugal barrier to form the temporary molecular ion ($C_2H_2^-$) which decays via the quantum mechanical tunneling of the extra electron through the barrier. The position (E_r) and width (Γ) of the resonance and the magnitude of the corresponding cross sections are highly sensitive to the treatment of non–local short range correlation (electron exchange and charge distortion) and long range polarisation effects.

Two well known local approximations for exchange effect in e–molecule problems are based on the Hara free–electron–gas–exchange (FEGE) [24] and semi–classical–exchange (SCE) [88] theories. The FEGE model has also been employed along with the orthogonalization procedure (OFEGE, see Ref. 89) where the continuum function is forced to be orthogonal with the bound function of the same symmetry. The FEGE approximation gives incorrect asymptotic behaviour, therefore, its asymptotically adjusted version (AAFEGE) has also been employed in the literature (see Ref. 89). Both the approximations (FEGE and SCE) have serious drawbacks when applied to low energy e–molecule case, particularly when the scattering event is dominated by resonance effects. The success of these local

potentials depends upon how well they reproduce the shape of the differential and integral cross sections or parameters (E_r and Γ) of a shape–resonance.

Unfortunately, the FEGE, AAFEGE and SCE models totally fail for the $^2\Pi_g$ e–C_2H_2 scattering (see later in Fig. 7.1.1). Here we employ a modified version of SCE approximation (to be denoted as MSCE), recently proposed by Gianturco and Scialla [90] for polyatomics. We also tune the FEGE model (to be denoted as TFEGE) with respect to the position of the $^2\Pi_g$ resonance of the e–C_2H_2 scattering. Since the electronic configuration of C_2H_2 molecule does not have a π_g bound orbital, the orthogonalisation techniques is not required for the present case of $^2\Pi_g$ symmetry.

Full details of the present method can be found else where [91]. In brief, we solve the following set of coupled differential equations (after carrying out all the single–center expansions of the potential and scattered function) for the radial components of the continuum function belonging to the $^2\Pi_g$ symmetry,

$$[\frac{d^2}{dr^2} - \frac{\ell(\ell+1)}{r^2} + k^2] f^{\Pi_g}_{\ell\ell_0}(r) = 2 \sum_{\ell'=2,4,..}^{\ell_{max}} \{V^{\Pi_g}_{\ell\ell'}(r) f^{\Pi_g}_{\ell'\ell_0}(r)\}, \qquad (7.1)$$

where the potential matrix $V^{\Pi_g}_{\ell\ell'}(r)$ for the $^2\Pi_g$ symmetry is given by,

$$V^{\Pi_g}_{\ell\ell'}(r) = -[(2\ell+1)(2\ell'+1)]^{\frac{1}{2}} \sum_{\lambda=0,2,..}^{\lambda_{max}} \frac{1}{2\lambda+1} v_\lambda(r) C(\ell\ell'\lambda;00) C(\ell\ell'\lambda;-1,1), \qquad (7.2)$$

where $C(\ell_1,\ell_2,\ell_3;m_1,m_2)$ is a Clebsch–Gordan coefficient. The potential expansion parameter, $v_\lambda(r)$ is a sum of static (v^{st}_λ), exchange (v^{ex}_λ) and polarisation (v^{pol}_λ) terms. The calculation of target charge density $[\rho(r,\theta)]$ and v^{st}_λ is done *ab initio* [92-93] by employing molecular wavefunctions [94] at the equilibrium geometry of C_2H_2. The $v^{pol}_\lambda(r)$ coefficients were determined in the correlation polarisation approximation [95].

Both the FEGE [24] and SCE [88] approximations for a local exchange potential depend on $\rho(r,\theta)$ and the incident electron energy E. The SCE potential is given by,

$$V^{SCE}_{ex}(r,\theta) = \frac{1}{2}[E - V_{st}(r,\theta)] - \frac{1}{2}[\{E - V_{st}(r,\theta)\}^2 + 4\pi\rho(r,\theta)]^{\frac{1}{2}}, \qquad (7.3)$$

The main assumption in the SCE approach is that the local momentum of the bound electrons can be disregarded with respect to that of the projectile electron. This makes the SCE model a high energy approximation. Very recently, Gianturco and Scialla [90] have introduced corrections in the SCE theory by including local momentum of the bound electrons, which can play a significant role for lower collision energies. Thus treating the bound electrons within the isotropic free–electron–gas (FEG) model, the MSCE potential is derived to be [90],

$$V_{\rm ex}^{\rm MSCE}(r,\theta) = \frac{1}{2}[E - V_{\rm st}(r,\theta) + \alpha)] - \frac{1}{2}[\{E - V_{\rm st}(r,\theta) + \alpha\}^2 + 4\pi\rho(r,\theta)]^{\frac{1}{2}}, \qquad (7.4)$$

where $\alpha = \frac{3}{10}[3\pi^2\rho(r,\theta)]^{\frac{2}{3}}$. The new MSCE potential can further be modified by realizing that the electronic density of the target is distorted by the impinging electron, i.e., when polarisation of the target wavefunction is taken into account. We would, therefore, call this potential as MSCEP when in the MSCE potential (Eq. 7.4) $V_{\rm st}$ is replaced by $V_{\rm st} + V_{\rm pol}$. We will present results in both the models, i.e., MSCE and MSCEP.

The FEGE potential is given by [24],

$$V_{\rm ex}^{\rm FEGE}(r,\theta) = \frac{2}{\pi}k_F(r,\theta)\left[\frac{1}{2} + \frac{1-\eta^2}{4\eta}\ln|\frac{1+\eta}{1-\eta}|\right], \qquad (7.5)$$

where $\eta = (k^2 + 2I_p + k_F^2)^{\frac{1}{2}}/k_F$, k_F is defined as $k_F = [3\pi^2\rho(r,\theta)]^{\frac{1}{3}}$ and I_p is the ionization potential of the target. In the limit $r \to \infty$, the local momentum k_F of the scattering electron does not approach the correct value of k. Consequently FEGE with $I_p = 0$ is the AAFEGE potential as mentioned earlier.

We solved the scattering problem (Eq. 7.1) for the $^2\Pi_g$ state with proper convergence tests on the K–matrix elements (including the eigenphase sums and the partial cross sections). This included the number of terms ($\lambda_{\rm max} = 20$) in the single–center expansion of the interaction potential, the size of the close–coupling K–matrix ($\ell_{\rm max} = 20$). In order to include the contribution of the long range quadrupole and polarisation fields in all the K–matrix elements, we integrated Eq. (7.1) up to a radius $r_{\rm max} \sim 10\ell/k$, where k is the wave number of the incident electron.

First, in Fig. 7.1.1, we have shown the $^2\Pi_g$ symmetry eigenphase sums (δ_s) in the SCE, FEGE and AAFEGE models including polarisation effect. The SCE and AAFEGE models do not exihibit any resonance phenomenon, while the FEGE potential (curve C) gives a weak structure around 4 eV. On the other hand, as mentioned earlier, the position of the e–C_2H_2 $^2\Pi_g$ resonance has been located in various experimental techniques somewhere around 2.5 eV [81].

In Fig. 7.1.2, we have shown the δ_s quantity in MSCEP, MSCE and TFEGE (with I_p = 5.25 eV) models including polarisation interaction. We see that the MSCE and MSCEP models reproduce the $^2\Pi_g$ shape resonance in the vicinity of 2 eV in good agreement with various experimental findings. It is to be noted that there is no tuning involved in the MSCE or MSCEP results of Fig. 7.1.2. On the other hand, the tuned results of the TFEGE approximation (in fact, we arbitrarily chose three values, 5.0, 5.25 and 5.50 eV, of I_p and found that the I = 5.25 eV is closest to the $^2\Pi_g$ parameters) also predict the features of the resonance; however, a tuning procedure is always inconvenient and requires prior knowledge of cross section behaviour. The values of (E_r, Γ) quantities in MSCEP, MSCE and TFEGE models are respectively, (2.20, 1.21), (2.08, 1.06) and (2.48, 1.32). Thus, we conclude that the MSCE (MSCEP) theory of Gianturco and Scialla [90] is a very good local approximation in order to represent the non–local exchange correlation in low energy electron–C_2H_2 scattering. We would emphasize that the MSCEP model is better than the MSCE one. We also found that it is the d–wave which is responsible for the $^2\Pi_g$ resonance behaviour.

Finally, in Fig. 7.1.3, we present our results in the MSCEP, MSCE and TFEGE models without including polarisation effects, i.e., at the static–exchange (SE) level. In general, the 2 eV shape–resonance structure in other isoelectronic molecules (CO and HCN, for example) occurs at a higher energy if polarisation potential is neglected in the SE calculation. As expected, the 2 eV resonance (Fig. 7.1.2) is shifted at higher energies in all the three MSCEP ($\sim$ 5 eV), MSCE ($\sim$ 4.5 eV) and TFEGE ($\sim$ 5.5 eV) models. No

previous static–exchange level results are available for the present C_2H_2 case. Our present MSCEP and MSCE results without polarisation effects, shown in Fig. 7.1.3, may be useful for future *ab initio* calculations on the C_2H_2 molecule.

7.2 Low Energy (0.01–20 eV) e–C_2H_2 Cross Sections

The electron (e^-) scattering from C_2H_2 molecules plays important role in many applied sciences [96]. However, there is a paucity of theoretical and experimental electron impact cross section data for this molecule [97]. Earliest measurements on the relative differential cross sections (DCS) were made by Hughes and McMillen [98] at 10–100 eV in the 10^0–150^0 angular range. Recent measurements of Kochem et al [99] on the elastic DCS covered a low energy (0.5–3.6 eV) regime from 5^0 to 110^0. Very recently absolute DCS for the electron C_2H_2 system have been measured by Khakoo et al [96] from 5 to 100 eV in an angular range of 10^0–125^0. There is no low energy theoretical work on the e^-–C_2H_2 system except the intermediate energy (10–100 eV) calculations by Mu–Tao et al [100] and of Thirumalai et al [101] (only at 10 eV). Thus, the present theoretical study is the first one in order to report low energy vibrationally and electronically elastic (rotationally summed) differential, intergral and momentum transfer cross sections at 0.01–20 eV.

The total cross section (σ_t) measurements on the e^-–C_2H_2 system are available due to Brüche [102] (1–33 eV), Hai–Xing and Moore [83], and Sueoka and Mori [82] (1–400 eV).

In our (see Section 7.1) investigation of the $^2\Pi_g$ shape–resonance phenomenon in C_2H_2 due to low energy electron impact, we found that this collision is very sensitive to the treatment of short–range correlation (electron exchange and relaxation of bound orbitals due to impinging electron) and long–range polarisation effects. In the cases of several features in the energy and angular dependence of the cross sections, the sensitivity of the cross sections with respect to exchange and polarisation forces is even more critical.

In a model potential approach, where non–local nature of exchange and polarisation effects is approximated by local forms, it is very difficult to describe all the observed features in the cross sections without any fitting procedure.

The MSCEP potential alongwith the correlation polarisation term was found to be more successful than the other models (see Section 7.1). Therefore, we will present our final results in the MSCEP model only.

We solved the scattering problem (Eq. 7.1) for various symmetries as follows:

$$\Sigma_g : \Lambda = 0, \quad \ell = 0, 2, 4, \ldots 20,$$

$$\Sigma_u : \Lambda = 0, \quad \ell = 1, 3, 5, \ldots 20,$$

$$\Pi_g : \Lambda = 1, \quad \ell = 2, 4, 6, \ldots 20,$$

$$\Pi_u : \Lambda = 1, \quad \ell = 1, 3, 5, \ldots 20,$$

$$\Delta_g : \Lambda = 2, \quad \ell = 2, 4, 6, \ldots 20,$$

$$\Delta_u : \Lambda = 2, \quad \ell = 3, 5, 7, \ldots 20,$$

$$\Phi_g : \Lambda = 3, \quad \ell = 4, 6, 8, \ldots, 20$$

$$\Phi_u : \Lambda = 3, \quad \ell = 3, 5, 7 \ldots, 20$$

Contribution from the higher order terms ($\Lambda > 3$) is very small and therefore neglected here. We carried out proper convergence tests on the K–matrix elements (including the eigenphase sums and the partial cross sections). This included the number of terms ($\lambda_{max} = 20$) in the single–center expansion of the interaction potential, the size of the close–coupling K–matrix ($\ell_{max} = 20$). In order to include the contribution of the long range quadrupole and polarisation fields in all the K–matrix elements, we integrated Eq. (7.1) up to a radius $r_{max} \sim 10\ell/k$, where k is the wave number of the incident electron.

In terms of the calculated body–frame **K**–matrix for a particular symmetry, the **S** and **T** matrices are defined as

$$\mathbf{S}^{\Lambda} = (\mathbf{1} + i\mathbf{K}^{\Lambda})(\mathbf{1} - i\mathbf{K}^{\Lambda})^{-1} \; ; \quad \mathbf{T}^{\Lambda} = \mathbf{1} - \mathbf{S}^{\Lambda}, \tag{7.6}$$

The integral cross sections (σ_{t}) for elastic (rotationally summed) scattering at energy k^2 is given by,

$$\sigma_{\mathrm{t}} = \frac{\pi}{k^2} \sum_{\ell\ell'\Lambda} |T^{\Lambda}_{\ell\ell'}|^2. \tag{7.7}$$

The expression for the DCS is obtained in a standard way by expanding it in terms of Legendre polynomials,

$$\frac{d\sigma}{d\Omega}(k^2, \theta) = \sum_{L} A_L P_L(\cos\theta). \tag{7.8}$$

The expansion A_L coefficients are given as [89],

$$A_L = \frac{(2L+1)}{4k^2} \sum_{ll'\bar{l}\bar{l}'} [(2l+1)(2l'+1)(2\bar{l}+1)(2\bar{l}'+1)]^{\frac{1}{2}} i^{l-l'}(-i)^{\bar{l}-\bar{l}'}(-1)^{L}$$
$$\begin{pmatrix} \bar{l} & l & L \\ 0 & 0 & 0 \end{pmatrix} \begin{pmatrix} l' & \bar{l}' & L \\ 0 & 0 & 0 \end{pmatrix} \sum_{j=|J-J'|}^{J+J'} (2j+1)(-1)^{j} W(ll'\bar{l}\bar{l}'; jL) M^{j}_{ll'} M^{j}_{\bar{l}\bar{l}'}{}^{*} \tag{7.9}$$

where the M–matrix is constructed as

$$M^{j}_{ll'} = \sum_{\Lambda} (-1)^{\Lambda} \begin{pmatrix} l & l' & j \\ \Lambda & -\Lambda & 0 \end{pmatrix} T^{\Lambda}_{ll'} \quad . \tag{7.10}$$

From equation (7.8), it is easy to derive simple form for the momentum transfer (σ_{m}) cross sections in terms of A_L coefficients, namely,

$$\sigma_{\mathrm{m}} = 4\pi[A_0 - \frac{1}{3}A_1]. \tag{7.11}$$

Figs. 7.2.1–7.2.4 show our DCS at 1, 2.0, 2.5 and 3 eV respectively along with the measurements of Kochem et al [99]. The present DCS at 40^0, 60^0, 90^0, 120^0 and 150^0 angles as function of energy (0–4 eV) are illustrated in Figs. 7.2.5–7.2.8 along with experimental data of Kochem et al [99]. For a better comparison between theory and experiment, all

the numbers of Kochem et al [99], shown in Figs. 7.2.1–7.2.8 are multiplied by a factor of two. First of all, we find a very good qualitative agreemnet between our theory and measurements of Kochem et al [99]. For example, the structure in the DCS in resonant region, observed in the measuremnets, is very well reproduced in the present parameter–free model. At 1 eV, a dip around 40^0 and a peak around 90^0 in the theoretical DCS is also present in the measured data of Kochem et al [99] (Fig. 7.2.1). Similaryly at 2 eV, there is a qualitative agreement between theory and experiment. At 2.5 and 3 eV (Figs. 7.2.3 and 7.2.4), we can see even a much better agreement between our DCS and the experimental results. We, however, notice that for this comparison between theory and experiment, the measured cross sections are multiplied by a factor of two.

We make a further comparison between our DCS and experimental DCS of Kochem et al as a function of energy, where measurements are available at few angles in the energy range of 0.2–3.6 eV. In Figs. 7.2.5–7.2.8, these DCS are shown at 40^0, 60^0, 90^0, 120^0 and 150^0 angles in the 0–4 eV range. Again, we see a good qualitative agreement between present calculations and observed data. As expected, the DCS around 2 eV region are significantly influenced by the $^2\Pi_g$ shape resonance phenomenon in both the forward and backward directions. A low energy (around 0.2 eV) minimum (known as the Ramsauer–Townsend (RT) effect) is also present, which seems to be supported by the trend in the low energy experimental points (see Figs. 7.2.5–7.2.7). Additional experimental studies below 1 eV are needed at this time in order to confirm the existence of RT effect for this molecule.

We now compare our DCS at higher energies (5–20 eV) with a very recent absolute experiment by Khakoo et al [96]. In fact, we provided our present calculated cross sections to this experimental group (Khakoo et al) before they obtained their final results. In Figs. 7.2.9–7.2.12, we have plotted our DCS at 5, 10, 15, and 20 eV respectively along with experimental points of Khakoo et al. At 10 eV, we have also included theoretical results of Thirumalai et al [101] and experimental relative DCS of Hughes and McMillen [98]. From

Figs. 7.2.9–7.2.12, we conclude that our model potential calculations for the e^-–C_2H_2 system describes the elastic scattering process very well as compared to a most recent experimental findings. The structure observed in the DCS at all these energies (5–20 eV) by Khakoo et al is very faithfully reproduced by our model. For example, a dip structure around 90^0 (5 eV), 80^0 (10 eV) and 75^0 (15 and 20 eV) is present in both the theoretical and experimental investigations. From magnitude point of view, theoretical results are a higher (within 20%) than the measured values. Other previous calculations by Mu-Tao et al [100] are very poor in the present energy region and therefore not shown in Figs. 7.2.10–7.2.12.

Fig. 7.2.13 displays our total (vibrationally and electronically elastic and rotationally summed) cross sections in a wide energy range 0.01–20 eV. There is low energy minimum around 0.2 eV which may be recognized as RT effect. The shape resonance feature around 2 eV and a broad hump around 7.0 eV, observed in the measurements of Sueoka and Mori [82] and also in the old experiment of Brüche [102], is clearly reproduced in our calculations. In fact the position and width of the $^2\Pi_g$ resonance, calculated in the present non-empirical model, agrees very well with previous theoretical and experimental results (see Sec. 7.1). The disagreement between our results and the experimental data (Fig. 7.2.13) with respect to the magnitude of the cross section around 2 eV (our calculated results are higher by about 50 % than the experiment) is consistent with the similar situation found in the e^-–CO scattering [103]. One reason of this discrepancy between theory and experiment has been attributed to the neglect of nuclear dynamics in the present theory (vibrational channel), which may influence elastic scattering significantly in this resonant region. It is also to be noted that the measurements of Sueoka and Mori [82] are relative and do not consider corrections due to forward scattering. Another set of experimental data may further resolve this discrepancy. Unfortunately, we do not have any other measuremnts on the abosolute value of the e^-–C_2H_2 total cross section. At 10 eV, the theoretical σ_t value of 26.85×10^{-16} cm^2 of Thirumalai et al [101] is in fair agreement with the present value

of 24.83×10^{-16} cm^2. The corresponding theoretical value of 63.6 of Lee Mu-Tao et al [100] does not seem to be realistic.

Finally, in Fig. 7.2.14, we have plotted our σ_m cross sections in the same energy regime (0.01–20 eV), where the shape of the cross section is very similar to the σ_t curve of Fig. 7.2.13. To the best of our knowledge, no theoretical or experimental data is available in the literature for comparison. At 10 eV, our value of 17.1×10^{-16}cm^2 compares well with the 18.9×10^{-16}cm^2 value of Thirumalai et al. In brief, the σ_m curve is also charaterized by low energy (0.2 eV) RT minimum, a shape resonance around 2 eV, and a broad hump around 7 eV.

We presented differential, integral and momentum transfer cross sections for the elastic scattering of low energy electrons from C_2H_2. No fitting procedure is involved in the present model potential approach, where exchange and polarisation effects are treated approximately. The numerical method is based on the fixed–nuclei, single–center and closed–coupling formalism. All the salient features in the cross sections, observed in various measurements for both the differential and total cross sections, are reproduced very well by the present theoretical model. This study also suggest that more experimental studies are required in order to understand some discrepancy between theory and experiment. In order to make a best comparison of our DCS with measurements of the German group (Kochem et al) we multiplied their numbers by a factor of two; no simple explanation is available for this discrepancy in the magnitude of the DCS. their values

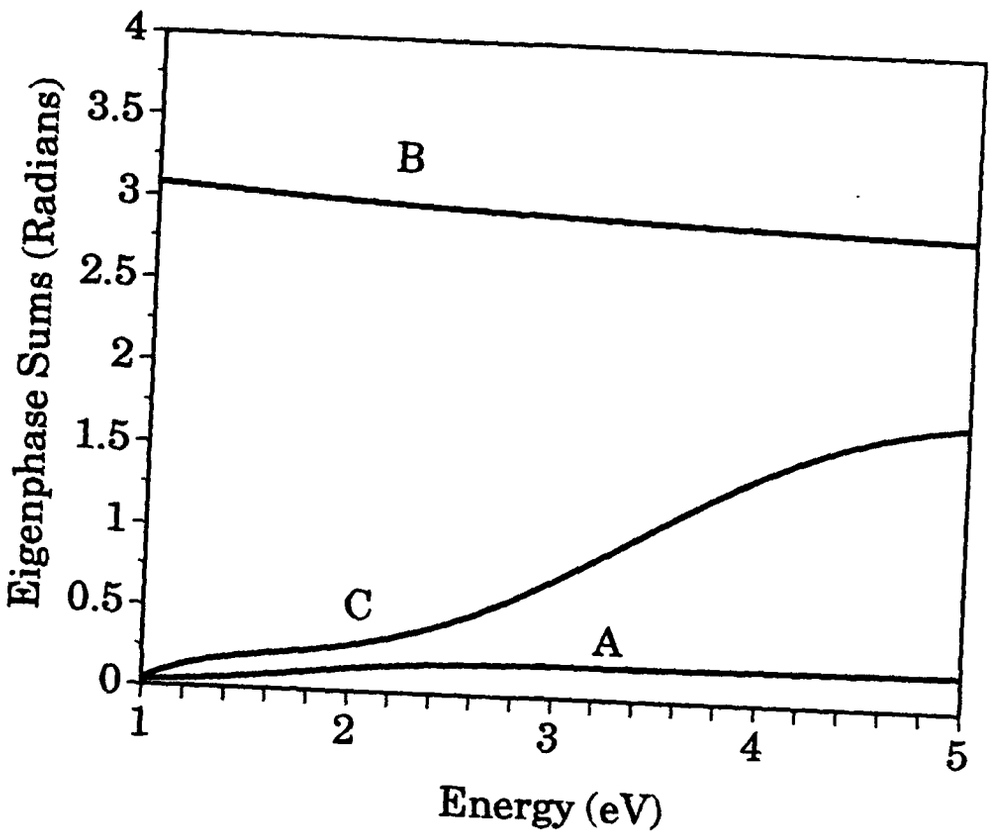

Figure 7.1.1 Eigenphase sums for the Πg e-C_2H_2 scattering in SCE (curve A), AAFEGE (curve (B) and FEGE (curve C) models.

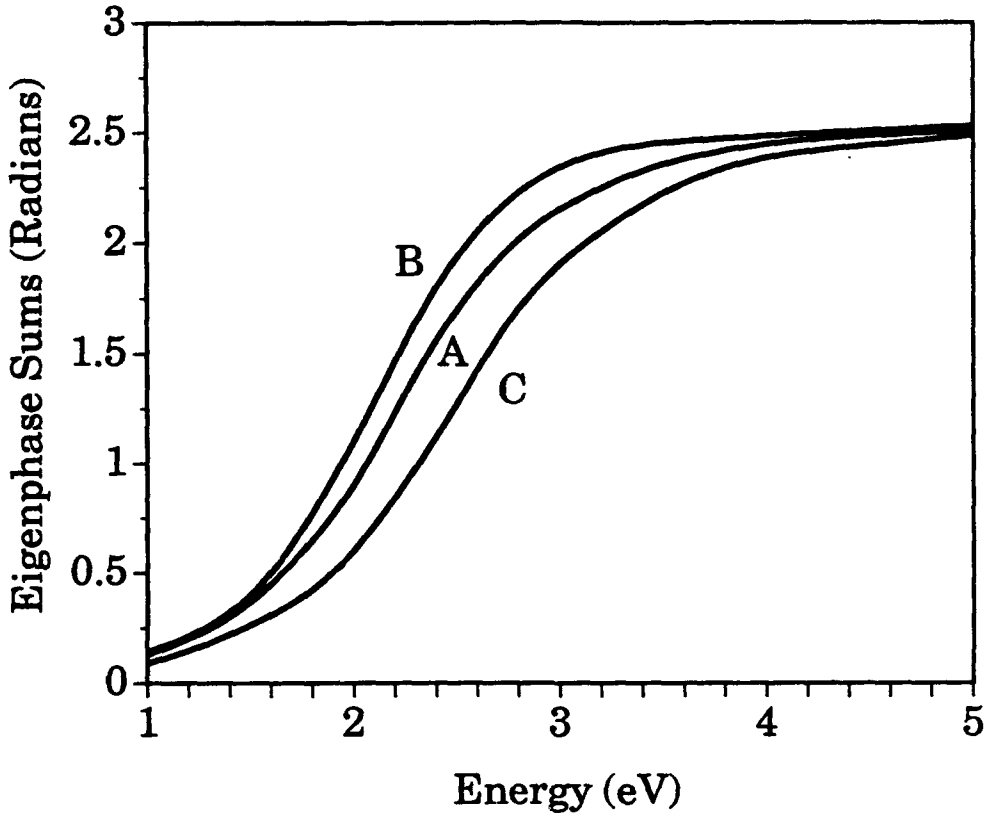

Figure 7.1.2 Eigenphase sums for the Πg e-C_2H_2 scattering in MSCEP (curve A), MSCE (curve (B) and TFEGE (curve C) models.

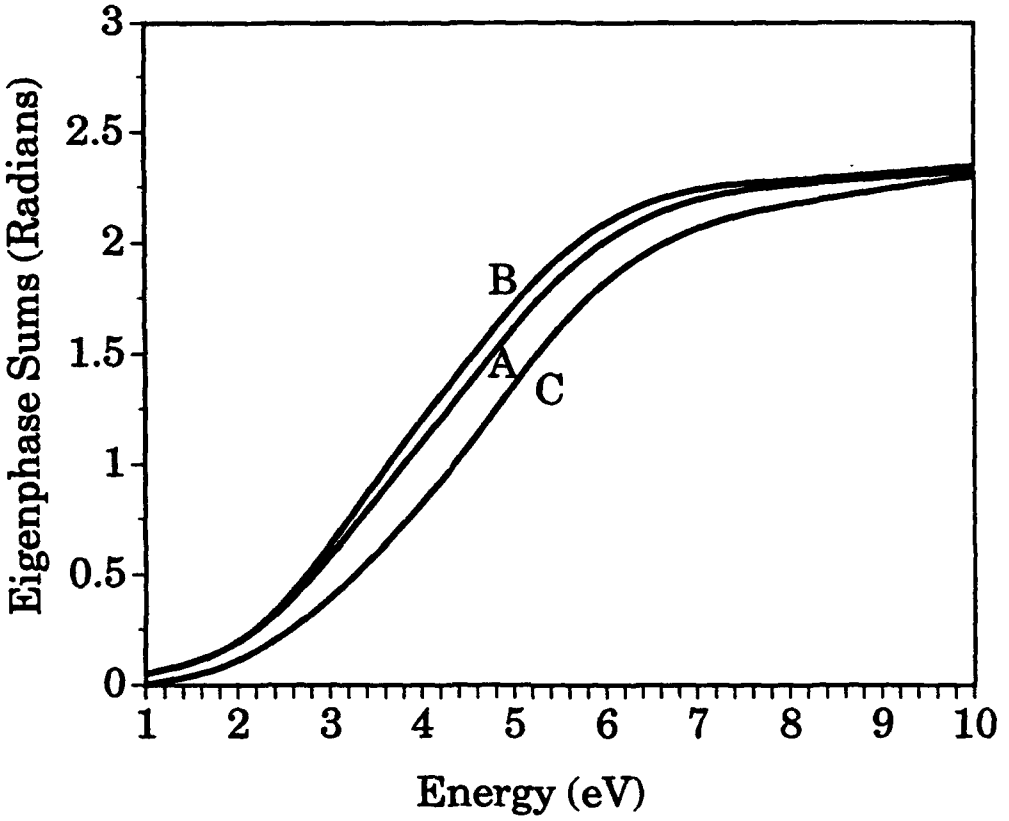

Figure 7.1.3 Eigenphase sums for the Πg e-C_2H_2 scattering in MSCEP (curve A), MSCE (curve (B) and TFEGE (curve C) models. Results are at the static-exchange (without polarization) level.

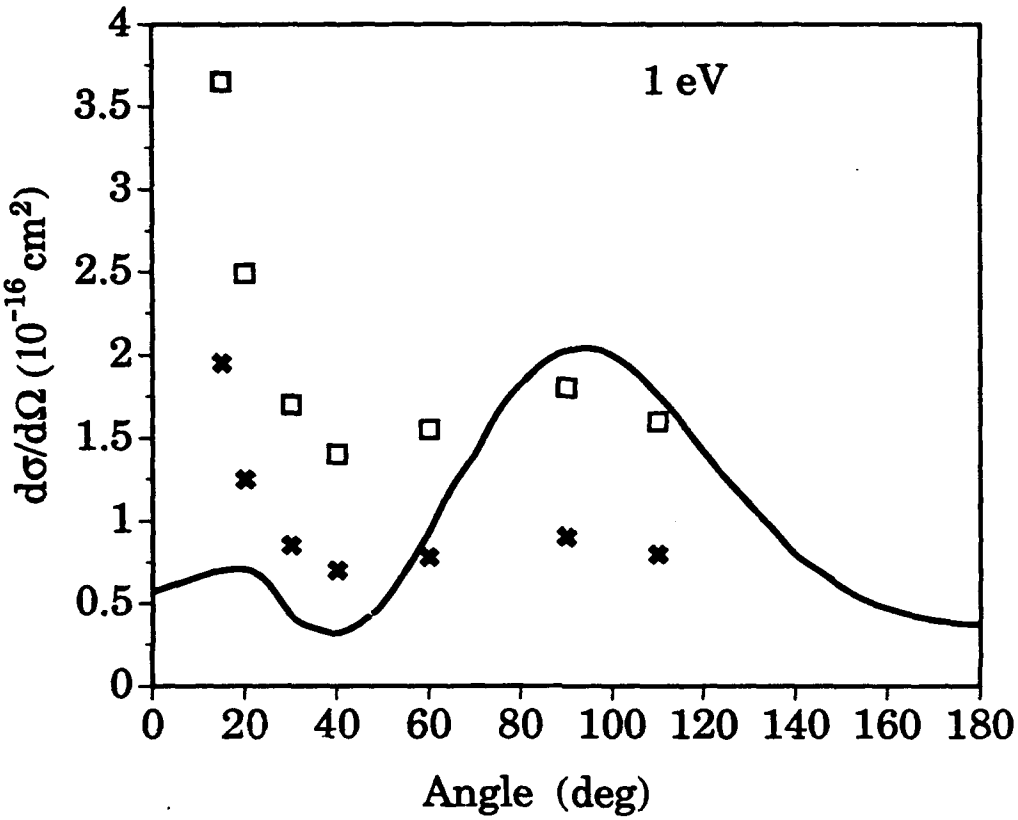

Figure 7.2.1 DCS for the e^--2h2 scattering at 1eV. Solid line, present calculations; Crosses and open boxes (multiplied by a factor of two), experimental data of Kochem et al (1985).

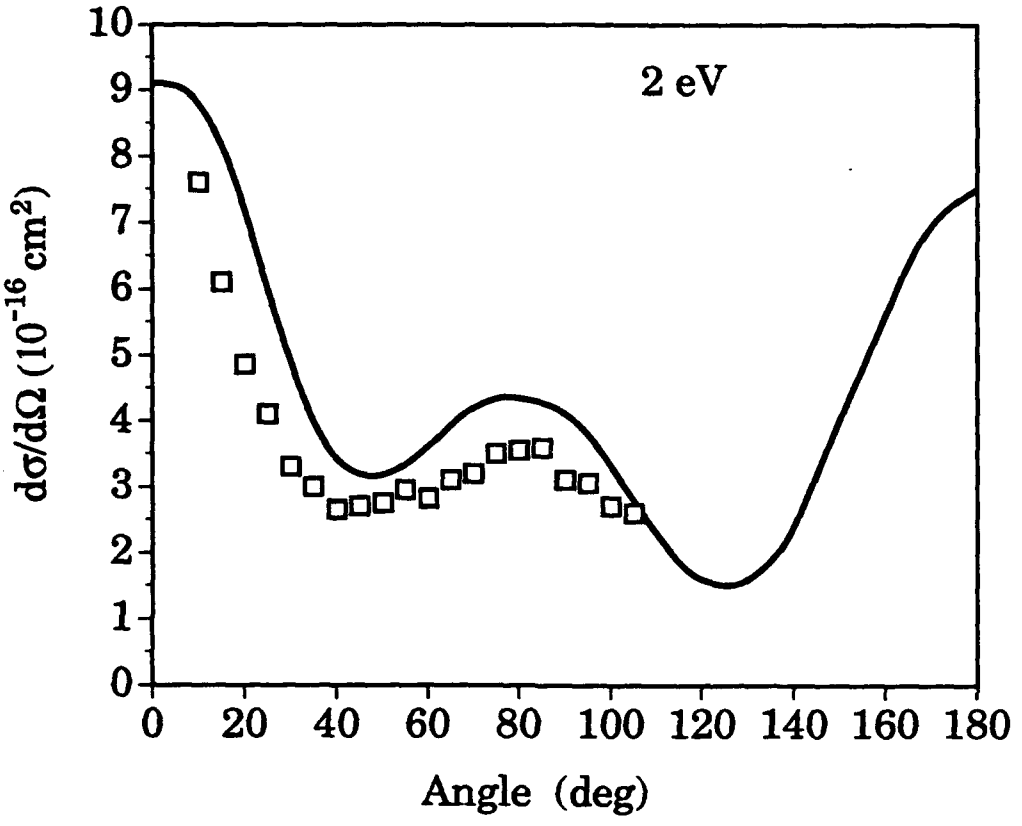

Figure 7.2.2 DCS for the e^--2h2 scattering at 2eV. Solid line, present calculations; Open boxes (multiplied by a factor of two), experimental data of Kochem et al (1985).

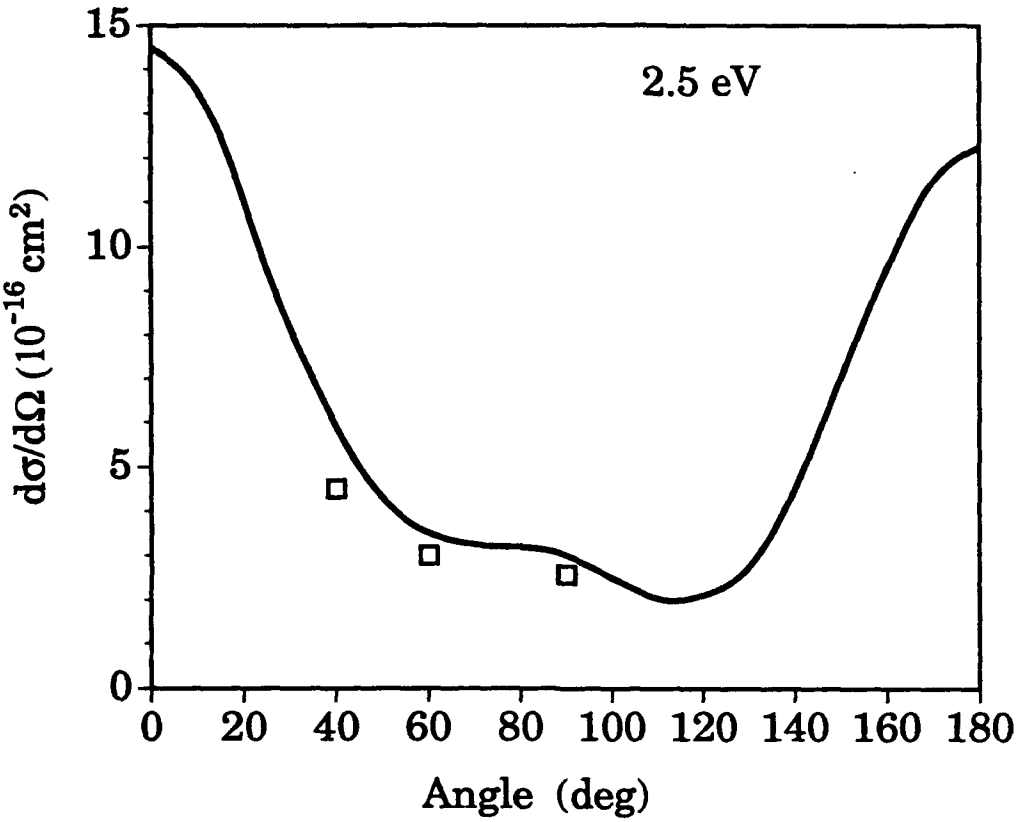

Figure 7.2.3 DCS for the e^--2h2 scattering at 2.5 eV. Solid line, present calculations; Open boxes (multiplied by a factor of two), experimental data of Kochem et al (1985).

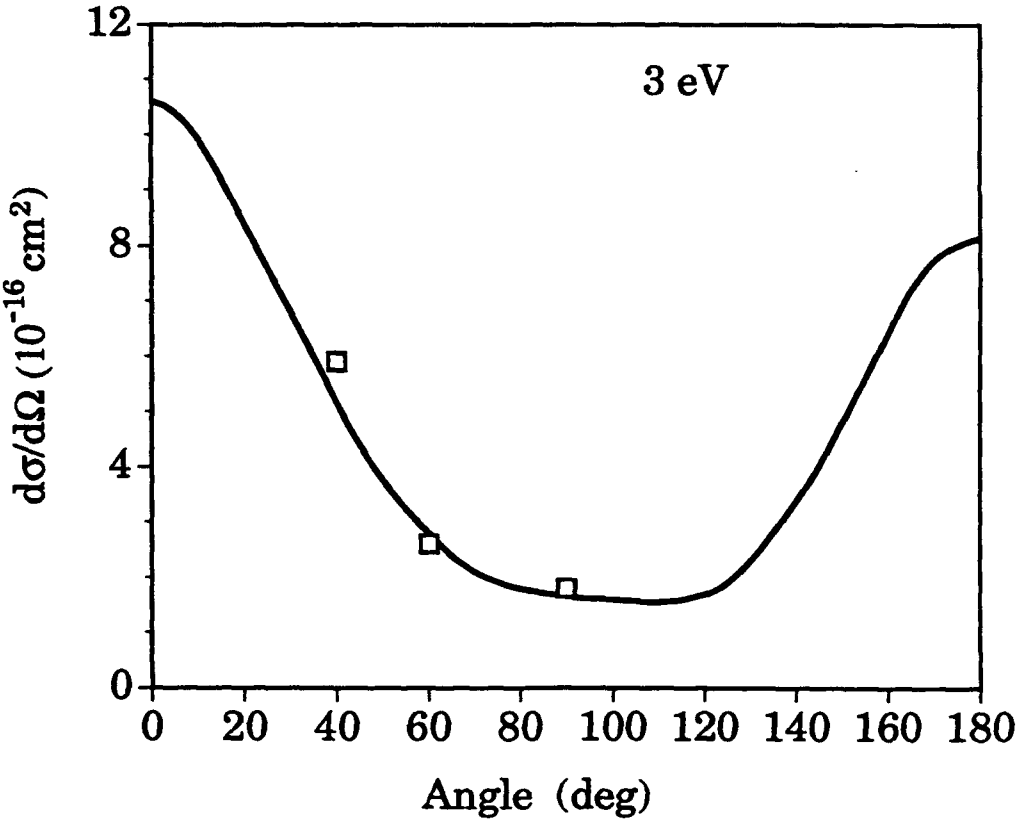

Figure 7.2.4 DCS for the e^--2h2 scattering at 3 eV. Solid line, present calculations; Open boxes (multiplied by a factor of two), experimental data of Kochem et al (1985).

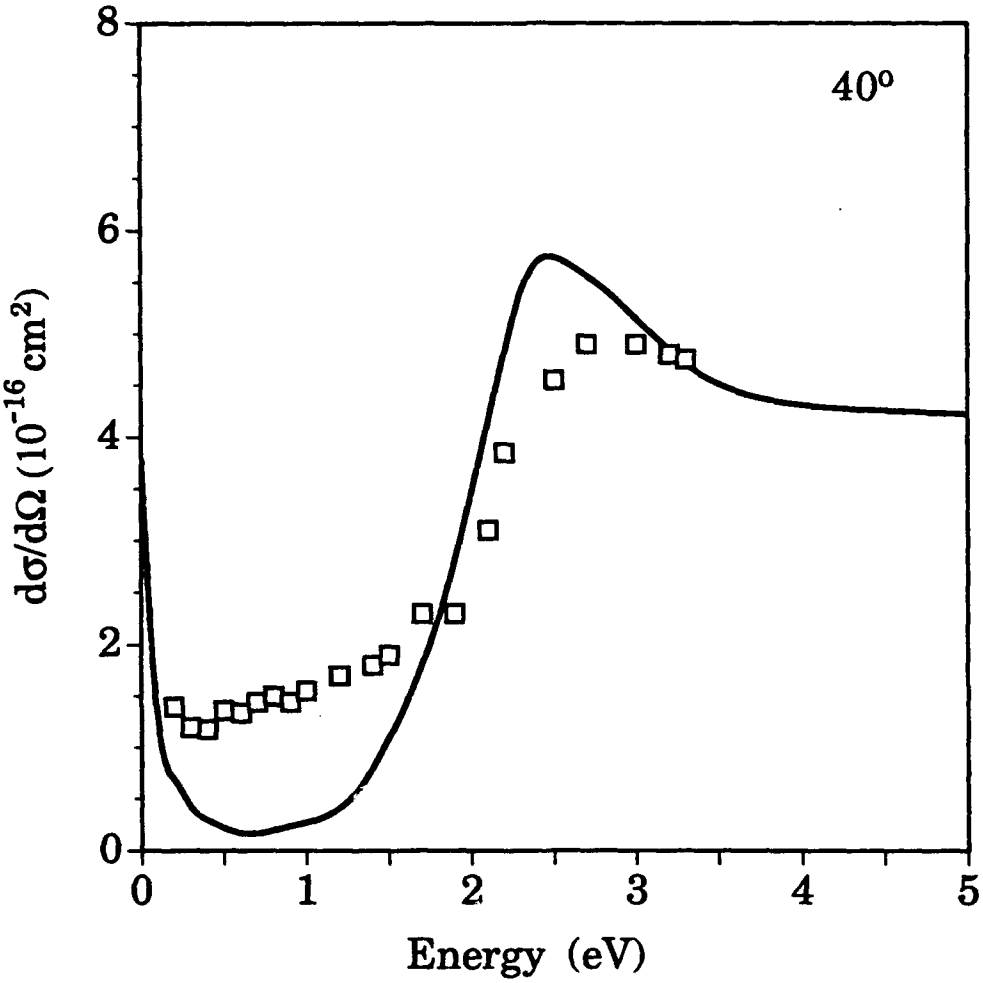

Figure 7.2.5 Present DCS (solid line) as a function of energy at 40° angle are compared with experimental data (multiplied by a factor of two) of Kochem et al (1985).

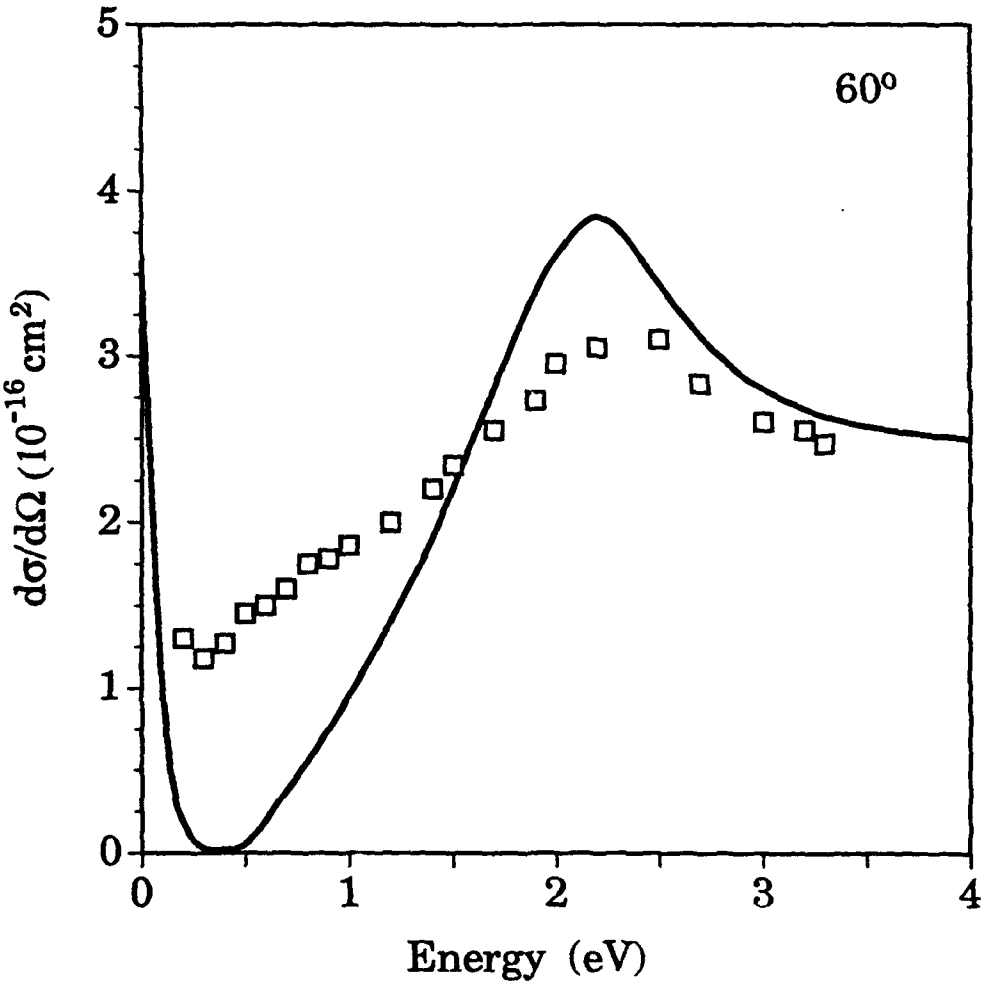

Figure 7.2.6 Present DCS (solid line) as a function of energy at 60° angle are compared with experimental data (multiplied by a factor of two) of Kochem et al (1985).

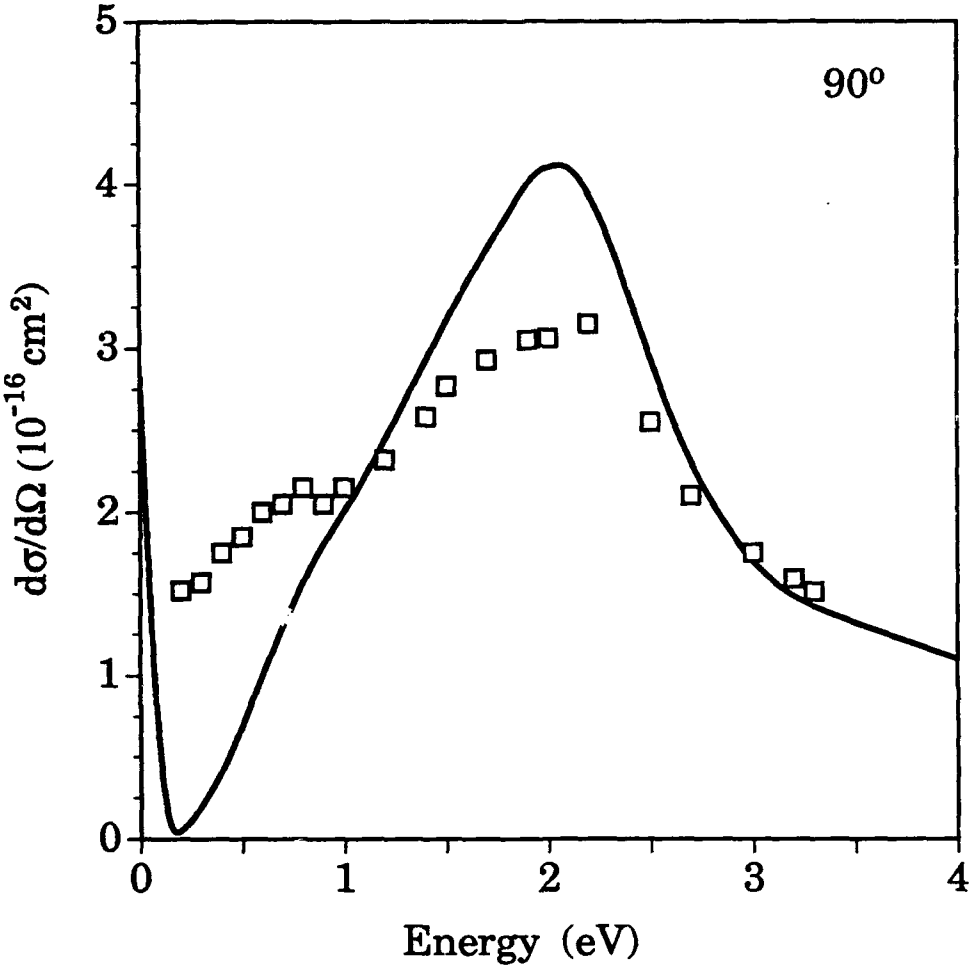

Figure 7.2.7 Present DCS (solid line) as a function of energy at 90° angle are compared with experimental data (multiplied by a factor of two) of Kochem et al (1985).

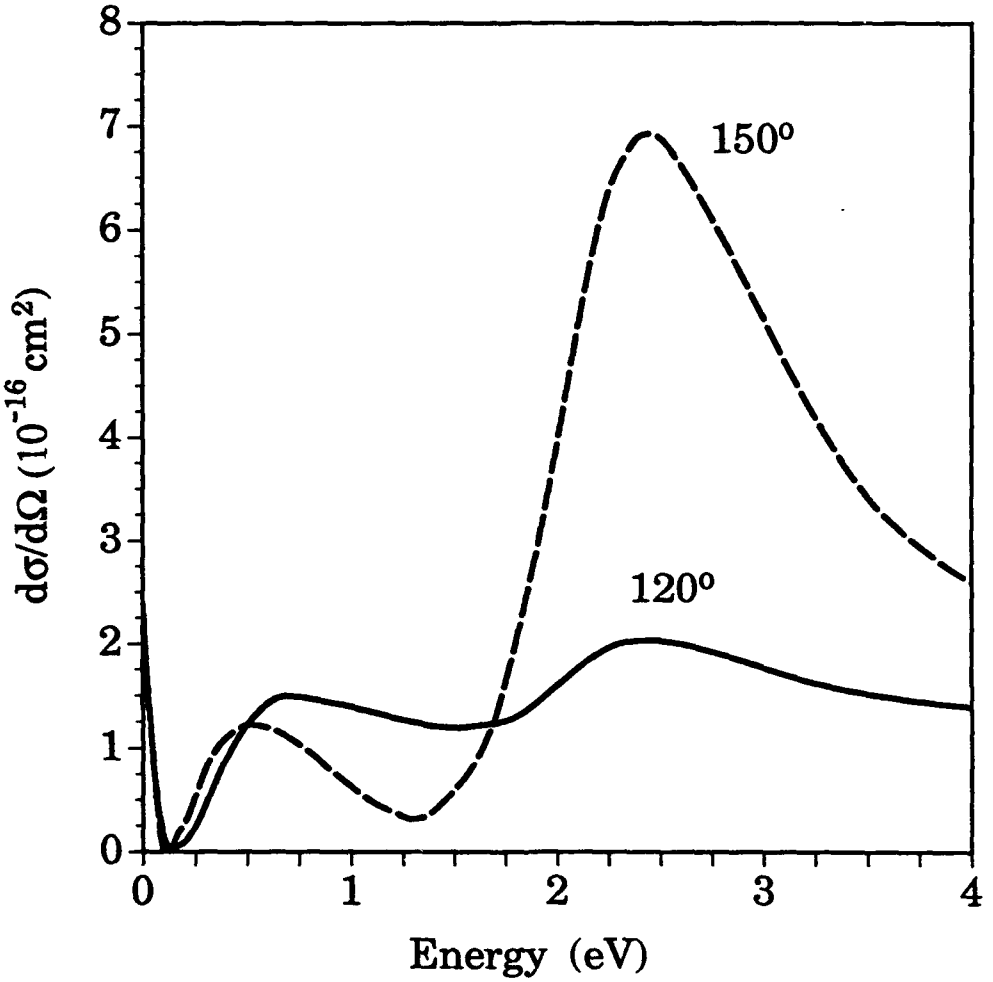

Figure 7.2.8 Present DCS as a function of energy at angles of 120° and 150°.

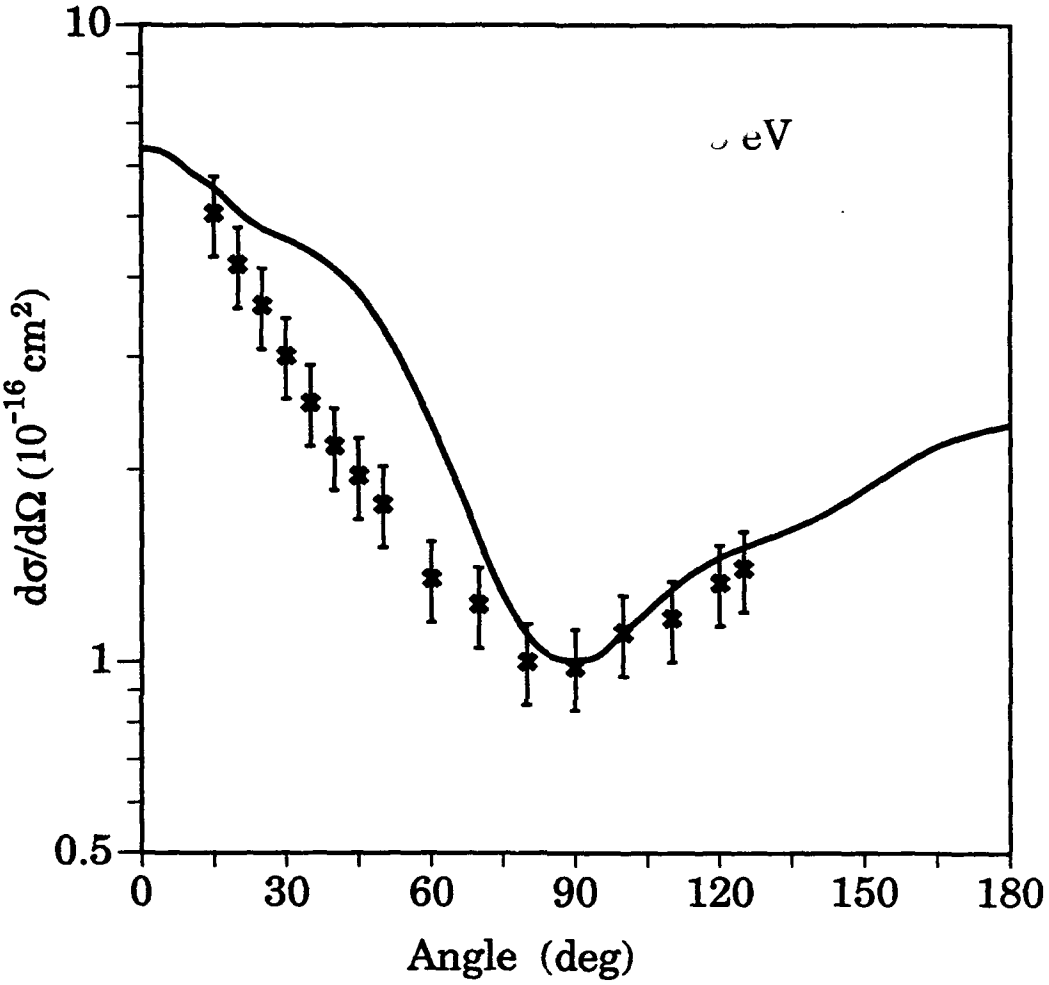

Figure 7.2.9 DCS for the e-2h2 scattering at 5 eV. Solid line, present calculations; Crosses, experimental data of Khakoo et al (1993).

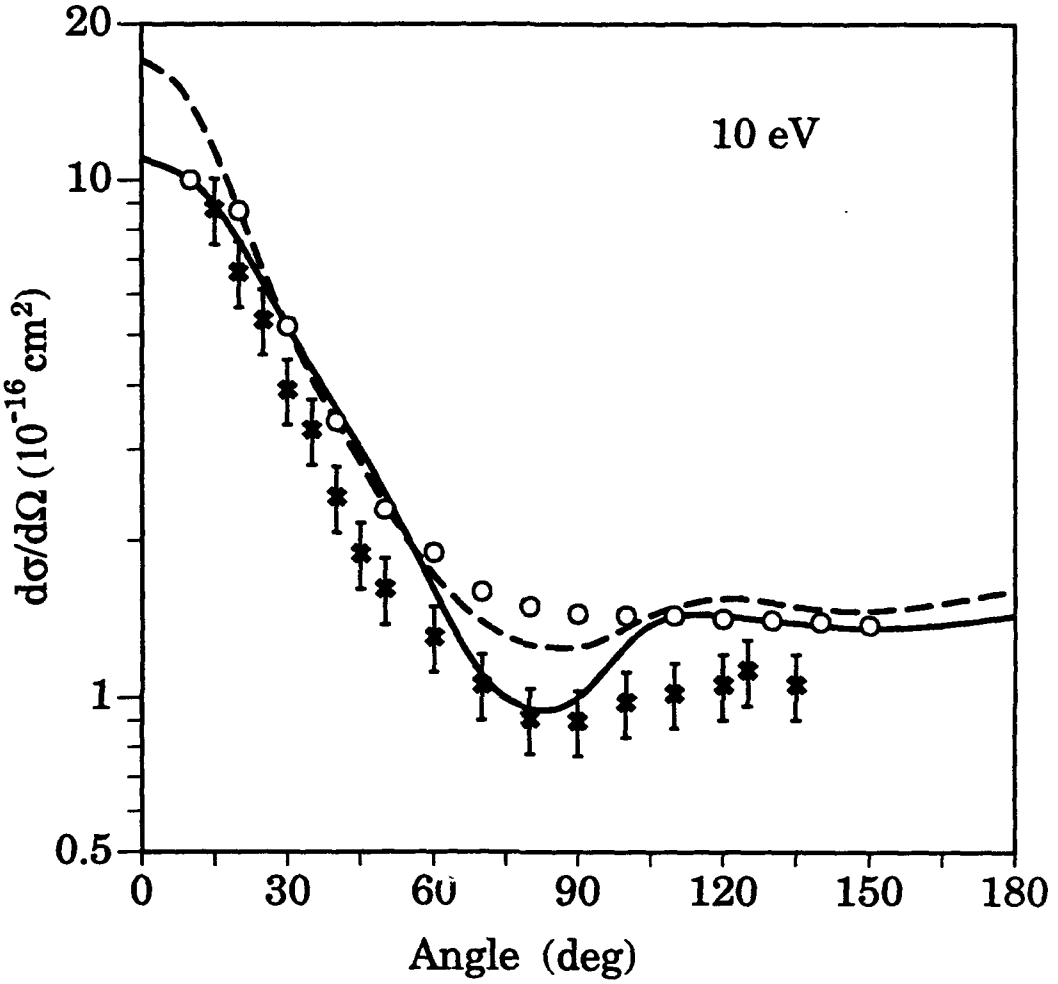

Figure 7.2.10 DCS for the e-2h2 scattering at 10 eV. Solid line, present calculations; Crosses, experimental data of Khakoo et al (1993) . The dash curve is the calculations of Thirumalai et al (1981), while open circles are relative measurements of Hughes and McMillen (1933).

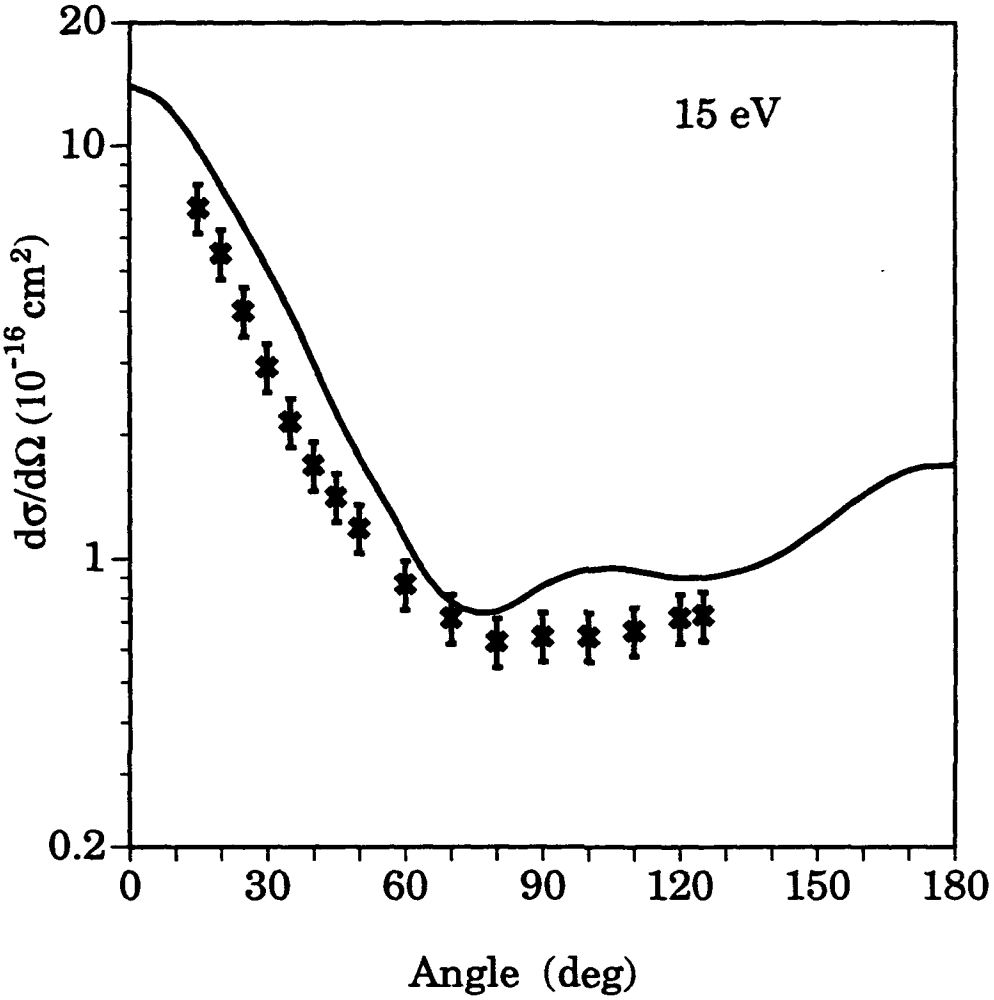

Figure 7.2.11 DCS for the e-2h2 scattering at 15 eV. Solid line, present calculations; Crosses, experimental data of Khakoo et al (1993).

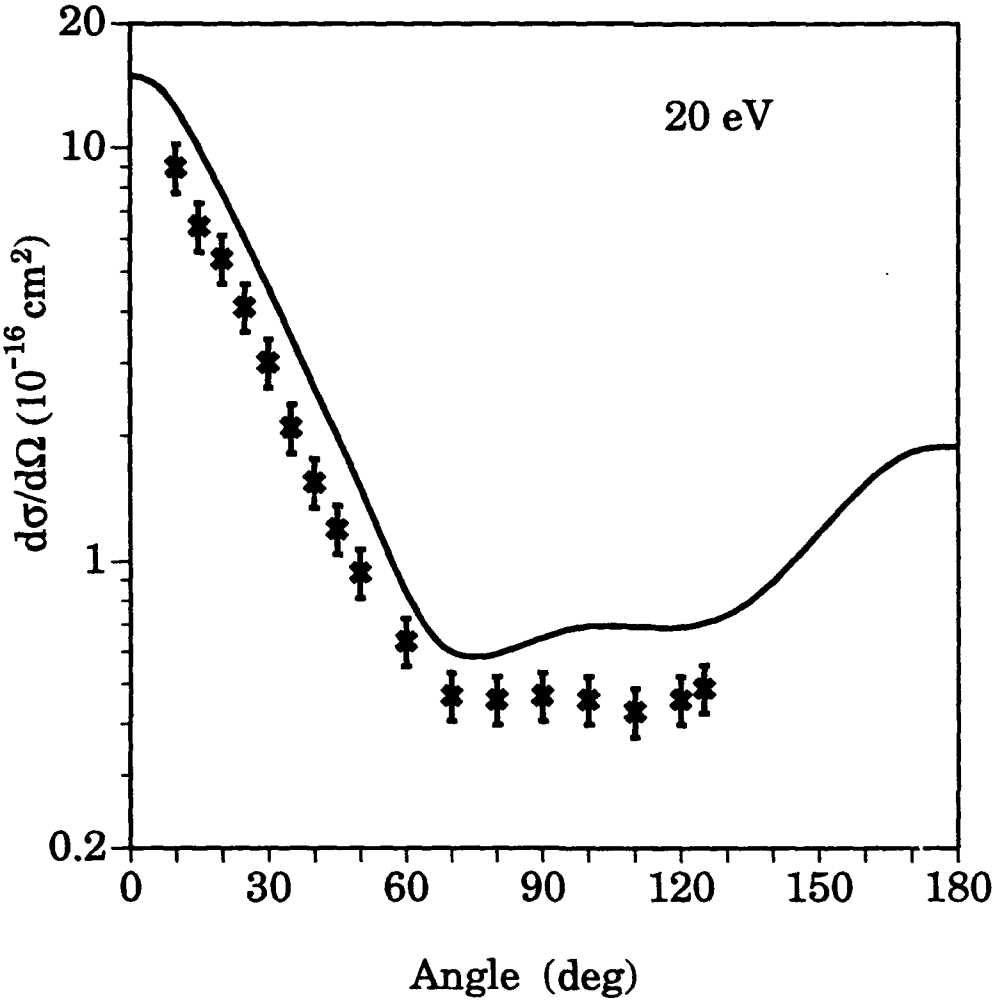

Figure 7.2.12 DCS for the e-2h2 scattering at 20 eV. Solid line, present calculations; Crosses, experimental data of Khakoo et al (1993) .

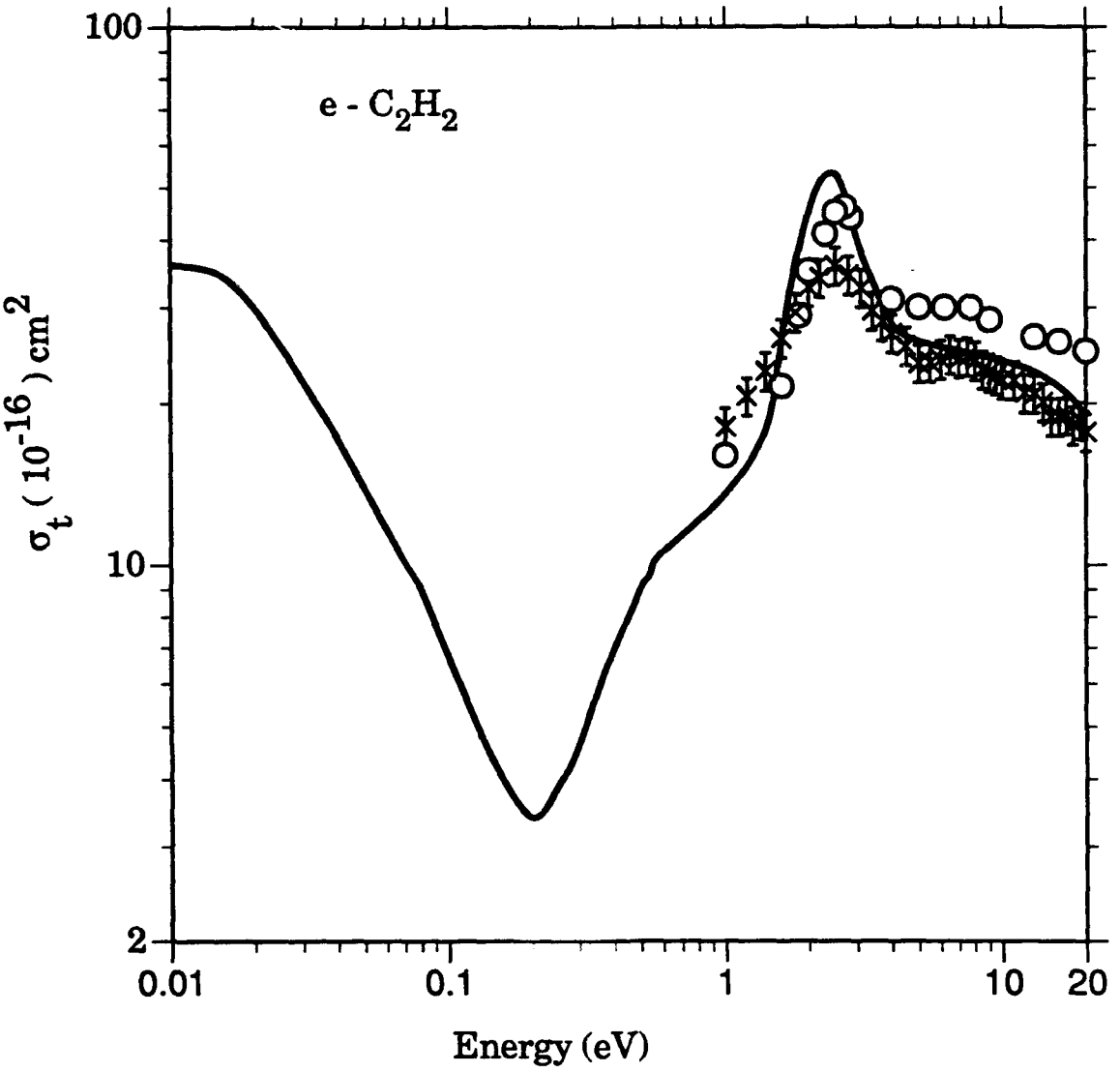

Figure 7.2.13 Integral cross sections for the e-2h2 collisions in the 0.01-20 eV range. Present calculations, solid line; x, experimental data of Sueoka and Mori (1989); o, experimental data of Brüche (1929).

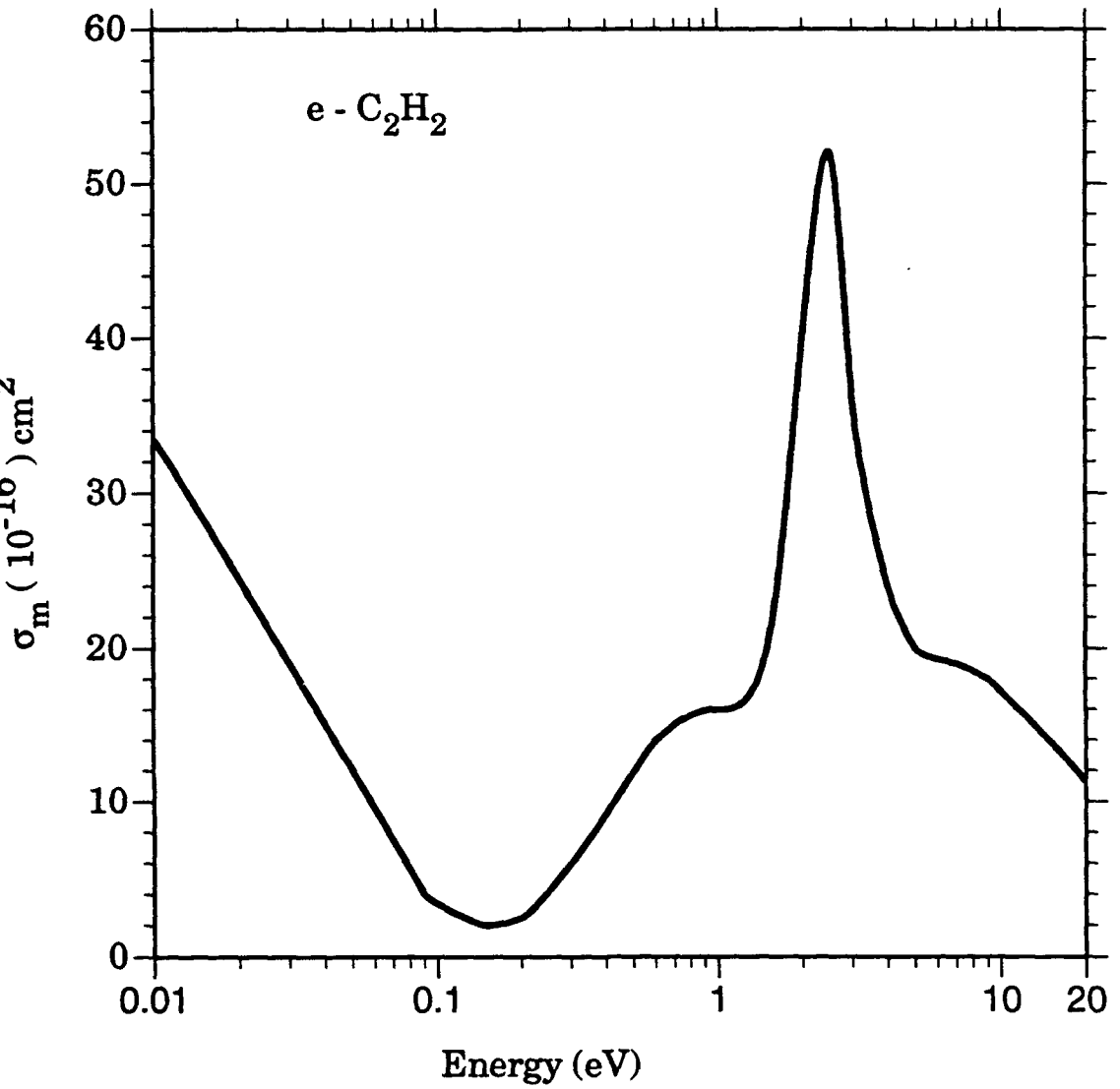

Figure 7.2.14 Present results on the momentum transfer cross sections for the e^--2h2 scattering in the 0.01-20 eV energy range.

8. EFFECT OF GAS TEMPERATURE ON THE CROSS SECTIONS

We made an extensive study of the effect of gas temperature on various elastic and inelastic (particularly the rotational excitation) cross sections [9, 18]. At a given temperature T, a typical polyatomic molecule has many rotational states populated. From theoretical point of view, it is easier to calculate rotational excitation cross sections from the ground state ($J = 0$) to any final J value of a given molecular system. In many practical cases, the transfer of rotational angular momentum J_t ($|J' - J| \leq J_t \leq J + J'$) in any scattering event involves very high values of J and J'. For spherical top molecules, the differential cross sections (DCS) for rotational excitation from any initial state J to a final state J' can be evaluated as follows [18],

$$\frac{d\sigma}{d\Omega}(J \rightarrow J'; k^2, \theta) = \sum_{J_t=|\Delta J|}^{2J+\Delta J} \frac{(2J+1+2\Delta J)}{(2J+1)(2J_t+1)} \frac{k'}{k_t} \frac{d\sigma}{d\Omega}(0 \rightarrow J_t; k^2, \theta), \qquad (8.1)$$

where k' and k_t are kinematic factors of the wavevector of projectile in the $J \rightarrow J'$ and $0 \rightarrow J_t$ cases respectively and $J' = J + \Delta J$. In the summation over J_t in Eq. (8.1), usually only a few terms are needed with small J_t values. Thus, given a set of cross sections for a few $0 \rightarrow J_t$ transitions only, Eq. (8.1) can easily be used to determine rotational excitation quantities from any initial J value including very high ones. This is essential when one needs to average the cross section over the distribution of rotational states at a given temperature. Eq. (8.1) is valid under the adiabatic–nuclear–rotation (ANR) approximation, i.e., the incident and scattered electron is moving much faster than the rotational motion of the molecule. In the present case of spherical top molecules and the energy range of 0.5-20 eV, the ANR approximation is valid and we used Eq. (8.1) to generate various cross sections with different initial J values for all possible final J' values allowed by the J_t selection rule.

If one neglects the kinematic factors (k' and k_t) from Eq. (8.1), the cross sections between the rotational states J and $J' = J \pm \Delta J$ can further be written as [14–15],

$$\frac{d\sigma}{d\Omega}(J \rightarrow J \pm \Delta J) = (1 \pm \frac{2\Delta J}{2J+1}) A(|\Delta J|), \qquad (8.2)$$

with

$$A(|\Delta J|) = \sum_{J_t=|\Delta J|}^{2J\pm\Delta J} \frac{d\sigma}{d\Omega}(0 \rightarrow J_t)/(2J_t+1). \tag{8.3}$$

where we assume that $2J - |\Delta J|$ is larger than any J_t that contributes appreciably to the sum in Eq. (8.3). In other words, we assume that $d\sigma/d\Omega(0 \rightarrow J_t)$ is almost zero for $J_t \geq 2J - |\Delta J|$, so that the upper limit of the summation in Eq. (8.3) is equivalent to infinity. Thus, we can easily write $|\Delta J|$ in the argument of A and not J or ΔJ.

The $d\sigma/d\Omega\,(0 \rightarrow J_t)$ can be expanded as,

$$\frac{d\sigma}{d\Omega}(0 \rightarrow J_t) = \frac{k_t}{k} \sum_L A_L(0 \rightarrow J_t) P_L(\cos\theta), \tag{8.4}$$

where $P_L(\cos\theta)$ are Legendre polynomials and the expansion A_L coefficients are given by [see Section 4.4],

$$A_L(0 \rightarrow J_t) = \frac{(-1)^L}{4k^2} \sum_{\ell\ell'\bar{\ell}\bar{\ell}'} BC(\ell L\bar{\ell};000)C(\ell' L\bar{\ell}';000)(-1)^{J_t} W(\ell\ell'\bar{\ell}\bar{\ell}';J_t L) M_{\ell\bar{\ell}}^{J_t m} M_{\ell'\bar{\ell}'}^{J_t m *}. \tag{8.5}$$

The **M** matrix is defined as,

$$M_{\ell\ell'}^{JM} = \sum_{mm'hh'p\mu} (-1)^m \bar{b}_{\ell hm}^{p\mu} C(\ell J\ell';mm'M) \bar{b}_{\ell' h'm'}^{p\mu} \mathbf{T}_{\ell h,\ell' h'}^{p\mu}, \tag{8.6}$$

and $B = [(2\ell+1)(2\ell'+1)(2\bar{\ell}+1)(2\bar{\ell}'+1)]^{\frac{1}{2}} i^{\ell-\ell'}(-i)^{\bar{\ell}-\bar{\ell}'}$. The C-coefficients are the usual Clebsch–Gordan coefiecients and the **T**–matrix is defined in terms of scattering **S** matrix as $\mathbf{T} = (\mathbf{S}-\mathbf{1})$ where $\mathbf{S} = (\mathbf{1}+i\mathbf{K})/(\mathbf{1}-i\mathbf{K})^{-1}$ is written in terms of reaction **K** matrix for each symmetry $(p\mu)$. In Eqs. (8.5)-(8.6), W(abcd;ef) is the well known Racah coefficient and the $\bar{b}_{lhm}^{p\mu}$ coefficients are expansion terms in the definition of symmetry adapted basis functions in terms of real spherical harmonics [1]. For the case of total and momentum transfer cross sections, Eq. (8.5) can be greatly simplified to give simple expressions [see Eqs. 4.4.9–4.4.10].

Here we have investigated the behavior of various scattering parameters on the initial rotational state J and temperature of the gas (CH_4 and SiH_4). This is important because

in rotational equilibrium at room temperature or higher, the gas molecules occupy many different rotational states. In addition, we also studied the dependence of the rotationally elastic and inelastic processes on the initial state J.

The basic scattering parameter is the differential cross section as a function of scattering angle (θ) and energy (k^2) for any rotational transition $J \rightarrow J+\Delta J$. A large set of cross sections can be obtained for state–to–state rotational transitions and rotationally summed quantities; however, it would be meaningful to derive compact information from this huge amount of cross section data. For example, the differential moments (the dependence on θ and k^2 is suppressed),

$$\frac{dS}{d\Omega}(\mu; J) = \sum_{J'}(E_{J'} - E_J)^{\mu} \frac{d\sigma}{d\Omega}(J \rightarrow J'), \tag{8.7}$$

and the integral moments $S(\mu; J)$ characterize the behavior of the electron–molecule system. The zeroth–order integral moment with $\mu = 0$, $S(0; J)$, is the usual integral (or total) cross section (summed $\sigma_t(J)$ or state–to–state $\sigma_t(J \rightarrow J')$), while first–order integral moment, $S(1; J)$, is the energy–loss or stopping cross section. Another useful parameter is the momentum transfer cross section (summed $\sigma_m(J)$ or state–to–state $\sigma_m(J \rightarrow J')$) which is obtained by integrating the differential cross section (Eq. 8.1) with the weighted factor of $(1 - \cos\theta)$. In Eq. (7.7), $E_J = BJ(J+1)$ is rotational energy of the molecule in Jth level and B is the molecular rotational constant. Higher order moments ($\mu \geq 2$) in Eq. 8.7 provide information on statistical fluctuations of the energy–loss spectrum from its mean value.

In practice, all observable physical quantities are connected with these moments averaged over the rotational distribution function $N(J;T)$, namely

$$< S(\mu) > = \sum_J N(J;T)S(\mu; J) \Big/ \sum_J N(J;T), \tag{7.8}$$

where $N(J;T) = g(J)e^{-E_J/\kappa T}$ is the Maxwellian distribution function, κ is the Boltzmann constant and $g(J) = (2J+1)^2$ is the statistical weight of the Jth state of a spherical top. In the definition of $N(J;T)$, we have neglected the effect of nuclear spins.

Another interesting aspect of the physics is the relationship between rotational excitation and de-excitation processes. Shimamura [14-15] has derived partial sum rules for the $J \rightarrow J \pm \Delta J$ rotational transitions. From Eqs. (8.2)-(8.3), we see that (denoting the cross section quantity in general by a)

$$\frac{a(J \rightarrow J + \Delta J)}{a(J \rightarrow J - \Delta J)} = \frac{2J + 1 + 2\Delta J}{2J + 1 - 2\Delta J}, \tag{8.9}$$

and the sum $a(J \rightarrow J + \Delta J) + a(J \rightarrow J - \Delta J)$ is a constant equal to $2A(|\Delta J|)$. However, if we include the effects of kinematic factors, particularly at the lower bound of the present energy region, Eq. (8.9) may be true only approximately. Shimamura [14–15] has also discussed the relationship between weighted rotational excitation and de-excitation quantities, i.e., $\Delta E^{+} a(J \rightarrow J + \Delta J)$ and $\Delta E^{-} a(J \rightarrow J - \Delta J)$. Here $\Delta E^{\pm}$ are transition energies given by $B\Delta J[\pm(2J + 1) + \Delta J]$. We have also discussed these partial sum rules and ratios for the CH_4 and SiH_4 cross sections [9, 18].

We have therefore carried out a systemetic study on the dependence of differential cross section (Eq. 8.1) and moments (Eq. 8.7) on the initial rotational state J and of the averaged quantities (using Eq. 8.8) on the gas temperature T. We compared our predictions with the theorems as discussed by Shimamura [11–17] regarding the J or T dependence of various physical quantities. All our results were presented only for the spherical top molecules (CH_4 and SiH_4). The basic scattering quantity, i.e., $d\sigma/d\Omega(0 \rightarrow J_t; k^2, \theta)$, is taken from our recent *ab initio* calculations [see Sections 6.1 and 6.2] on the e–CH_4 and SiH_4 systems. These calculations treat electron–exchange interaction exactly via iterative procedure and the charge correlation and polarization effects are included approximately in a parameter-free perturbative approach (see Section 4.5).

Our previous calculations [4] on the e–CH_4 state–to–state rotational transitions were in qualitative agreement with the experimentally extracted values of Müller *et al.* [53]. There were, however, some differences between theory and experiment for these rotationally inelastic channels where cross sections are very small compared to the pure elastic case.

For example, for the $0 \rightarrow 3$ transition, calculated values show zero cross section in the forward direction, while experimental points exihibit no such behaviour. This was one of the purposes of this study, i.e., to resolve this discrepancy between theory and experiment.

For the CH_4 and SiH_4 gases, we summarise our findings [9, 18] as follows:

1. The rotationally summed differential, integral and momentum transfer cross sections and various moments are independent of initial rotational state J and hence on the gas temperature T. The higher order moments depend very weakly on the initial J value.
2. we found that the partial-sum rule [14–15] for any physical quantity, say a,

$$a(J \rightarrow J + \Delta J) + a(J \rightarrow J - \Delta J) = 2A(|\Delta J|), \tag{8.10}$$

   is approximately true. Here $A(|\Delta J|)$ can be differential, integral, and momentum transfer cross sections or the moments (Eq. 8.2–8.3).
3. There is a significant effect of rotational averaging on the rotational excitation cross sections. The pure rotationally elastic channel is not affected with rotational avarag-ing. In general, the averaged DCS are smaller and exihibit less structure in the DCS as compared with the unaveraged DCS. (see Ref. 9)

9. ELECTRON–MOLECULE SCATTERING AT HIGH ENERGIES

The total cross sections (σ_t) (including elastic plus all energetically possible inelastic channels) for electron–molecule systems are important in many applied sciences [104–107]. In the intermediate and high energy region (roughly from ionization threshold up to several keV), almost all inelastic channels (rotational, vibrational and electronic excitation, ionization, dissociative processes etc.) are open. In this energy regime, a conventional close–coupling theory (see Sec. 3) of electron–molecule complex is an arduous task and almost impossible to carry out with present day fast supercomputers. It is, therefore, not surprising that almost all previous calculations on the σ_t for electron–molecule systems have been restricted to low energy region (typically below or around the first ionization threshold) only.

Although it is the low–energy electron molecule scattering where the cross sections exhibit a rich structure and several complex phenomenon, however, a knowledge of high–energy σ_t values for several molecular gases is required [104–107]. The importance of σ_t in radiation physics and chemistry has been discussed in the literature [108]. Such cross sections are available mostly through experimental studies and theoretical σ_t values in the literature are scarce (see Table 7.1 of Ref. 10), even for the simplest H_2 molecule.

The goal of this calculation was the following. First, to suggest a general and quite simple theoretical method which can predict σ_t values in a wide energy range for any molecular system for which Hartree-Fock level wave functions are available. The other molecular quantities needed for the calculation are the polarizability, ionization potential and various permanent multipole moments (dipole, quadrupole etc.) of the isolated molecule; second, to provide a simple fitted formula (see Eq. 9.18) from our calculated data for the total cross section; third, to provide Born–Bethe parameters [109–113] for all the molecules listed above; fourth, to emphasize the fact that individual elastic (σ_{el}) and inelastic (σ_{abs}) (or absorption) cross sections (giving rise to the final σ_t quantity) should compare quite well with the corresponding experimental, or more accurate theoretical results. For example, in

the present case, our inelastic (or absorption) cross sections should be an upper bound to the experimental total ionization, electronic excitation and dissociation channels together. The σ_t parameter has been measured for a large number of molecules from low to high energies [10].

Finally, we also examined correlation between molecular and scattering parameters. A quantitative as well as qualitative correlation picture was presented [10] which depicts several interesting aspects of the electron–molecule scattering at high energies. In particular, the nuclear charge Z or the occupation number of the target plays important role in the values of σ_t for all the targets. Such correlations would allow us better to understand the scattering mechanism and to estimate cross sections for those molecules where experimental or theoretical studies are difficult to perform.

The basic philosophy of the present method is based on the assumption that the non–spherical nature (providing torque to the molecule for rotational excitation) of the molecular system does not play significant role in shaping up the total cross section of the high–energy electron–molecule collisions. The collision time is too short and rotational excitation cross sections are insignificant relative to elastic, ionization, etc. processes. In addition, the contribution from vibrational excitation process is assumed to be negligble.

We first assume that the fixed–nuclei approximation is valid in this energy region and the interaction of the electron molecule system can be represented by a local complex optical potential, namely:

$$V_{\mathrm{opt}}(\mathbf{r}) = V_{\mathrm{R}}(\mathbf{r}) + iV_{\mathrm{abs}}(\mathbf{r}), \tag{9.1}$$

where the real part is a sum of three terms :

$$V_{\mathrm{R}}(\mathbf{r}) = V_{\mathrm{st}}(\mathbf{r}) + V_{\mathrm{ex}}(\mathbf{r}) + V_{\mathrm{pol}}(\mathbf{r}). \tag{9.2}$$

The static potential, $V_{\mathrm{st}}(\mathbf{r})$, is calculated from the unperturbed target wave function Ψ_0 at the Hartree–Fock level. The $V_{\mathrm{pol}}(\mathbf{r})$ represents approximately the short–range correlation and long–range polarization effects, while the $V_{\mathrm{ex}}(\mathbf{r})$ term accounts for electron exchange

interaction. In this energy region, a local and real potential model for exchange and polarization effects is adequate. The $V_{\rm abs}$ in Eq. (9.1) is the absorption potential. Due to the non–spherical nature of a molecule, the optical potential (Eq. 9.1) is not isotropic. A general expression for $V_{\rm opt}(\mathbf{r})$ for any target can be written in terms of the following multipole expansion around the center–of–mass (COM) of the molecule [1]:

$$V_{\rm opt}^{p\mu}(\mathbf{r}) = \sum_{\ell h} v_{\ell h}(r) X_{\ell h}^{(p\mu)}(\hat{\mathbf{r}}), \tag{9.3}$$

where $(p\mu)$ denotes the ground–state symmetry of molecule and the symmetry adapted X functions are defined in terms of real spherical harmonics $S_{\ell m}^{\pm}(\hat{\mathbf{r}})$ as [1]:

$$X_{\ell h}^{(p\mu)}(\hat{\mathbf{r}}) = \sum_{m=0}^{+\ell} b_{\ell h m}^{(p\mu)} S_{\ell m}^{q}(\hat{\mathbf{r}}). \tag{9.4}$$

For closed–shell systems, the $(p\mu)$ is the totally symmetric $^1A_1$ (non–linear molecules) or $^1\Sigma_g^+$ (linear molecules) irreducible representation. The anisotropic terms, $\ell = 1, 2, \ldots$, in expansion (9.3), provide torque to excite rotational levels in the molecule. As mentioned earlier, our main assumption in this work is that such higher–order terms are weak and can be treated separately in the first Born theory and added incoherently to the elastic part.

First we determine the target charge density $\rho(\mathbf{r})$ of a given molecule:

$$\rho(\mathbf{r}) = \int |\Psi_0|^2 d\mathbf{r}_1 d\mathbf{r}_2 \ldots d\mathbf{r}_Z = 2 \sum_{\alpha} |\phi_\alpha(\mathbf{r})|^2, \tag{9.5}$$

where Z is the number of electrons in the target, ϕ_i is the ith molecular orbital and a factor of 2 appears due to spin integration and α sum being over each doubly occupied orbital. It can be shcwn that for closed–shell molecules, $\rho(\mathbf{r})$ belongs to totally symmetric one-dimensional irreducible representation ($^1A_1$, $^1\Sigma_g^+$ or $^1\Sigma^+$) of the molecular point group [1]. All the four potential terms ($V_{\rm st}$, $V_{\rm ex}$, $V_{\rm pol}$ and $V_{\rm abs}$) are functions of $\rho(\mathbf{r})$. For example:

$$V_{\rm st}(\mathbf{r}) = \int \rho(\mathbf{r}_1) |\mathbf{r} - \mathbf{r}_1|^{-1} \, d\mathbf{r}_1 \; - \sum_{i=1}^{M} Z_i |\mathbf{r} - \mathbf{R}_i|^{-1}. \tag{9.6}$$

The V_{ex} is taken in the Hara free-electron-gas-exchange (HFEGE) model [24] and V_{pol} is calculated in the correlation-polarization (COP) approximation [114–116].

The imaginary part of the optical potential, $V_{abs}(\mathbf{r})$, is the absorption potential which represents approximately the combined effect of all the inelastic channels. An *ab initio* calculation of absorption potential is still an open problem. Here we employ a semi-empirical absorption potential as discussed by Truhlar and coworkers [117]. The V_{abs} is a function of molecular charge density, incident electron energy and the mean excitation energy , Δ, of the target :

$$V_{abs}(r) = -\rho(r)(v_{loc}/2)^{1/2}(8\pi/5k^2k_f^3)H(k^2 - k_f^2 - 2\Delta)(A_1 + A_2 + A_3), \tag{9.7}$$

where:

$$v_{loc}(r) = k^2 - V_{st}(r) - V_{ex}(r) - V_{pol} \tag{9.8a}$$

$$A_1 = 5k_f^3/2\Delta, \tag{9.8b}$$

$$A_2 = -k_f^3(5k^2 - 3k_f^2)/(k^2 - k_f^2)^2, \tag{9.8c}$$

$$A_3 = 2H(2k_f^2 + 2\Delta - k^2)\frac{(2k_f^2 + 2\Delta - k^2)^{5/2}}{(k^2 - k_f^2)^2}. \tag{9.8d}$$

where $\frac{1}{2}k^2$ is the energy of the incident electron in Hartrees. Here $H(x)$ is a Heaviside function defined by, $H(x) = 1$, for $x \geq 0$ and $H(x) = 0$ for $x < 0$. Here also, we consider only the spherical term in the single-center expansion of the absorption potential.

After generating the full optical potential (Eq. 9.1) of a given electron molecule system, we treat it exactly in a partial-wave analysis by solving the following set of first-order coupled differential equations for the real (χ_ℓ) and imaginary($\bar{\chi}_\ell$) parts of the complex phase-shift function under the variable-phase-approach (VPA) [118]:

$$\chi'_\ell(kr) = -\frac{2}{k}[2V_R(r)(A^2 - B^2) + 2V_{abs}(r)AB], \tag{9.9}$$

$$\bar{\chi}'_\ell(kr) = -\frac{2}{k}[2V_R(r)AB - 2V_{abs}(r)(A^2 - B^2)]. \tag{9.10}$$

where:

$$A = \cosh \bar{\chi}_\ell(kr)[\cos \chi_\ell(kr) j_\ell(kr) - \sin \chi_\ell(kr) \eta_\ell(kr)], \tag{9.11a}$$

$$B = -\sinh \bar{\chi}_\ell(kr)[\sin \chi_\ell(kr) j_\ell(kr) - \cos \chi_\ell(kr) \eta_\ell(kr)], \tag{9.11b}$$

and $j_\ell(kr)$ and $\eta_\ell(kr)$ are the usual Riccati–Bessel functions. The Eqs. (9.9) and (9.10) are integrated up to a sufficiently large r different for different ℓ and k values. Thus the final S–matrix is written as:

$$S_\ell(k) = exp(-2\bar{\chi}_\ell)\, exp(i2\chi_\ell), \tag{9.12}$$

and the corresponding DCS are defined as:

$$\frac{d\sigma}{d\Omega} = \frac{1}{4k^2}\left|\sum_{\ell=0}^{\ell_{max}}(2\ell+1)[S_\ell(k)-1]P_\ell(\cos\theta)\right|^2, \tag{9.13}$$

where $P_\ell(\cos\theta)$ is a Legendre polynomial of order ℓ. The integrated elastic ($\sigma_{\rm el}$), absorption ($\sigma_{\rm abs}$) and $\sigma_{\rm t}$ cross sections are described in terms of the S–matrix as follows:

$$\sigma_{\rm el}^\ell = \frac{\pi}{k^2}(2\ell+1)|1-S_\ell(k)|^2; \quad \sigma_{\rm el} = \sum_{\ell=0}^{\ell_{\rm max}} \sigma_{\rm el}^\ell, \tag{9.14}$$

$$\sigma_{\rm abs}^\ell = \frac{\pi}{k^2}(2\ell+1)[1-|S_\ell(k)|^2]; \quad \sigma_{\rm abs} = \sum_{\ell=0}^{\ell_{\rm max}} \sigma_{\rm abs}^\ell, \tag{9.15}$$

$$\sigma_{\rm t}^\ell = \frac{2\pi}{k^2}(2\ell+1)[1-{\rm Re}S_\ell(k)]; \quad \sigma_{\rm t}^{\rm S} = \sum_{\ell=0}^{\ell_{\rm max}} \sigma_{\rm t}^\ell. \tag{9.16}$$

We note that $\sigma_{\rm t}^{\rm S} = \sigma_{\rm el} + \sigma_{\rm abs}$ is the contribution from the spherical term only. In the above analysis the inelasticity or the absorption factor is defined by $|S_\ell(k)| = exp(-2\bar{\chi}_\ell)$.

We presented [10] total cross sections for a large number of molecules divided in terms of isoelectronic sequence such as, 2– (H_2), 6– (Li_2), 10– (HF, CH_4), 14– (CO, N_2, C_2H_2, HCN), 16– (O_2), 18– (HCl, H_2S, PH_3, SiH_4) and 22– (CO_2) electron systems. All the calculated results were compared with measured data and we found a very good agreement

between theory and experiment. In particular, the present theory was successful above 100 eV for almost all the above species.

We also emplyed our high energy cross sections ($\sigma_{\rm el}$, $\sigma_{\rm abs}$ and $\sigma_{\rm t}$) to determine Born–Bethe parameters [109–113]. The Bethe theory defines the total inelastic ($\sigma_{\rm abs}$) cross section, while the Born approximation gives the total elastic ($\sigma_{\rm el}$) cross section. Thus, a combined Born–Bethe theory expresses the total cross section in terms of the following analytic formula:

$$\frac{E}{R}\frac{\sigma_{\rm t}}{\pi a_0^2} = \left[A_{\rm el} + B_{\rm el}\frac{R}{E} + C_{\rm el}\left(\frac{R}{E}\right)^2 \ldots\right] + \left[4M_{\rm tot}^2 \ln\left(4C_{\rm tot}\frac{E}{R}\right) + \ldots\right], \qquad (9.17)$$

where E is the incident energy in eV, R is the Rydberg energy, a_0 is the Bohr radius. The constants $A_{\rm el}, B_{\rm el}, C_{\rm el}, M_{\rm tot}$ and $C_{\rm tot}$ have physical significance. The $M_{\rm tot}^2$ is related with the optical oscillator strength of the molecule. To our knowledge, there were hardly any results in the literature on the Born–Bethe parameters (Eq. 9.17) for most of the molecules studied here. In addition, we fit a general formula for the $\sigma_{\rm t}$ from our calculated values in the following form:

$$\frac{E}{R}\frac{\sigma_{\rm t}}{4\pi a_0^2} = a' \ln\frac{E}{R} + b'\frac{R}{E} + c', \qquad (9.18)$$

and provided the values of constants a', b' and c' for the present set of molecules [10].

In order to further analyse our total cross section results, we have made Bethe plots ($\sigma_{\rm abs}E/(4\pi R a_0^2)$ vs. $\ln(E/R)$) for all the molecules [10]. From these plots we found the Bethe theory valid, which says that the Bethe plot should be a straight line with a gradient of $M_{\rm tot}^2$.

We further put together the above description of high energy electron scattering with a variety of diatomic and polyatomic molecules. It is always useful to know the variation of cross sections in different targets. We have already seen that isoelectronic collisional systems possess similar cross sections both in quantity and quality. Except very highly polarizable Li_2 or the simple H_2 molecules, we might expect some kind of correlation between σ_t and any molecular property (number of electrons Z, polarizability, multipole

moments, molecular size etc.). A general feature above 100 eV, common for all the above targets, is the decrease of σ_t with increase in impact energy. We clearly found [10] that the σ_t values increase with an increase in Z, i.e., there is strong correlation between the total cross section and the size of the target. On the other hand, we did not see such a correlation with respect to target polarizability. However, at lower energies (around 100 eV), the σ_t seems to have a strong dependence on α_0. From our σ_t–Z correlation diagram [10] a rough estimate of the total cross section can be made for any molecular system with Z smaller or greater than 22.

11. CONCLUSIONS

During a period of three years, several important developments and calculations were made on the electron–molecule scattering. We presented rotationally elastic, inelastic and summed cross sections for electron scattering with several polyatomic molecules (CH_4, SiH_4, GeH_4, H_2O, H_2S and NH_3) in a highly sophisticated close–coupling non–empirical theory. Exchange effects were included exactly, while polarization corrections were considered approximately but without involving any fitting parameter. Results were compared with measurements where such data were available. No previous theoretical investigation is available on these molecules in such detail and energy range. The present study has drawn several important conclusions: (1) exchange effects at the exact level and model polarization potentials can describe low energy e–molecule scattering quite accurately, (2) polarization effects should be included in a theory where target orbitals are relaxed in the presence of incoming particle, (3) the effect of gas temperature on the cross sections is crucial for rotationally inelastic channels, (4) a single–center approach can be useful for many polyatomics without any convergence problem, (5) the iterative scheme is quite promising tool in future if employed in an optimized way as suggested in this study.

For the first time, a large variety of molecules are studied at intermediate and high energies. The total cross section (sum of elastic plus all possible inelastic channels) for several selected gases were calculated and presented in tabular form in the energy range of 10–5000 eV. Such theoretical data are not found in the literature for most of the targets studied here. In addition we also reported Born–Bethe parameters for all these molecules. An attempt was made to find a correlation between molecular properties and the corresponding total cross section quantity.

Several computers codes were modified and developed in order to deal with big molecules and also polar ones. Our Single–center–expansion scheme was made possible to work for much heavier systems (e.g. GeH_4, SF_6, CF_4, etc.) than the typical CH_4, etc.

ones. An interface program was developed which generates SCE quantities from molecular wave functions. This progress was realized in terms of some actual calculations on some molecules of larger size.

This work is still in progress in two ways: (1), to investigate electron interactions in large systems, and (2) to employ the present set of programs for vibrational and electronic excitation of polyatomic molecules. Some preliminary progress has been made for the CH_4 and H_2O molecules. However, this work requires a huge amount of effort in terms of manual and computational facilities.

11. REFERENCES

[1]. F. A. Gianturco and Ashok Jain, Phys. Rep., **143**, 348 (1986).

[2]. P. McNaughten and D. G. Thompson, J. Phys. **B21**, L703 (1988).

[3]. Ashok Jain, C. A. Weatherford, P. McNaughten and D. G. Thompson, Phys. Rev. **A40**, 6730 (1989).

[4]. P. McNaughten, D. G.Thompson and Ashok Jain, J. Phys. **B23**, 2405S (1990).

[5]. Ashok Jain and D. G. Thompson, J. Phys. **B24**, 1087 (1991).

[6]. Ashok Jain, F. A. Gianturco and D. G. Thompson, J. Phys. **B24**, L255 (1991).

[7]. Ashok Jain, Phys. Rev. **A44**, 772 (1991).

[8]. F. A. Gianturco, V. Di Martino and Ashok Jain, Nuovo Cim. **14**, 411 (1992).

[9]. Ashok Jain, Air force Report No. WL–TR–91–2074 (1991).

[10]. Ashok Jain, Air force Report No. WL–TR–92–2079 (1992).

[11]. I Shimamura, Chem. Phys. Lett., **73**, 328 (1980).

[12]. I. Shimamura, Prog. of Theo. Phys., **68**, 178 (1982).

[13]. I. Shimamura, J. Phys. **B15**, 93 (1982).

[14]. I Shimamura, Phys. Rev. **A28**, 1357 (1983).

[15]. I Shimamura, Phys. Rev. **A23**, 3350 (1981).

[16]. I Shimamura, Z. Phys. **A309**, 107 (1982).

[17]. I Shimamura, Phys. Rev. **A42**, 1318 (1990).

[18]. Ashok Jain, Z Phys. **D21**, 153 (1991).

[19]. Ashok Jain, K. L. Baluja, V. Di martino and F. A. Gianturco, Chem. Phys. Lett. **183**, 34 (1991).

[20]. Ashok Jain and K. L. Baluja, Phys. Rev. **A45**, 202 (1992).

[21]. Ashok Jain, J. Phys. **B25**, L439 (1992).

[22]. Ashok Jain, J. Phys. **B26**, 4833 (1993).

[23]. See for example a review by N. F. Lane, Rev. Mod. Phys. **52**, 29 (1980) for the subject of ANA. See also M. A. Morrison, Aus. J. Phys. **36**, 239 (1983).

[24]. S. Hara, J. Phys. Soc. Japan, **22**, 710 (1967).

[25]. S. S. Salvini and D. G. Thompson, J. Phys. **B14**, 3797 (1981).

[26]. Ashok Jain and D. G. Thompson, J. Phys. **B15**, L631 (1982).

[27]. J. A. Pople and P. Schofield, Phil. Mag. **2**, 591 (1957).

[28]. A. Temkin, Phys. Rev. **107**, 1004 (1957).

[29]. D. M. Chase, Phys. Rev. **104**, 838 (1956).

[30]. Ashok Jain, Ph.D. thesis (Queen's University, Belfast) (1983).

[31]. D. W. Norcross and L A Collins, Adv. At. Mol. Phys. **18**, 341 (1982).

[32]. D. W. Norcross and N T Padial, Phys. Rev. **A25**, 226 (1982).

[33]. G Herzberg, in " Molecular Spectra and Molecular Structure, " Vol. III. (Krieger, 1990)

[34]. HONDO version 7.0 (Dupius–Watts–Villar–Hurst) (1987).

[35]. L. A. Collins and D W Norcross, Phys. Rev. **A18**, 478 (1978).

[36]. J Ferch, B Granitz and W raith, J. Phys. **B18**, L445 (1985).

[37]. A. Garscadden, G L Duke and W F Bailey, Appl. Phys. Lett. **43**, 1012 (1983).

[38]. H -X Wan, J H Moore and J A Tossell, J. Chem. Phys. **91**, 7340 (1989).

[39]. W J Pollock, Trans. Faraday Soc. **64**, 2919 (1968).

[40]. J C Giordan, J. Am. Chem. Soc. **105**, 6544 (1983).

[41]. S Mori, Y Katayama and O Sueoka, At. Coll. Res. Jpn. **11**, 19 (1985).

[42]. M Tronc, A Hitchcock and F Edard, J. Phys. **B22**, L207 (1989).

[43]. Y Ohmori, M Shimozuma and H Tagashira, J. Phys. **D19**, 1029 (1986).

[44]. M Kurachi and Y Nakamura, J. Phys. D, Appl. Phys. **22**, 107 (1989).

[45]. M Hayashi (private communication).

[46]. H Tanaka, L Boesten, H Sato, M Kimura, M A Dillon and D Spence, J. Phys. **B23**, 577 (1990).

[47]. A Jain and D G Thompson, J. Phys. **B20**, 2861 (1987).

[48]. A K Jain, A N Tripathi and A Jain, J. Phys. **B20**, L389 (1987).

[49]. F A Gianturco, L C Pantano and S Scialla, Phys. Rev. **A36**, 557 (1987).

[50]. A Jain, J. Chem. Phys. **78**, 1289 (1987).

[51]. J Yuan, J. Phys. **B22**, 2589 (1989).

[52]. C Winstead and V McLoy, Phys. Rev. **A42**, 5357 (1990).

[53]. R Müller, K Jung, K H Kochem, W Sohn and H Ehrhardt, J. Phys. **B 18**, 3971 (1985).

[54]. L Boesten and L Tanaka (private communication).

[55]. O Sueoka, S Mori and Y Katayama, J. Phys. **B20**, 3237 (1987).

[56]. C Szmytkowski, K Maciag, G Karwasz and D Filipovic (private communication).

[57]. T W Shyn (private communication).

[58]. H P Pritchard, M A P Lima and V McKoy, Phys. Rev. **A39**, 2392 (1989).

[59]. S D Parker, C W McCurdy and T N Rescigno, Bull. Am. Phys. Soc. **36**, 1266 (1991).

[60]. A Jain and D G Thompson, J. Phys. **B16**, 2593 (1983).

[61]. C. Szmytkowski, Chem. Phys. Lett. **136**, 363 (1987).

[62]. O. Suoka and S. Mori, J. Phys. **B19**, L373 (1986).

[63]. V. F. Sokolov and Y. A. Sokolova, Sov. Tech. Phys. Lett. **7**, 268 (1981).

[64]. E. Bruche, Ann. Phys. **1**, 93 1929.

[65]. H. Nishimura and K. Yano, J. Phys. Soc. Jpn., **57**, 1951 (1988).

[66]. A. Danjo and H. Nishimura, J. Phys. Soc. Jpn., **54**, 811 (1985).

[67]. T. W. Shyn and S. Y. Cho, Phys. Rev., **A36**, 5138 (1987).

[68]. K.Jung, T. Antoni, R. Müeller, K. H. Kochem, H. Ehrhardt, J. Phys. **B15**, 3535 (1982).

[69]. W. R. Johnstone and W. R. Newell, J. Phys. **B24**, 3633 (1991).

[70]. F. A. Gianturco and D. G. Thompson, J. Phys. **B13**, 3077 (1980).

[71]. L. M. Brescansin, M. A. P. Lima, T. L. Gibson and V. McKoy, J. Chem. Phys. **85**, 1854 (1986).

[72]. F. A. Gianturco and S. Sialla, J. Chem. Phys. **87**, 6468, (1987).

[73]. H. Sato, M. Kimura and K. Fujima, Chem. Phys. Lett. **145**, 21 (1988).

[74]. T. N. rescigno and B. H. Lengsfield, Z. Phys. **D24**, 117 (1992).

[75]. C. Szmytkowski and K Maciag, Chem. Phys. Lett. **129**, 321 (1986).

[76]. K. Rohr, J. Phys. **B11**, 4109 (1978).

[77]. S. J Buckman, private communication, (1992).

[78]. Ashok Jain and D. G. Thompson, J. Phys. **B17**, 443 (1983).

[79]. F. A. Gianturco, to be published in J. Phys. B (1992).

[80]. T. S. Rescigno, private communication, (1992).

[81]. V Krumbach, B M Nestmann and S D Peyerimhoff, J. Phys. **B22**, 4001-19 (1989).

[82]. O Suoka and S Mori, J. Phys. **B22**, 963 (1989).

[83]. W Hai–Xing and J H Moore, (as quoted in Krumbach et al 1989)

[84]. K D Jordan and P D Burrow, Acc. Chem. Res. **11**, 341 (1978).

[85]. M Tronc and L Malegat *Wavefunctions and Mechanism from Electron Scattering* (1984)

[86]. K H Kochem, W Sohn, K Jung, H Erhardt and E S Chang, J. Phys. **B18** 1253 (1985).

[87]. J A Tossel, J. Phys. **B18**, 387 (1985).

[88]. M E Riley and D G Truhlar, J. Chem. Phys. **63**, 2182 (1975).

[89]. S S Salvini and D G Thompson, J. Phys. **B14**, 3797 (1981).

[90]. F A Gianturco and S Sialla, J. Phys. **B20**, 3171 (1987).

[91]. M A Morrison, N F Lane and L A Collins, Phys. Rev. **A15**, 2186 (1977).

[92]. L A Collins, D W Norcross and G B Schmid, Comp. Phys. Commun. **21**, 79 (1982).

[93]. M A Morrison, Comp. Phys. Commun. **21**, 63 (1980). *Processes* ed. F A Gianturco and G Stefani (Berlin: Springer) pp. 24.

[94]. A D McLean and M Yoshimine, Int. Journal of Quantum. Chem., **iS**, 313 (1967).

[95]. N T Padial and D W Norcross, Phys. Rev. **A28**, 1590 (1984).

[96]. M A Khakoo, T Jayaweera, S Wang and S Trajmar, J. Phys. **B26**, 4844 (1993)

[97]. H Tawara, Y Itikawa, H Nishimura, H Tanaka and Y Nakamura Nuclear Fusion Supplement, **2**, 41 (1992).

[98]. L Hughes and J H McMillen, Phys. Rev. **44**, 876 (1933).

[99]. K H Kochem, W Sohn, K Jung, H Erhardt and E S Chang, J. Phys. **B18** 1253-66 (1985).

[100]. L Mu–Tao , L Brescansin, M A P Lima, L E Machado and E P Leal, J. Phys. **B23**, 4331 (1990).

[101]. D Thirumalai,K Onda and D G Truhlar, J. Chem. Phys. **74**, 526 (1981).

[102]. E Brüche, Ann. Phys., Lpz., **2**, 909 (1929).

[103]. Ashok Jain and D W Norcross, Phys. Rev. **A45**, 1644 (1992).

[104]. *Molecular Processes in Space*, ed. by Watanabe *et al*, (Plenum Publications, New York 1990).

[105]. A. V. Phelps, Ann. de Geophys., **28**, 611 (1972).

[106]. M. Hayashi, in *Swarm Studies and Inelastic Electron–Molecule Collisions*, ed. by Pirchford *et al*, (Springer–Verlag, New York 1985).

[107]. M. Inokuti, in *Proceedings of the Workshop on Electronic and Ionic Collision Cross–Section needed in the Modelling of Radiation Interactions with Matter*, (Argonne National Laboratory, 84–28, 1983).

[108]. R. L. Platzman, Int. J. Appl. Radiat. Isot. **10**, 116 (1961).

[109]. M. Inokuti, Y. K. Kim and R. L. Platzman, Phys. Rev. **164**, 55 (1967).

[110]. M. Inokuti, Rev. Mod. Phys., **43**, 297 (1971).

[111]. M. Inokuti, R. P. Saxon and J. L. Dehmer, J. Radiat. Phys. Chem. **7**, 109 (1975).

[112]. M. Inokuti and M. R. C. McDowell, J. Phys. **B7**, 2382 (1974).

[113]. M. Inokuti, Y. Itikawa and J. E. Turner, Rev. Mod. Phys., **50**, 23 (1978).

[114]. Ashok Jain and D. G. Thompson, J. Phys. **B16**, 1113 (1983).

[115]. J. K. O'Connel and N. F. Lane, Phys. Rev. **A27**, 1893 (1983).

[116]. N. T. Padial and D. W. Norcross, Phys. Rev. **A29**, 1742 (1984).

[117]. G. Staszewska, D. W. Schwenke, D. Thirumalai and D. G. Truhlar, J. Phys. **B16**, L281 (1983); Phys. Rev. **A28**, 2740 (1983); G. Staszewska, D. W. Schwenka and D. G. Truhlar, J. Chem. Phys. **81**, 335 (1984); Phys. Rev. **A29**, 3078 (1984).

[118]. F. Calogero, *Variable Phase Approach to Potential Scattering*, (Academic Press, New York 1974).

APPENDIX

PARTIAL DIFFERENTIAL EQUATION APPROACH TO ELECTRON, POSITRON-MOLECULE SCATTERING

By

Charles A. Weatherford

TABLE OF CONTENTS

1. ABSTRACT

This is to be considered as a final report on a subsection of the Air Force contract 27256-PH-SAH (Dr. Ashok Jain, Principal Investigator, Dr. Charles A. Weatherford, Co-Investigator).

The present portion of the research involves an attempt to go beyond the standard approach to electron-polyatomic scattering, wherein the use of the partial differential equation (PDE) approach to electron or positron molecule scattering in the low to intermediate energy regime is utilized. The research attempts to avoid single-center expansions of bound and continuum wavefunctions.

The body of the report consists of a narrative describing the rationale for three papers which constitute the appendix (two are unpublished, and one is accepted for publication in the Physical Review A), as well as a description of the new application of finite elements to the PDE approach to electron-polyatomic scattering.

2. INTRODUCTION

The present document c utes the final report on a subsection of the contract 27256-PH-SAH (Dr. Ashok Jain, Principal Investigator, Dr. Charles A. Weatherford, Co-Investigator) for the benefit of the United States Air Force. The present project is entitled "Partial Differential Equation Approach to Electron, Positron-Molecule Scattering." The research in scattering theory involved the calculation of electron collision cross sections for low to intermediate energy interactions with various diatomic and polyatomic molecules. This subsection involves the application and extension of the Partial Differential Equation (PDE) method[1-10] to electron-molecule sc ng In doing so, single-center expansions are avoided and thus new methods of calculating he required multicenter integrals have been developed.

Among the computational techniques that have been used to compute the scattering cross sections, one of the most common elements is the expansion of the continuum wave function in partial waves - that is, in spherical harmonics. The resulting variational treatment leads to sets of coupled integro-ordinary differential equations.[11-17] Over the past number of years, the direct solution of the partial differential equations (PDEs) has been accomplished[1-10] with great success. The code is still in the development stage, however. The code is being generalized to use a finite element representation of the Laplacian. Also, no attempt has as yet been made to exploit the multiprocessor environment of the newest supercomputers. In the present research, we have adapted the finite element PDE (FEPDE) code to a mutiprocessor environment.[18] Specifically, we are using the massively parallel environment (Connection Machine, CM-5). In doing so, we have begun to use multigrid[19-21] technology.

In the remainder of this report, we will present: section 3 briefly explains the rationale for the three papers included in the present report as appendices; section 4.A describes the basics of the Partial Differential Equation Theory; section 4.B describes the generalization to a finite element discretization; section 5 contains the references; the Appendices are given as section 6.

3. RATIONALE FOR APPENDICES

The present research constitutes an attempt to establish an *ab initio* computational approach to electron and positron-polyatomic scattering. As such, it avoids single-center expansions of the bound and continuum wavefunctions. The longer-range objective is to also go beyond phenomenological potentials and construct a method with an *ab initio* potential including polarization effects.

Appendix 6.A ("Addition Theorems for Coulomb Sturmians in Coordinate and Momentum Space") consists of an as yet, unsubmitted paper describing a new approach (developed by the author) to calculate all required bound-state molecular multicenter integrals using exponential basis functions. The method is still being developed, but show great promise.

Appendix 6.B ("Schrödinger Equation Mesh Requirements in the Finite Difference Discretization for Non-Spherical Potentials") describes a mesh convergence study using the finite difference discretization of the continuum Schrödinger equation. The convergence turned out to be rather disappointing. This along with ease of coding considerations, has led the author to adopt the finite element discretization descrived in Section V.B of this report.

Finally, Appendix 6.C (" Completion of hybrid theory calculation of the Π_g resonance in electron-N_2 scattering describes the latest calculation which has been completed using the finite difference discretization of the continuum Schrödinger Equation. This paper is to be published in the April 1994 issue of the Physical Review A.

4. PDE APPROACH TO ELECTRON-MOLECULE SCATTERING

Narrative A:

Partial Differential Equation Theory

This proposal concerns the Quantum Scattering description of two colliding systems. It considers the solution of the time-independent Schrödinger equation with two bodies in both the initial and final channels. The non-relativistic velocity regime is considered. The collision energy is low enough so that the Born approximation is not valid. Although the basic equations to be solved are prototypes for a large number of collision systems in atomic and molecular physics and quantum chemistry, the theory herein presented, specializes to electron-molecule scattering.

The central idea behind the theory is the desire to avoid partial-wave expansions of the scattering wavefunction. This is particularly desirable when the interaction potentials are highly non-spherical. The Partial Differential Equation (PDE) method has proven to be an extremely stable and efficient solution technique for the close-coupling equations that occur in electron-molecule scattering[1-10]. This has proven to be especially true on vector computers. It is anticipated that the use of parallel processors will also allow for an even greater efficiency of computation.

The basic equations to be solved are illustrated by the static exchange equation [3]

$$[\hat{\nabla}^2 + k^2]F(\vec{r}) = 2V(\vec{r})F(\vec{r}) - 2\sum_{i=1}^{N_E} \hat{W}_{\alpha_i}(\vec{r})\Phi_{\alpha_i}(\vec{r}). \tag{1}$$

This is the most simple but reasonably realistic equation that is encountered in electron-molecule scattering. F represents the Continuum orbital; $\vec{r}$ represents the continuum electron position vector; $\hat{W}$, the exchange kernel, is given by

$$\hat{W}_{\alpha_i}(\vec{r}) = \int d\vec{x}\ \Phi_{\alpha_i}(\vec{x})\frac{1}{|\vec{r}-\vec{x}|}F(\vec{x}). \tag{2}$$

Φ is a bound orbital of the target molecule. Realize that

$$\hat{\nabla}^2(|\vec{r}-\vec{x}|^{-1}) = -4\pi\delta(\vec{r}-\vec{x}). \tag{3}$$

Then, two coupled equations, which must be solved simultaneously, are then obtained

$$\begin{aligned}[\hat{\nabla}^2 + k^2]F(\vec{r}) =& 2V(\vec{r})F(\vec{r}) \\ & -2\sum_{i=1}^{N_E}\Phi_{\alpha_i}(\vec{r})\hat{W}_{\alpha_i}(\vec{r})\end{aligned} \tag{4}$$

$$\hat{\nabla}^2\hat{W}_{\alpha_i}(\vec{r}) = -4\pi\Phi^*_{\alpha_i}(\vec{r})F(\vec{r}) \tag{5}$$

$\hat{W}$ plays the part of a pseudo-continuum orbital. It has the value of zero on the large r boundary. There are as many inhomogeneous equations like (5) as there are bound molecular orbitals.

Eqs. (4) and (5) are elliptic PDEs. They are solved by applying a finite element approximation to $\hat{\nabla}^2$ to produce

$$\underline{A}\underline{F} = \underline{B} \tag{6}$$

$\underline{A}$ is the block tridiagonal coefficient matrix, $\underline{F}$ is the solution vector, and $\underline{B}$ is the boundary vector.

At the $r = \rho$ boundary, the partial-wave solutions are extracted by expanding the PDE solution, for each symmetry m, in partial waves.

$$F^m(\vec{r}) = \sum_{l_i} a_{l_i} \sum_{l_j} f^m_{l_i l_j}(r) Y^m_{l_j}(\theta,\phi) \tag{7}$$

The $a's$ are arbitrary amplitudes. The $f's$ have the form

$$f_{l_i l_j}(r) = S_{l_i}(r)P_{l_i l_j}(r) + C_{l_i}(r)Q_{l_i l_j}(r) \tag{8}$$

The S and C are spherical Bessel functions if the target is neutral and Coulomb functions if the target is charged. The value $r = \rho$ is determined by the range of the exchange contribution. The P and Q can be combined into a multidimensional vector I and propagated to an approximate ∞.

$$\underline{I}(r_f) = \underline{T}(r_f)\underline{I}(r_i) \tag{9}$$

$\underline{T}$ is the propagator. The reaction matrix is then computed by

$$\underline{K} = \underline{QP}^{-1} \tag{10}$$

We have generalized the PDE method to treat charged targets and multichannels in the fixed nuclei approximation (FNA). This means that the S and C are Coulomb funtions for charged targets. To treat general open shell targets, we must expand

$$\begin{aligned}\Psi^m =& \hat{A}\sum_{i=1}^{n_T}\Phi_i(1,\ldots,N)F_{ij}^m(N+1) \\ &+\sum_{a=1}^{n_c}\beta_i(1,\ldots,N+1)C_{a,j}\end{aligned} \tag{11}$$

Here, the β's are correlation terms. This results in the equation

$$\begin{aligned}[\hat{\nabla}^2 + k_i^2]F_{ik}^m(\vec{r}) =& 2\sum_{j=1}^{n_t}[V_{ij}(\vec{r}) + \hat{W}_{ij}(\vec{r})]F_{jk}^m(\vec{r}) \\ &+2\sum_{a=1}^{n_c}U_{ia}(\vec{r})C_{ak}\end{aligned} \tag{12}$$

Note that the Lagrange multipliers are not needed since the orthogonality is enforced by the specification of the value of 0 on the $r = \rho$ boundary in the B vector. They can be put in as an internal check (which we do). The C in (12) satisfies

$$\sum_{b=1}^{n_c}\Omega_{ab}C_{bj} + \sum_{i=1}^{n_t}\langle U_{ia}|F_{ij}^m\rangle = 0 \tag{13}$$

where $a = (1,\ldots,n_c)$ and $j = (1,\ldots,n_t)$, and j is fixed. U and Ω are defined by

$$U_{ia}(\vec{r}) = \sum_{\alpha_i=1}^{n_c}\langle\Phi_{\alpha_i}|\hat{H}_{N+1} - E|\beta_a\rangle \tag{14}$$

$$\Omega_{ab} = \langle\beta_a|\hat{H}_{N+1} - E|\beta_b\rangle \tag{15}$$

We might note that the correlation terms are of two types: (1) those that are required to relax orthogonality and ; (2) those that are required to produce projectile-target correlation (both short and long range).

Eqs. (12) are solved in the standard manner. See for example, Ref. 22. In this procedure, F is expanded as (drop the m symmetry notation)

$$F_{ik}(\vec{r}) = F_{ik}^{(0)}(\vec{r}) + \sum_{a=1}^{n_c} F_i^{(a)}(\vec{r}) C_{ak} \tag{16}$$

Then the actual equations to be solved are

$$[\hat{\nabla}^2 + k_i^2] F_{ik}^{(0)}(\vec{r}) = 2 \sum_{j=1}^{n_t} [V_{ij}(\vec{r}) + \hat{W}_{ij}^{(0)}(\vec{r})] F_{jk}^{(0)}(\vec{r}) \tag{17}$$

$$\begin{aligned} [\hat{\nabla}^2 + k_i^2] F_i^{(a)}(\vec{r}) =& 2 \sum_{j=1}^{n_t} [V_{ij}(\vec{r}) + \hat{W}_{ij}^{(a)}(\vec{r})] F_j^{(a)}(\vec{r}) \\ & + 2 U_{ia}(\vec{r}) \end{aligned} \tag{18}$$

The W's are here defined by

$$\hat{\nabla}^2 \hat{W}_{ij}^{(0)}(\vec{r}) = -4\pi \sum_{k=1}^{n_t} \overline{\Phi}_{ik}^*(\vec{r}) F_{kj}^{(0)}(\vec{r}) \tag{19}$$

$$\hat{\nabla}^2 \hat{W}_{ij}^{(a)}(\vec{r}) = -4\pi \sum_{k=1}^{n_t} \overline{\Phi}_{ik}^*(\vec{r}) F_k^{(a)}(\vec{r}) \tag{20}$$

Thus the formalism is similar to that of Ref. 22. The primary difference is that we are solving PDE's instead of ordinary differential equations.

Each of the Eqs. (17) and (18) may be solved independly on different processors and then combined after solution. For those correlation terms included in Eq. (12) that are not required to relax orthogonality, an optical potential will be constructed in the manner of Schneider and Collins[23].

Narrative B:

Finite Element Discretization

A short outline of the Finite Element method is presented below:

- Time-independent Schrödinger equation for e^--molecule scattering in the Fixed Nuclei Approximation in 3D using spherical coordinates:

$$\left[\frac{\partial^2}{\partial r^2}+\frac{2}{r}\frac{\partial}{\partial r}+\frac{1}{r^2}\frac{\partial^2}{\partial\theta^2}+\frac{cot\theta}{r^2}\frac{\partial}{\partial\theta}+\frac{1}{r^2 sin^2\theta}\frac{\partial^2}{\partial\phi^2}+k^2\right]\Psi(r,\theta,\phi)= 2V(r,\theta,\phi)\Psi(r,\theta,\phi) \tag{21}$$

- Solve by the method of Finite Elements:

1. Divide solution space into non-overlapping domains called "finite elements" ;
2. Define local basis functions within each element–in the present case, 5th order Hermite polynomials;
3. Discretize in each element by the Galerkin method and implicitly form global element matrix;
4. Form global connected matrix by enforcing continuity of the solution and its derivatives across element boundaries;
5. Form boundary reduced connected matrix and boundary vector; $\mathbf{A}; \vec{B} \ni$

$$\mathbf{A}\vec{X}=\vec{B} \tag{22}$$

6. Solve simultaneous equations by direct LU

$$\vec{X}=\mathbf{A}^{-1}\vec{B} \tag{23}$$

- Hermite Interpolation

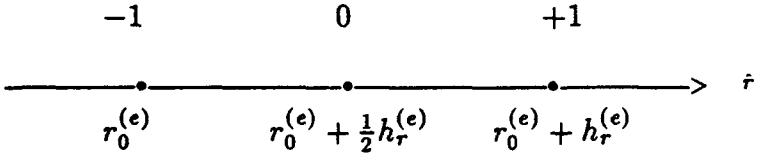

In terms of local variables $x_i : \{-1, 0, +1\}_{i=1}^{3}$

$$\psi^{(e)}(x) = \sum_{i=1}^{6} \psi_i^{(e)} p_i(x) \tag{24}$$

where

$$\begin{bmatrix} \psi_1^{(e)} \\ \psi_2^{(e)} \\ \psi_3^{(e)} \\ \psi_4^{(e)} \\ \psi_5^{(e)} \\ \psi_6^{(e)} \end{bmatrix} = \begin{bmatrix} \psi^{(e)}(x_1) \\ \frac{\partial}{\partial x}\psi^{(e)}|_{x_1} \\ \psi^{(e)}(x_2) \\ \frac{\partial}{\partial x}\psi^{(e)}|_{x_2} \\ \psi^{(e)}(x_3) \\ \frac{\partial}{\partial x}\psi^{(e)}|_{x_3} \end{bmatrix} \tag{25}$$

and $p_i(x)$ is determined from

$$p_i(x) = \sum_{j=1}^{6} g_{ij} x^{j-1} \tag{26}$$

$$p_i(x_j) = \delta_{ij} \quad for \quad i = 1,3,5 \quad and \quad j \epsilon \{x_1, x_2, x_3\} \tag{27}$$

$$\frac{d}{dx} p_i(x)|_{x_j} = \delta_{ij} \quad for \quad i = 2,4,6 \quad and \quad j \epsilon \{x_1, x_2, x_3\} \tag{28}$$

$$p_1(x) = g_{11} + g_{12}x + g_{13}x^2 + g_{14}x^3 + g_{15}x^4 + g_{16}x^5 \tag{29}$$

$$\frac{d}{dx} p_2(x) = g_{22} \quad 2g_{23}x + 3g_{24}x^2 + 4g_{25}x^3 + 5g_{26}x^4 \tag{30}$$

$$p_3(x) = g_{31} + g_{32}x + g_{33}x^2 + g_{34}x^3 + g_{35}x^4 + g_{36}x^5 \tag{31}$$

$$\frac{d}{dx} p_4(x) = g_{42} + 2g_{43}x + 3g_{44}x^2 + 4g_{45}x^3 + 5g_{46}x^4 \tag{32}$$

$$p_5(x) = g_{51} + g_{52}x + g_{53}x^2 + g_{54}x^3 + g_{55}x^4 + g_{56}x^5 \tag{33}$$

$$\frac{d}{dx} p_6(x) = g_{62} + 2g_{63}x + 3g_{64}x^2 + 4g_{65}x^3 + 5g_{66}x^4 \tag{34}$$

Now implement conditions (27) and (28)

$$\begin{bmatrix} g_{11} & g_{12} & g_{13} & g_{14} & g_{15} & g_{16} \\ g_{21} & g_{22} & g_{23} & g_{24} & g_{25} & g_{26} \\ g_{31} & g_{32} & g_{33} & g_{34} & g_{35} & g_{36} \\ g_{41} & g_{42} & g_{43} & g_{44} & g_{45} & g_{46} \\ g_{51} & g_{52} & g_{53} & g_{54} & g_{55} & g_{56} \\ g_{61} & g_{62} & g_{63} & g_{64} & g_{65} & g_{66} \end{bmatrix} \begin{bmatrix} 1 & 0 & 1 & 0 & 1 & 0 \\ -1 & 1 & 0 & 1 & 1 & 1 \\ 1 & -2 & 0 & 0 & 1 & 2 \\ -1 & 3 & 0 & 0 & 1 & 3 \\ 1 & -4 & 0 & 0 & 1 & 4 \\ -1 & 5 & 0 & 0 & 1 & 5 \end{bmatrix} = \vec{1} \tag{35}$$

The expression for $\psi^{(e)}$ in terms of global variables can now be written using

$$\begin{aligned} r &= r_0^{(e)} + h_r^{(e)} \frac{(1+x)}{2} \\ x &= -1 + \frac{2}{h_r^{(e)}}[r - r_0^{(e)}] \end{aligned} \tag{36}$$

In order to go to a global representation of (4), $\psi^{(e)}(r)$, it is not necessary to let $x \rightarrow r$ in $p_i(x)$. The global operators can be transformed to local operators which operate only on the piecewise continuous polynomials within each element

$$\frac{d}{dr} = \frac{dx}{dr}\frac{d}{dx} = \frac{2}{h_r^{(e)}}\frac{d}{dx} \tag{37}$$

$$\frac{d^2}{dr^2} = \left[\frac{2}{h_r^{(e)}}\right]^2 \frac{d^2}{dx^2} \tag{38}$$

So we can simply say

$$\Psi^{(e)}(r) = \sum_{i=1}^{6} \psi_i^{(e)} p_i(x) \tag{39}$$

However, the problem with (19) is that $\psi_i^{(e)}$, for $i = 2, 4, 6$, represents derivatives of $\Psi^{(e)}(r)$ with respect to the local variable x and we need it to represent derivatives with respect to the global variable r.

$$\frac{\partial \psi^{(e)}(x)}{\partial x} = \frac{\partial r}{\partial x}\frac{\partial \psi^{(e)}(r)}{\partial r} = \frac{1}{2} h_r^{(e)} \frac{\partial \psi^{(e)}(r)}{\partial r} \tag{40}$$

thus

$$\Psi^{(e)}(r) = \sum_{i=1,3,5} \psi_i^{(e)} p_i(x) + \sum_{i=2,4,6} \frac{1}{2} h_r^{(e)} \frac{\partial \psi^{(e)}(r)}{\partial r} p_i(x) \tag{41}$$

Let us now write

$$\Psi^{(e)}(r) = \sum_{i=1}^{6} \Psi_i^{(e)} P_i^{(e)}(x) \tag{42}$$

such that

$$\Psi_i^{(e)} = \left\{ \begin{array}{ll} \psi_i^{(e)} & for\ i = 1,3,5 \\ \frac{\partial \psi^{(e)}(r)}{\partial r}|_{r_i = r_0^{(e)} + h_r^{(e)} \frac{(1+x_i)}{2}} & for\ i = 2,4,6 \end{array} \right\} \tag{43}$$

and

$$P_i^{(e)}(x) = \left\{ \begin{array}{ll} p_i(x) & for\ i = 1,3,5 \\ h_r^{(e)} p_i(x) & for\ i = 2,4,6 \end{array} \right\} \tag{44}$$

In Fig. 1, a short description is presented of the derivation of the scattering amplitude in the fixed-nuclei approximation for electron-polyatomic scattering.

In Fig. 2, a comparison at the static level is made between the results of Jain, using the single-center partial-wave method, and the present finite element method for e-CH_4, in the A_1 symmetry. This demonstrates that the basic discretization is working. It remains to incorporate the exchange effect and to account for polarization.

FIXED-NUCLEI AMPLITUDE FOR e-POLYATOMIC SCATTERING

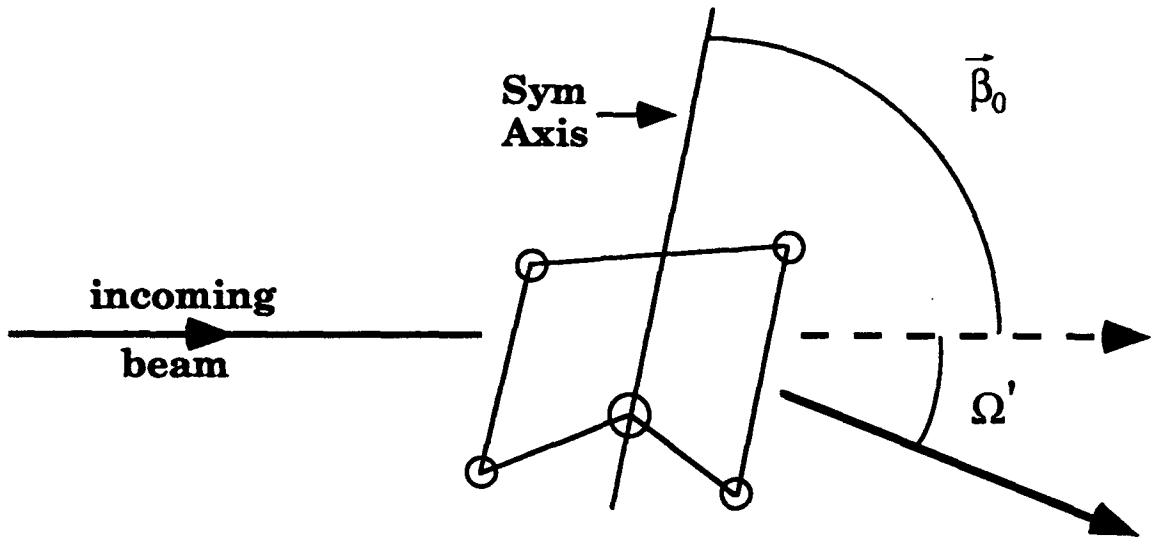

Incoming Wave Transformed To Body Frame

$$Y_{l_1}^0(\Omega') = \sum_m Y_{l_1}^m(\Omega) D_{0m}^{(l_1)^*}(\vec{\beta}_0)$$

Scattering Of $Y_l^m(\Omega)$ By Polyatomic In Body Frame

$$\hat{S}Y_l^m(\Omega) \rightarrow \sum_{l_2} \sum_{m_2} a_{mm_2}^{(l_1 l_2)} Y_{l_2}^{m_2}(\Omega)$$

Transform $Y_{l_2}^{m_2}(\Omega)$ Back To Lab Frame

$$Y_{l_2}^{m_2}(\Omega) = \sum_{m'} D_{m_2 m'}^{(l_2)}(\vec{\beta}_0) Y_{l_2}^{m'}(\Omega')$$

In Total

$$\hat{S}Y_{l_1}^0(\Omega') = \sum a_{mm_2}^{(l_1 l_2)} D_{0m}^{(l_1)^*}(\vec{\beta}_0) D_{m_2 m'}^{(l_2)}(\vec{\beta}_0) Y_{l_2}^{m'}(\Omega')$$

General Form Of Fixed Nuclei Scattering Amplitude:

$$f(\vec{\beta}_0; \Omega') = \sum D_{0m}^{(l_1)^*}(\vec{\beta}_0) a_{mm_2}^{(l_1 l_2)} D_{m_2 m'}^{(l_2)}(\vec{\beta}_0) Y_{l_2}^{m'}(\Omega')$$

Figure 1. Short derivation of the form of the scattering amplitude for e-polyatomic scattering in the fixed-nuclei approximation.

5. REFERENCES

1. A. Temkin, in *Symposium on Electron – Molecule Collisions*, edited by I. Shimamura and M. Matsuzawa, (University of Tokyo, Tokyo, 1979), p. 59.
2. E.C. Sullivan and A. Temkin, Comput. Phys. Commun. **25**, 97 (1982).
3. K. Onda and A. Temkin, Phys. Rev. **A28**, 621 (1983).
4. C.A. Weatherford, K. Onda, and A. Temkin, Phys. Rev. **A31**, 3620 (1985).
5. C.A. Weatherford, *Proceedings of the* 1986 *NSESCC Users Conference*, edited by H. Eiserke (Goddard Space Flight Center, 1986).
6. C.A. Weatherford, F.B. Brown, and A. Temkin, Phys. Rev. **A35**, 4561 (1987).
7. C.A. Weatherford, F.B. Brown, and A. Temkin, *Proceedings of the Fifteenth International Conference on the Physics of Electronic and Atomic Collisions*, Brighton, United Kingdom, edited by M.J. Coggiola, D.L. Huestis, and R.P. Saxon, 268 (1987).
8. C.A. Weatherford, and A. Temkin, *Proceedings of the Fifteenth International Conference on the Physics of Electronic and Atomic Collisions Invited Papers*, Brighton, United Kingdom, edited by P. Burke and D. West, (1987).
9. W.M. Huo and C.A. Weatherford, *Proceedings of the Sixteenth International Conference on the Physics of Electronic and Atomic Collisions*, New York, N.Y., edited by A. Dalgarno, R.S. Freund, M.S. Lubell, and T.B. Lucatorto, 294 (1989).
10. A. Temkin and C.A. Weatherford, *Proceedings of the Sixteenth International Conference on the Physics of Electronic and Atomic Collisions Invited Papers*, New Haven, CT, edited by A. Herzenberg (1989).
11. N.F. Mott and H.S.W. Massey, *The Theory of Atomic Colisions* (Oxford Press, 2nd edition, 1949).
12. M.L. Goldberger and K.M. Watson, *Collision Theory*, (Wiley, 1964)
13. C.J. Joachain, *Quantum Collision Theory*, (North-Holland, 1975).

14. R.G. Newton, *Scattering Theory of Waves and Particles*, (Springer-Verlag, 2nd edition, 1982)
15. R.K. Nesbet, *Variational Methods in Electron – Atom Scattering Theory*, (Plenum, 1980).
16. J.R. Taylor, *Scattering Theory*, (Wiley, 1972).
17. N.F. Lane, Rev. Mod. Phys. **52**, 1980, 29 (1980).
18. K.A. Gallivan, M.T. Heath, E. Ng, J.M. Ortega, B.W. Peyton, R.J. Plemmons, C.H. Romine, A.H. Sameh, R.G. Voigt, *Parallel Algorithms for Matrix Computations*, (SIAM, 1990).
19. W. Hackbusch, *Multi – Grid Methods and Applications*, (Springer-Verlag, 1985).
20. W.L. Briggs, *A Multigrid Tutorial*, (SIAM, 1987).
21. S.F. McCormick, *Multilevel Projection Methods for Partial Differential Equations*, (SIAM, 1992).
22. W. Eissner and M.J. Seaton, J. Phys. B**5**, 2187 (1972).
23. B.I. Schneider and L.A. Collins, Phys. Rev. A**28**, 166 (1983).

6. APPENDICES

ADDITION THEOREMS FOR COULOMB STURMIANS IN COORDINATE AND MOMENTUM SPACE

by

Charles A. Weatherford
Physics Department
and
Institute For Molecular Computations
Florida A&M University
Tallahassee, FL 32307, USA

1. PRELIMINARIES

The problem of performing multicenter integrals over Slater-Type Orbitals is one of the classic problems of Quantum Chemistry.[1] Two of the most successful techniques for the evaluation of such integrals are the Löwdin α-function method[2-5] and the Fourier Transform technique.[6-8] An interesting variant of the Fourier Transform technique is based on the Fock hyperspherical projection of the momentum space hydrogenic orbitals onto a four dimensional hypersphere.[9,10] Some important applications of the Fock projection to the Slater integral problem are given in references 11 and 12.

We are interested in performing the following $4-$*center* electron repulsion integral:

$$E^{(nlm)_a(nlm)_b}_{(nlm)_c(nlm)_d}(\alpha_a,\alpha_b,\alpha_c,\alpha_d;\vec{A},\vec{B},\vec{C},\vec{D}) \equiv$$
$$\int d\vec{r}_1 S^{*m_a}_{(nl)_a}(\alpha_a,\vec{r}_1+\vec{A}\,)S^{m_b}_{(nl)_b}(\alpha_b,\vec{r}_1+\vec{B}\,) \qquad (1)$$
$$\times \int d\vec{r}_2 \frac{1}{|\vec{r}_1-\vec{r}_2|} S^{*m_c}_{(nl)_c}(\alpha_c,\vec{r}_2+\vec{C}\,)S^{m_d}_{(nl)_b}(\alpha_d,\vec{r}_2+\vec{D}\,)$$

The $S-$functions are Coulomb Sturmians (CSs).[13] The CSs are defined by[7]

$$S_{nl}^{m}(\alpha,\vec{r}) \equiv (-1)^{n+l-1}\alpha^{3/2}N_{nl}\; e^{-\alpha r}L_{n-l-1}^{(2l+1)}(2\alpha r)\mathcal{Y}_{l}^{m}(2\alpha\vec{r}\,) \tag{2}$$

where the phase factor $(-1)^{n+l-1}$ has been introduced in the manner of Koga and Matsuhashi.[14] Then

$$N_{nl} = 2^{3/2}\left[\frac{(n-l-1)!}{2n(n+l)!}\right]^{1/2} \tag{3}$$

is the normalization constant, L is a Laguerre polynomial (same definition as given in Arfken[15]) given by

$$L_{n}^{(\beta)}(x) = \binom{n+\beta}{n}\,{}_1F_1(-n;\beta+1;x) \tag{4}$$

where ${}_1F_1$ is a confluent hypergeometric function[16] and $\mathcal{Y}$ is a solid spherical harmonic given by

$$\mathcal{Y}_{l}^{m}(\vec{r}) = r^{l}Y_{l}^{m}(\hat{r}) \tag{5}$$

and Y is a regular spherical harmonic.[15] The series for L terminates in the present case and gives

$$L_{n-l-1}^{(2l+1)}(2\alpha r) = \sum_{\tau=1}^{n-l} B_{\tau nl}(2\alpha r)^{\tau-1} \tag{6}$$

$$B_{\tau nl} = \frac{(-1)^{\tau-1}(n+l)!}{(n-l-\tau)!(2l+\tau)!(\tau-1)!} \tag{7}$$

The E integral is the most general integral which is encountered when non-correlated basis functions are used in an LCAO procedure for CI calculations. In the present work, addition theorems (which separate integration variables) are derived for Coulomb Sturmian functions and modified Coulomb Sturmian functions (Ψ),

$$\Psi_{nl}^{m}(\alpha,\vec{r}) \equiv \frac{n}{\alpha r}S_{nl}^{m}(\alpha,\vec{r}) \tag{8}$$

in coordinate and momentum space. The Coulomb Sturmians and their Fourier Transforms, are complete in the sense of distributions in Sobolev space[7] $W_2^{(1)}(\mathbf{R}^3)$, which is

a proper subset of Hilbert space $L^2(\mathbf{R}^3)$. In this regard, a standard Slater Type Orbital (STO) defined by

$$\chi_{nl}^{m}(\alpha,\vec{r}) = N_n \alpha^{n+1/2} r^{n-1} e^{-\alpha r} Y_l^{m_j}(\hat{r}) \tag{9}$$

and

$$N_n = \frac{2^{n+\frac{1}{2}}}{[(2n)!]^{\frac{1}{2}}} \tag{10}$$

may be expanded in a finite linear combination of Coulomb Sturmians and *vice versa*.[17]

$$\chi_{(nl)_i}^{m_i}(\alpha,\vec{r}\,) = \alpha^{1/2} \sum_{n_f=l_i+1}^{n_i} b_{n_f}^{(nl)_i} S_{n_f l_i}^{m_i}(\alpha,\vec{r}\,) \tag{11}$$

with

$$\begin{aligned} b_{n_f}^{(nl)_i} &= (-1)^{n_f+l_i}\left[\frac{2n_f(l_i+1)(n_f-l_i-1)!(n_f+l_i)!}{(2n_i)!}\right]^{\frac{1}{2}} \\ &\times \sum_{\sigma=1}^{n_f-l_i} \frac{(-1)^{\sigma}(n_i+l_i+\sigma-1)!}{(n_f-l_i-\sigma)!(2l_i+\sigma)!(\sigma-1)!} \end{aligned} \tag{12}$$

and *vice versa*

$$S_{(nl)_i}^{m_i}(\alpha,\vec{r}\,) = \alpha^{-1/2} \sum_{n_f=l_i+1}^{n_i} a_{n_f}^{(nl)_i} \chi_{n_f l_i}^{m_i}(\alpha,\vec{r}\,) \tag{13}$$

$$\begin{aligned} a_{n_f}^{(nl)_i} &= (-1)^{n_i+l_i-1}\left[\frac{(n_i-l_i-1)!(n_i+l_i)!}{n_i}\right]^{\frac{1}{2}} \\ &\times \frac{[(n_f)!]^{\frac{1}{2}}}{(n_i-n_f)!(n_f+l_i)!(n_f-l_i-1)!} \end{aligned} \tag{14}$$

It is useful to "equalize" the screening parameters in one electron, single center densities, composed of CSs basis functions. To accomplish this, it is first useful to equalize the screening parameters for densities composed of STOs. Some trivial algebra produces

$$\Upsilon_{(nl)_1(nl)_2}^{m_1 m_2}(\alpha,\beta,\vec{r}) = B_{n_1 n_2}(\alpha,\beta)\Upsilon_{(nl)_1(nl)_2}^{m_1 m_2}(\gamma,\gamma,\vec{r}) \tag{15}$$

where

$$B_{n_1 n_2}(\alpha,\beta) = \frac{N_{n_1}(\alpha)N_{n_2}(\beta)}{N_{n_1}(\gamma)N_{n_2}(\gamma)} \tag{16}$$

where $\gamma = \frac{\alpha+\beta}{2}$ and Υ is the STO one electron density defined by

$$\Upsilon^{m_1 m_2}_{(nl)_1(nl)_2}(\alpha,\beta,\vec{r}) \equiv \chi^{*m_2}_{(nl)_2}(\beta,\vec{r}\,)\chi^{m_1}_{(nl)_1}(\alpha,\vec{r}\,) \tag{17}$$

Then, defining the one electron, single center, CS density by

$$\Omega^{m_1 m_2}_{(nl)_1(nl)_2}(\alpha,\beta,\vec{r}) \equiv S^{*m_2}_{(nl)_2}(\beta,\vec{r}\,)S^{m_1}_{(nl)_1}(\alpha,\vec{r}\,) \tag{18}$$

the required expression (which equalizes the CS screening parameters for the density Ω), is obtained by first using Eq. (13) for each CS in Ω, then using Eq. (15) to equalize the screening parameters in Υ, and then using Eq. (11) to recover the required Ω with equalized screening parameters. The result is

$$\Omega^{m_1 m_2}_{(nl)_1(nl)_2}(\alpha,\beta,\vec{r}) = \sum_{n_3=l_1+1}^{n_1}\sum_{n_5=l_1+1}^{n_3}\sum_{n_4=l_2+1}^{n_2}\sum_{n_6=l_2+1}^{n_4} A^{(nl)_1(nl)_2}_{n_3 n_4 n_5 n_6}(\alpha,\beta)\Omega^{m_1 m_2}_{(n_6 l_1)(n_5 l_2)}(\gamma,\gamma,\vec{r}) \tag{19}$$

where

$$A^{(nl)_1(nl)_2}_{n_3 n_4 n_5 n_6}(\alpha,\beta) = \frac{(\alpha+\beta)}{2\alpha^{1/2}\beta^{1/2}} a^{(nl)_2}_{n_3} b^{n_3 l_2}_{n_5} a^{(nl)_1}_{n_4} b^{n_4 l_1}_{n_6} B_{n_3 n_4}(\alpha,\beta) \tag{20}$$

It is also useful to linearize the product of two CSs. To this end, we linearize the product of two STOs as per the following formula:

$$\Upsilon^{m_1 m_2}_{(nl)_1(nl)_2}(\alpha,\beta,\vec{r}) = C_{n_1 n_2}(\alpha,\beta)\sum_{l_3=|l_1-l_2|,2}^{l_1+l_2} D^{(lm)_1(lm)_2}_{l_3}\chi^{m_1-m_2}_{n_1+n_2-1,l_3}(\alpha+\beta,\vec{r}) \tag{21}$$

where

$$C_{n_1 n_2}(\alpha,\beta) = \frac{N_{n_1}(\alpha)N_{n_2}(\beta)}{N_{n_1+n_2-1}(\alpha+\beta)} \tag{22}$$

and

$$D_{l_3}^{(lm)_1(lm)_2} = (-1)^{m_1}\left[\frac{(2l_1+1)(2l_2+1)(2l_3+1)}{4\pi}\right]^{1/2} \begin{pmatrix} l_1 & l_2 & l_3 \\ 0 & 0 & 0 \end{pmatrix}\begin{pmatrix} l_1 & l_2 & l_3 \\ m_1 & -m_2 & m_2-m_1 \end{pmatrix} \tag{23}$$

Thus, the linearization of the Cs density is easily shown to give

$$\Omega_{(nl)_1(nl)_2}^{m_1 m_2}(\alpha,\beta,\vec{r}) = \sum_{n_f=|l_1-l_2|+1}^{n_1+n_2-1} \sum_{l_f=|l_1-l_2|,2}^{l_1+l_2} P_{(nl)_f}^{(nl)_1(nl)_2}(\alpha,\beta) S_{(nl)_f}^{m_1-m_2}(\alpha+\beta,\vec{r}) \tag{24}$$

where

$$\begin{aligned} P_{(nl)_f}^{(nl)_1(nl)_2}(\alpha,\beta) &= \int d\vec{r}\, \Psi_{(nl)_f}^{*m_1-m_2}(\alpha+\beta,\vec{r})\Omega_{(nl)_1(nl)_2}^{m_1 m_2}(\alpha,\beta,\vec{r}) \\ &= \frac{n_f}{[\alpha\beta(\alpha+\beta)]^{1/2}} D_{l_f}^{(lm)_1(lm)_2} \sum_{n_3=l_2+1}^{n_2} a_{n_3}^{(nl)_2} \sum_{n_4=l_1+1}^{n_1} a_{n_4}^{(nl)_1} \\ &\times \qquad C_{n_3 n_4}(\alpha,\beta)\; b_{n_f}^{(n_3+n_4-1,l_f)} \end{aligned} \tag{25}$$

It is important to note that all of the sums in Eqs. 24 and 25 are finite.

The CSs satisfy a partial differential equation[7] given by

$$[\nabla_{\vec{r}}^2 - \alpha^2] S_{nl}^m(\alpha,\vec{r}) = -\frac{1}{2\alpha^2}\Psi_{nl}^m(\alpha,\vec{r}) \tag{26}$$

This can be contrasted with the partial differential equation satisfied by the STOs

$$[\nabla_{\vec{r}}^2 - \alpha^2]\chi_{nl}^m(\alpha,\vec{r}) = V_{nl}(\alpha,r)\chi_{nl}^m(\alpha,\vec{r}) \tag{27}$$

where

$$V_{nl}(\alpha,r) = -\frac{2\alpha n}{r} - \frac{[l(l+1)-n(n-1)]}{r^2} \tag{28}$$

It can be easily demonstrated that the CSs satisfy a homogeneous Fredholm integral equation of the second kind[15]

$$S_{nl}^{m}(\alpha,\vec{r}) = \frac{1}{2\alpha^2}\int d\vec{x} G(\alpha,|\vec{r}-\vec{x}|)\Psi_{nl}^{m}(\alpha,\vec{x}) \tag{29}$$

where G is the Green's function (same as for the modified Helmholtz equation) and is given by

$$G(\alpha,|\vec{r}-\vec{x}|) = \frac{e^{-\alpha|\vec{r}-\vec{x}|}}{4\pi|\vec{r}-\vec{x}|} \tag{30}$$

The Green's function satisfies the partial differential equation

$$[\nabla_{\vec{r}}^2 - \alpha^2]G(\alpha,|\vec{r}-\vec{x}|) = -\delta(\vec{r}-\vec{x}) \tag{31}$$

The translation operator $\hat{T}_{\vec{A}} = e^{\vec{A}\cdot\vec{\nabla}_{\vec{A}}}$ (note that $\vec{\nabla}_{\vec{A}}$ has to be expressed in Cartesian coordinates for this expression to be valid) is defined by

$$\hat{T}_{\vec{A}}F(\vec{r}) = F(\vec{r}+\vec{A}) = F(\vec{r}_A) \tag{32}$$

where $\vec{r}_A = \vec{r}+\vec{A}$. Now an important characteristic of the Laplacian, which is well known, is its invariance with respect to translations

$$\nabla_{\vec{r}+\vec{A}}^2 = \nabla_{\vec{r}}^2 \tag{33}$$

Applying the translation operator to both sides of Eq. (26) and using Eq. (33) yields

$$[\nabla_{\vec{r}}^2 - \alpha^2]S_{nl}^{m}(\alpha,\vec{r}+\vec{A}) = -\frac{1}{2\alpha^2}\Psi_{nl}^{m}(\alpha,\vec{r}+\vec{A}) \tag{34}$$

It may be noted, in passing, that Eq. (34) can be used to generate an algebraic eigenvalue equation by expanding $S_{nl}^{m}(\alpha,\vec{r}+\vec{A})$ in terms of $S_{nl}^{m}(\alpha,\vec{r})$ and letting $\nabla_{\vec{r}}^2$ operate. Then premultiplication by $S_{nl}^{*m}(\alpha,\vec{r})$ is used and finally, integration over $d\vec{r}$. The result is an eigenvalue equation in which the exact eigenvalues are known. However, the coefficients (eigenvectors) in the aforementioned expansion, which result from the diagonalization of the coefficient matrix, are the desired quantities and unfortunately, these components have first order errors in them, as opposed to second order errors in the approximate eigenvalues.

Thus this procedure proves too slowly convergent[18] to be useful, without some systematic way of correcting the eigenvectors.

The integral equation solution to Eq. (34) can, nevertheless, be written

$$S_{nl}^{m}(\alpha,\vec{r}+\vec{A}) = \frac{1}{2\alpha^2}\int d\vec{x}\; G(\alpha,|\vec{r}-\vec{x}|)\Psi_{nl}^{m}(\alpha,\vec{x}+\vec{A}) \tag{35}$$

This can be contrasted with the result of applying the translation operator directly to both sides of Eq. (29) to give

$$S_{nl}^{m}(\alpha,\vec{r}+\vec{A}) = \frac{1}{2\alpha^2}\int d\vec{x}\; G(\alpha,|\vec{r}+\vec{A}-\vec{x}|)\Psi_{nl}^{m}(\alpha,\vec{x}) \tag{36}$$

Finally, the CSs satisfy the orthonormality conditions[7]

$$\int d\vec{r}\; \Psi_{(nl)_1}^{*m_1}(\alpha,\vec{r}\,)S_{(nl)_2}^{m_2}(\alpha,\vec{r}\,) = \delta_{(nlm)_1(nlm)_2} \tag{37}$$

and

$$\int d\vec{r}\; S_{(nl)_1}^{*m_1}(\alpha,\vec{r}\,)\Psi_{(nl)_2}^{m_2}(\alpha,\vec{r}\,) = \delta_{(nlm)_1(nlm)_2} \tag{38}$$

and the closure conditions[19]

$$\hat{1} = \sum_{nlm} |S_{nl}^{m}\rangle\langle\Psi_{nl}^{m}\,| \tag{39}$$

and

$$\hat{1} = \sum_{nlm} |\Psi_{nl}^{m}\rangle\langle S_{nl}^{m}\,| \tag{40}$$

and the single-center (equal screening constant), coordinate-space overlap of two CSs is given by[7,18]

$$\begin{aligned} O_{(nl)_1(nl)_2}^{m_1 m_2} &\equiv \int d\vec{r}\; S_{(nl)_2}^{*m_2}(\alpha,\vec{r}\,)S_{(nl)_1}^{m_1}(\alpha,\vec{r}\,) \\ &= \delta_{(lm)_1(lm)_2}\left[\gamma_{n_1 l_1}^{+}\delta_{n_2,n_1+1} + \delta_{n_2,n_1} + \gamma_{n_2 l_2}^{-}\delta_{n_2,n_1-1}\right] \end{aligned} \tag{41}$$

where

$$\gamma_{nl}^{\pm} = [\frac{(n \mp l)(n \pm l \pm 1)}{4n(n \pm 1)}]^{1/2} \tag{42}$$

When a sum, such as $\sum_{nlm}$ is indicated, it means

$$\left\{ \begin{array}{ll} n: & 1 \rightarrow \infty \\ l: & 0 \rightarrow n-1 \\ m: & -l, -l+1, \ldots, +l \end{array} \right\}$$

or, the order could be changed so that

$$\left\{ \begin{array}{ll} l: & 0 \rightarrow \infty \\ m: & -l, -l+1, \ldots, +l \\ n: & l+1 \rightarrow \infty \end{array} \right\}$$

The particular order used needs to be numerically tested. Note that the integrands of Eqs. (37), (38) and (41) are composed of CSs with the same screening parameters. The expression given in Eq. (41) is derived from Eq. (37) using the following recursion relation:

$$\begin{aligned} \alpha r \; S_{nl}^{m}(\alpha, \vec{r}) \; &= \; \frac{\gamma_{nl}^{+}}{(n+1)} \; S_{n+1,l}^{m}(\alpha, \vec{r}) \\ &\times n \; S_{nl}^{m}(\alpha, \vec{r}) \; + \; \frac{\gamma_{nl}^{-}}{(n-1)} \; S_{n-1,l}^{m}(\alpha, \vec{r}) \end{aligned} \tag{43}$$

These equations will prove useful in the discussions given below.

2. FOCK HYPERSPHERE AND ADDITION THEOREMS

The derivation of computable expressions for the integral in Eq. (1) involves the use of the relationship between Coulomb Sturmians and four dimensional spherical harmonics (Fock hyperspherical projection) and proceeds by representing the translation operator in coordinate space, and the translation operator in momentum space, on a basis of Coulomb Sturmians and their Fourier Transforms respectively. The resulting matrix representations of the translation operator in coordinate and momentum space are respectively, finite linear combinations of Coulomb Sturmians and their Fourier Transforms, and are both unitary. This can be demonstrated by the use of closure relations for the Coulomb Sturmians and their Fourier Transforms, which will be derived.

Filter and Steinborn[20] have given an addition theorem for orthonormalized Slaters (ONSs, orthonormalized functions built up from the STOs by analytical Gram-Schmidt orthonormalization) by using the translation operator explicitly and deriving a formula for the matrix elements of the translation operator. These results have been applied to the calculation of the ground state wavefunction of H_2^+ with somewhat disappointing results.[21]

The present work derives an addition theorem for the CSs, similar in structure, to the addition theorem of Filter and Steinborn for the ONSs. The present derivation, however, is quite different in approach. As is presented below, the present work exploits the Fourier transform of a CS[7] and the relationship of the Fourier transform to four-dimensional spherical harmonics[22] using the Fock hyperspherical projection.[9] The method is similar in many respects to techiniques of Shibuya and Wulfman[10] and to the work of Alper[11] and Novosadov.[12] The differences between these techniques and the present technique will be implicit in the derivation presented, and in the approach by which the addition theorem is used to evaluate the multicenter integrals. The work of Alper[11] is perhaps most closely related to the present methods.

The symmetric definition of the three-dimensional Fourier transform is first applied to a CS so that

$$S_{nl}^{m}(\alpha,\vec{r}) = (2\pi)^{-3/2} \int d\vec{p}\, e^{i\vec{r}\cdot\vec{p}}\, \overline{S}_{nl}^{\ m}(\alpha,\vec{p}) \tag{44}$$

$$\overline{S}_{nl}^{\ m}(\alpha,\vec{p}) = (2\pi)^{-3/2} \int d\vec{r}\, e^{-i\vec{p}\cdot\vec{r}}\, S_{nl}^{m}(\alpha,\vec{r}) \tag{45}$$

where $\overline{S}_{nl}^{\ m}$ is the Fourier transform of the CS (CSFT). Thus, it can be shown[7] that the single-center (equal screening constant), momentum-space overlap of two CSs is

$$\begin{aligned} O_{(nl)_1(nl)_2}^{m_1 m_2} &= \int d\vec{p}\, \overline{S}^{*m_2}_{(nl)_2}(\alpha,\vec{p}\,)\overline{S}^{m_1}_{(nl)_1}(\alpha,\vec{p}\,) \\ &= \delta_{(lm)_1(lm)_2}\left[\gamma^{+}_{n_1 l_1}\delta_{n_2,n_1+1} + \delta_{n_2,n_1} + \gamma^{-}_{n_2 l_2}\delta_{n_2,n_1-1}\right] \end{aligned} \tag{46}$$

The Fourier transform of Ψ can also be taken. Weniger[7] demonstrated the relationship between a CSFT and a four-dimensional spherical harmonic (the FDSH is the one used by Judd, Ref. 23) given by

$$Y_{nl}^{m}(\tau,\theta,\phi) = \frac{(\alpha^2+p^2)^2}{4\alpha^{5/2}}\overline{S}_{nl}^{\ m}(\alpha,\vec{p}) \tag{47}$$

where the relationship between τ (hyperangle) and α (screening parameter) is defined by

$$\xi = \frac{2\alpha p_x}{\alpha^2+p^2} = sin(\tau)sin(\theta)cos(\phi) \tag{48a}$$

$$\eta = \frac{2\alpha p_y}{\alpha^2+p^2} = sin(\tau)sin(\theta)sin(\phi) \tag{48b}$$

$$\zeta = \frac{2\alpha p_z}{\alpha^2+p^2} = sin(\tau)cos(\theta) \tag{48c}$$

$$\chi = \frac{\alpha^2-p^2}{\alpha^2+p^2} = cos(\tau) \tag{48d}$$

Thus α is a scaling parameter and

$$\xi^2+\eta^2+\zeta^2+\chi^2 = 1 \tag{49}$$

It is clear then that a point $\vec{p}$ of three-dimensional space is mapped (one-to-one) onto a surface of a four-dimensional unit sphere described by the angular variables ξ,η,ζ,χ. The following relationships are then determined.

$$sin^{i}(\tau) = \left[\frac{2\alpha p}{\alpha^2+p^2}\right]^{l} \tag{50}$$

$$d\hat{\Omega}_{\alpha}(\vec{p}) \equiv sin^2(\tau)sin(\theta)d\tau d\theta d\phi = \left[\frac{2\alpha}{\alpha^2+p^2}\right]^3 d\vec{p} \tag{51}$$

Do not confuse the four-dimensional spherical differential surface element $d\hat{\Omega}$ with the single center charge density of Eq. (18). The orthonormality conditions for the CSFTs and FDSHs are given by

$$\begin{aligned}\int_0^{\pi} d\tau\ sin^2(\tau)\int_0^{\pi} d\theta\ sin(\theta)\int_0^{2\pi} d\phi\ Y^{*\ m_1}_{(nl)_1}(\tau,\theta,\phi)Y^{m_2}_{(nl)_2}(\tau,\theta,\phi)&\\ = \int d\vec{p}\,\overline{S}^{*\ m_1}_{(nl)_1}(\alpha,\vec{p}\,)\overline{\Psi}^{\ m_2}_{(nl)_2}(\alpha,\vec{p}\,)&\\ = \int d\vec{p}\,\overline{\Psi}^{*\ m_1}_{(nl)_1}(\alpha,\vec{p}\,)\overline{S}^{\ m_2}_{(nl)_2}(\alpha,\vec{p}\,)&\\ = \delta_{(nlm)_1(nlm)_2}&\end{aligned} \tag{52}$$

where

$$\begin{aligned}\overline{\Psi}^{m}_{nl}(\alpha,\vec{p}\,) &= \frac{(\alpha^2+p^2)}{2\alpha^2}\overline{S}^{\ m}_{nl}(\alpha,\vec{p}\,) \\ &= \frac{2\alpha^{1/2}}{(\alpha^2+p^2)}Y^{m}_{nl}[\hat{\Omega}_{\alpha}(\vec{p})]\end{aligned} \tag{53}$$

The Shibuya and Wulfman[10] expansion of a plane wave in terms of CSs and FDSHs is given by

$$e^{i\vec{p}\cdot\vec{r}} = [\alpha 2^5\pi^3]^{1/2}\sum_{nlm}\frac{1}{(\alpha^2+p^2)}S^{m}_{nl}(\alpha,\vec{r})Y^{*\ m}_{nl}[\hat{\Omega}_{\alpha}(\vec{p})] \tag{54}$$

Eq. (54) may be compared with the expansion of a plane wave in terms of CSs and CSFTs given by

$$e^{i\vec{p}\cdot\vec{r}} = (2\pi)^{3/2}\sum_{nlm}\overline{\Psi}^{\ *\ m}_{nl}(\alpha,\vec{p}\,)S^{m}_{nl}(\alpha,\vec{r}\,) \tag{55}$$

or

$$e^{i\vec{p}\cdot\vec{r}} = (2\pi)^{3/2}\sum_{nlm}\overline{S}^{\ *\ m}_{nl}(\alpha,\vec{p}\,)\Psi^{m}_{nl}(\alpha,\vec{r}\,) \tag{56}$$

For later use, the Fourier transform representation of a three-dimensional Dirac delta function and the Coulomb potential may be written as

$$\delta(\vec{p}_2-\vec{p}_1) = \frac{1}{(2\pi)^3}\int d\vec{r}\ e^{i\vec{r}\cdot(\vec{p}_2-\vec{p}_1)} \tag{57}$$

$$\frac{1}{|\vec{r}_1-\vec{r}_2|} = \frac{1}{2\pi^2}\int d\vec{p}\ \frac{e^{i\vec{p}\cdot(\vec{r}_1-\vec{r}_2)}}{p^2} \tag{58}$$

The derivation of the addition theorem begins by applying the translation operator defined by Eq. (32) to both sides of Eq. (44). The result is

$$S^{m}_{nl}(\alpha,\vec{r}\pm\vec{R}\,) = (2\pi)^{-3/2}\int d\vec{p}\ e^{i\vec{r}\cdot\vec{p}}\ e^{\pm i\vec{R}\cdot\vec{p}}\ \overline{S}^{\ m}_{nl}(\alpha,\vec{p}) \tag{59}$$

The Shibuya and Wulfman plane wave expansion of Eq. (55), is used for the $\vec{r}$-containing plane wave term in the integrand of Eq. (59). The result is

$$S^{m_i}_{(nl)_i}(\alpha,\vec{r}\pm\vec{R}\,)=\sum_{(nlm)_f}Q_{(nlm)_i(nlm)_f}(\alpha,\pm\vec{R})S^{m_f}_{(nl)_f}(\alpha,\vec{r}) \tag{60}$$

where

$$Q_{(nlm)_i(nlm)_f}(\alpha,\pm\vec{R})=\int d\vec{p}e^{\pm i\vec{p}\cdot\vec{R}}\,\overline{\Psi}^{\,*\,m_f}_{(nl)_f}(\alpha,\vec{p}\,)\overline{S}^{\,m_i}_{(nl)_i}(\alpha,\vec{p}\,) \tag{61}$$

Then Eqs. (51) and (53) along with

$$\frac{1}{\alpha^2+p^2}=\frac{\pi}{2^{3/2}\alpha^2}\left[2Y^0_{10}[\hat{\Omega}_\alpha(\vec{p})]+Y^0_{20}[\hat{\Omega}_\alpha(\vec{p})]\right] \tag{62}$$

is used to transform the volume integral over $\vec{p}$ to an integral over the surface of a four-dimensional unit sphere with the result

$$Q_{(nlm)_i(nlm)_f}(\alpha,\pm\vec{R})=\int d\hat{\Omega}_\alpha(\vec{p})e^{\pm i\vec{p}\cdot\vec{R}}\,Y^{\,*\,m_f}_{(nl)_f}[\hat{\Omega}_\alpha(\vec{p})]Y^{\,m_i}_{(nl)_i}[\hat{\Omega}_\alpha(\vec{p})] \tag{63}$$

Note that $Y^0_{10}(\Omega)=[\pi 2^{1/2}]^{-1/2}$ and $Y^0_{20}(\Omega)=[\pi 2^{1/2}]^{-1/2}cos(\tau)$. The explicit evaluation of the integral in Eq. (63) proceeds by using Eq. (53), (55), and (62) along with

$$Y^{\,*\,m}_{nl}(\Omega)=(-1)^{l-m}Y^m_{nl}(\Omega) \tag{64}$$

and a very important linearization property of FDSHs.[23] This is a property of the FDSHs which allows the product of two FDSHs on the same hypersurface, to be written as a finite linear combination of a single FDSH on the same surface, and is central to the present strategy. This expression was earlier by Shibuya and Wulfman[10] and used to great advantage by Alper.[11] Actually, the result is probably most directly attributable to Biedenharn[22]. It may be expressed as

$$Y^{m_1}_{(nl)_1}[\hat{\Omega}_\alpha(\vec{p})]Y^{m_2}_{(nl)_2}[\hat{\Omega}_\alpha(\vec{p})]=$$

$$\times\sum_{n_3=|n_1-n_2|+1,2}^{n_1+n_2-1}\ \sum_{l_3=|l_1-l_2|,2}^{l_1+l_2}C(n_1l_1m_1,n_2l_2m_2;n_3l_3,m_1+m_2)\;Y^{m_1+m_2}_{n_3l_3}[\hat{\Omega}_\alpha(\vec{p})] \tag{65}$$

The ',2' on the sum indicates every other term is used. The C is defined by

$$C(n_1 l_1 m_1, n_2 l_2 m_2; n_3 l_3 m_3) = \left[\frac{(2l_1+1)(2l_2+1)n_1 n_2 n_3}{2\pi^2}\right]^{1/2} \times (l_1 m_1, l_2 m_2 | l_3, m_1+m_2) \begin{Bmatrix} \frac{(n_1-1)}{2} & \frac{(n_1-1)}{2} & \frac{l_1}{2} \\ \frac{(n_2-1)}{2} & \frac{(n_2-1)}{2} & \frac{l_2}{2} \\ \frac{(n_3-1)}{2} & \frac{(n_3-1)}{2} & \frac{l_3}{2} \end{Bmatrix} \tag{66}$$

The $(\cdots)$ term is a $Clebsch - Gordon\ coefficient$,[24] and

$$\begin{Bmatrix} \cdots \\ \cdots \\ \cdots \end{Bmatrix}$$

is a Wigner $9j$ coefficient.[24] The efficient evaluation of the $9j$ symbol is critical to the ultimate computational success of the present program. However, present and projected computer technology offers great encouragement in this regard. Even now, textbooks have reasonably adequate computer codes included in the appendices.[25]

The direct evaluation of Q is now straightforward, resulting in

$$Q_{(nlm)_1(nlm)_2}(\alpha, \pm\vec{R}) = \times \alpha^{-3/2} \sum_{n=max(|n_1-n_2|,1)}^{n_1+n_2} \sum_{l=|l_1-l_2|,2}^{min(n-1,l_1+l_2)} \Lambda_{nl}^{(nlm)_1(nlm)_2} S_{nl}^{m_1-m_2}(\alpha, \vec{R}) \tag{67}$$

Then

$$\Lambda_{nl}^{(nlm)_1(nlm)_2} = 2(-1)^{l_2-m_2}\pi^{5/2} B[(nl, m_1-m_2), (nlm)_1, (nlm)_2] \tag{68}$$

and

$$B[(nl, m_1-m_2), (nlm)_1, (nlm)_2] \equiv 2\Gamma[(nl, m_1-m_2), (nlm)_1, (n_2 l_2, -m_2), (100)] \Gamma[(nl, m_1-m_2), (nlm)_1, (n_2 l_2, -m_2), (200)] \tag{69}$$

where in general

$$\Gamma[(nlm)_1(nlm)_2(nlm)_3(nlm)_4] \equiv \int d\hat{\Omega}_\alpha(\vec{p})\ Y^{*\,m_1}_{(nl)_1}[\hat{\Omega}_\alpha(\vec{p})] Y^{m_2}_{(nl)_2}[\hat{\Omega}_\alpha(\vec{p})] Y^{m_3}_{(nl)_3}[\hat{\Omega}_\alpha(\vec{p})] Y^{m_4}_{(nl)_4}[\hat{\Omega}_\alpha(\vec{p})] \tag{70}$$

The evaluation of Γ proceeds by using Eqs. (52) and (65) to give

$$\begin{aligned}
&\Gamma[(nlm)_1(nlm)_2(nlm)_3(nlm)_4] = \\
&\times \sum_{n_5=|n_3-n_4|+1,2}^{n_3+n_4-1} \sum_{l_5=|l_3-l_4|,2}^{l_3+l_4} C(n_3 l_3 m_3, n_4 l_4 m_4; n_5 l_5, m_3+m_4) \\
&\times \sum_{n_6=|n_5-n_2|+1,2}^{n_5+n_2-1} \sum_{l_6=|l_5-l_2|,2}^{l_5+l_2} C(n_2 l_2 m_2, n_5 l_5, m_3+m_4, n_5 l_5, m_2+m_3+m_4) \\
&\times \quad \delta_{n_1,n_6}\delta_{l_1,l_6}\delta_{m_1,m_2+m_3+m_4}
\end{aligned} \tag{71}$$

Now, an addition theorem for Ψ can be derived, in an analogous fashion to the one given in Eq. (60) for S with the result of

$$\Psi^{m_i}_{(nl)_i}(\alpha, \vec{r} \pm \vec{R}\,) = \sum_{(nlm)_f} Q_{(nlm)_i(nlm)_f}(\alpha, \pm\vec{R}) \Psi^{m_f}_{(nl)_f}(\alpha, \vec{r}) \tag{72}$$

Note that the coefficient matrix Q is the same as in Eq. (60).

In a very similar manner, an addition theorem can be given for $\overline{S}$. It is

$$\overline{S}^{m_i}_{(nl)_i}(\alpha, \vec{p} \pm \vec{\rho}\,) = \sum_{(nlm)_f} R_{(nlm)_i(nlm)_f}(\alpha, \beta, \pm\vec{\rho}) \overline{S}^{m_f}_{(nl)_f}(\beta, \vec{p}) \tag{73}$$

with

$$R_{(nlm)_i(nlm)_f}(\alpha, \beta, \pm\vec{\rho}) = \int d\vec{r} e^{\mp i\vec{r}\cdot\vec{\rho}}\ \Psi^{*\,m_f}_{(nl)_f}(\beta, \vec{r}\,) S^{m_i}_{(nl)_i}(\alpha, \vec{r}\,) \tag{74}$$

The explicit evaluation of R is then possible and results in

$$\begin{aligned}
&R_{(nlm)_1(nlm)_2}(\alpha, \beta, \pm\vec{\rho}) = \\
&\qquad \times \sum_{n=max(|n_1-n_2|,1)}^{n_1+n_2} \sum_{l=|l_1-l_2|,2}^{min(n-1, l_1+l_2)} G^{(nlm)_1(nlm)_2}_{nl}(\alpha, \beta)\ \overline{\Psi}^{m_1-m_2}_{nl}(\alpha+\beta), \vec{\rho})
\end{aligned} \tag{75}$$

and

$$G^{(nlm)_1(nlm)_2}_{nl}(\alpha, \beta) = (2\pi)^{3/2} \frac{n_2(\alpha+\beta)}{n\beta} P^{(nlm)_1(nlm)_2}_{nl}(\alpha, \beta) \tag{76}$$

and where P is given by Eq. (25).

Finally, an addition theorem can be given for $\overline{\Psi}$. The result is

$$\overline{\Psi}^{m_i}_{(nl)_i}(\alpha,\vec{p}\pm\vec{\rho}\,) = \sum_{(nlm)_f} T_{(nlm)_i(nlm)_f}(\alpha,\beta,\pm\vec{\rho})\overline{\Psi}^{m_f}_{(nl)_f}(\beta,\vec{p}) \tag{77}$$

where it can be easily shown that

$$T_{(nlm)_i(nlm)_f}(\alpha,\beta,\pm\vec{\rho}) = Q^*_{(nlm)_f(nlm)_i}(\beta,\alpha,\mp\vec{\rho}) \tag{78}$$

The R and Q matrices can be shown to be unitary. This can be accomplished using closure relations. The closure relations for the FDSHs were given by Schwinger[26]

$$\delta(\Omega-\Omega\,') = \sum_{nlm} Y^{*m}_{nl}(\Omega\,')Y^m_{nl}(\Omega) \tag{79}$$

In this regard, an important relationship is

$$\delta[\hat{\Omega}_\alpha(\vec{p}) - \hat{\Omega}_\alpha\,'(\vec{p}\,')] = (\frac{\alpha^2+p^2}{2\alpha})^3\delta(\vec{p}-\vec{p}\,') \tag{80}$$

The following completeness relations can then be derived from Eqs. (39), (40), (79), and (80)

$$\delta(\vec{r}_1-\vec{r}_2) = \sum_{nlm}\Psi^{*m}_{nl}(\alpha,\vec{r}_2)S^m_{nl}(\alpha,\vec{r}_1) = \sum_{nlm} S^{*m}_{nl}(\alpha,\vec{r}_2)\Psi^m_{nl}(\alpha,\vec{r}_1) \tag{81}$$

$$\delta(\vec{p}_1-\vec{p}_2) = \sum_{nlm}\overline{\Psi}^{*m}_{nl}(\alpha,\vec{p}_2)\overline{S}^m_{nl}(\alpha,\vec{p}_1) = \sum_{nlm}\overline{S}^{*m}_{nl}(\alpha,\vec{p}_2)\overline{\Psi}^m_{nl}(\alpha,\vec{p}_1) \tag{82}$$

The unitarity of Q and R can then be readily demonstrated. Therefore

$$\sum_{(nlm)_3}[\underline{Q}(\alpha,\vec{R})]_{(nlm)_1(nlm)_3}[\underline{\widetilde{Q}}^*(\alpha,\vec{R})]_{(nlm)_3(nlm)_2} = \delta_{(nlm)_1(nlm)_2} \tag{83}$$

$$\sum_{(nlm)_3}[\underline{\widetilde{Q}}^*(\alpha,\vec{R})]_{(nlm)_1(nlm)_3}[\underline{Q}(\alpha,\vec{R})]_{(nlm)_3(nlm)_2} = \delta_{(nlm)_1(nlm)_2} \tag{84}$$

and similarly for R

$$\sum_{(nlm)_3} [\underline{R}(\alpha,\beta,\vec{P})]_{(nlm)_1(nlm)_3} [\underline{\widetilde{R}}^*(\alpha,\beta,\vec{P})]_{(nlm)_3(nlm)_2} = \delta_{(nlm)_1(nlm)_2} \tag{85}$$

$$\sum_{(nlm)_3} [\underline{\widetilde{R}}^*(\alpha,\beta,\vec{R})]_{(nlm)_1(nlm)_3} [\underline{R}(\alpha,\beta,\vec{R})]_{(nlm)_3(nlm)_2} = \delta_{(nlm)_1(nlm)_2} \tag{86}$$

A number of important relationships can be proven for Q and R including

$$Q^*_{(nlm)_1(nlm)_2}(\alpha,\vec{R}) = Q_{(nlm)_2(nlm)_1}(\alpha,-\vec{R}) \tag{87}$$

$$R^*_{(nlm)_1(nlm)_2}(\alpha,\beta,\vec{P}) = R_{(nlm)_2(nlm)_1}(\beta,\alpha,-\vec{P}) \tag{88}$$

$$Q_{(nlm)_1(nlm)_2}(\alpha,\vec{0}) = \delta_{(nlm)_1(nlm)_2} \tag{89}$$

$$R_{(nlm)_1(nlm)_2}(\alpha,\alpha,\vec{0}) = \delta_{(nlm)_1(nlm)_2} \tag{90}$$

$$0 \le |Q_{(nlm)_1(nlm)_2}(\alpha,\vec{R})| \le 1 \tag{91}$$

$$0 \le |R_{(nlm)_1(nlm)_2}(\alpha,\beta,\vec{R})| \le 1 \tag{92}$$

A number of other relations are defined by Koga et al.[14,27,28] for the Q-function which they call the S function. Corresponding relationships can be found for the R function.

3. MULTICENTER INTEGRALS OVER COULOMB STURMIANS

The addition theorems are useful for application to problems which involve the evaluation of multicenter integrals over exponentially decaying orbitals. Thus, applications to the calulation of molecular wavefunctions for discrete and continuum processes can be considered. In particular, the general 4-center electron repulsion integral, defined in Eq. (1), will be analytically evaluated. Now, introducing Eq. (58) into Eq. (1) results in

$$\begin{aligned} E^{(nlm)_a(nlm)_b}_{(nlm)_c(nlm)_d}(\alpha_a,\alpha_b,\alpha_c,\alpha_d;\vec{A},\vec{B},\vec{C},\vec{D}) = \frac{1}{2\pi^2}\int d\vec{P}\ \frac{1}{P^2}\ e^{+i\vec{P}\cdot\vec{R}_{CB}} \\ \times F^*_{(nlm)_a(nlm)_b}(\alpha_a,\alpha_b;\vec{R}_{AB};\vec{P}\ )\ F_{(nlm)_d(nlm)_c}(\alpha_d,\alpha_c;\vec{R}_{DC};\vec{P}\ ) \end{aligned} \tag{93}$$

where

$$\left\{ \begin{array}{l} \vec{R}_{CB} \equiv \vec{C} - \vec{B} \\ \vec{R}_{AB} \equiv \vec{A} - \vec{B} \\ \vec{R}_{DC} \equiv \vec{D} - \vec{C} \end{array} \right\} \tag{94}$$

and F is called a 2-center form factor and is given by

$$F_{(nlm)_1(nlm)_2}(\alpha_1, \alpha_2; \vec{R}; \vec{P}\ ) \equiv \int d\vec{r}\ S^{*m_2}_{(nl)_2}(\alpha_2, \vec{r}) S^{m_1}_{(nl)_1}(\alpha_1, \vec{r} + \vec{R}) e^{-i\vec{P}\cdot\vec{r}} \tag{95}$$

or, by introducing the appropriate Fourier transforms,

$$F_{(nlm)_1(nlm)_2}(\alpha_1, \alpha_2; \vec{R}; \vec{P}) \equiv \int d\vec{\rho}\ \overline{S}^{*m_2}_{(nl)_2}(\alpha_2, \vec{\rho} - \vec{P}) \overline{S}^{m_1}_{(nl)_1}(\alpha_1, \vec{\rho}\ ) e^{-i\vec{R}\cdot\vec{\rho}} \tag{96}$$

It is important to realize that E in Eq. (93) depends only on the differences between internuclear vectors (defined in Eq. (94)) and not on the vectors themselves. Also, the efficient evaluation of the 2-center form factors (F) is of critical importance.

In order to evaluate the form factors, the 2-center overlap of two CSs in coordinate and momentum space needs to be defined and evaluated. Thus

$${}^{r}O^{m_i m_j}_{(nl)_i(nl)_j}(\alpha, \beta; \vec{R}) \equiv \int d\vec{r}\ S^{*m_j}_{(nl)_j}(\beta, \vec{r}) S^{m_i}_{(nl)_i}(\alpha, \vec{r} + \vec{R}) \tag{97}$$

and

$${}^{p}O^{m_i m_j}_{(nl)_i(nl)_j}(\alpha, \beta; \vec{P}) \equiv \int d\vec{\rho}\ \overline{S}^{*m_j}_{(nl)_j}(\beta, \vec{\rho}) \overline{S}^{m_i}_{(nl)_i}(\alpha, \vec{\rho} + \vec{P}) \tag{98}$$

It should be clear that

$${}^{r}O^{m_i m_j}_{(nl)_i(nl)_j}(\alpha, \alpha; \vec{0}) = O^{m_i m_j}_{(nl)_i(nl)_j} \tag{99}$$

$${}^{p}O^{m_i m_j}_{(nl)_i(nl)_j}(\alpha, \alpha; \vec{0}) = O^{m_i m_j}_{(nl)_i(nl)_j} \tag{100}$$

where $O^{m_i m_j}_{(nl)_i(nl)_j}$ is defined in Eq. (41). Also, using Eq. (19)

$${}^{r}O^{m_1 m_2}_{(nl)_1(nl)_2}(\alpha, \beta, \vec{0}) = \sum_{n_3=l_1+1}^{n_1} \sum_{n_5=l_1+1}^{n_3} \sum_{n_4=l_2+1}^{n_2} \sum_{n_6=l_2+1}^{n_4} A^{(nl)_1(nl)_2}_{n_3 n_4 n_5 n_6}(\alpha, \beta) O^{m_1 m_2}_{(n_6 l_1)(n_5 l_2)} \delta_{l_1 l_2} \delta_{m_1 m_2} \tag{101}$$

In order to evaluate ${}^{r}O^{m_i m_j}_{(nl)_i(nl)_j}$ and ${}^{p}O^{m_i m_j}_{(nl)_i(nl)_j}$, the translation formulas in Eqs. (60) and (73), along with Eq. (101), are used to produce

$$ {}^{r}O^{m_i m_j}_{(nl)_i(nl)_j}(\alpha,\beta;\vec{R}) = \sum_{n_1=max(1,n_i-1)}^{n_i+1} Q_{(nlm)_i(n_1 l_j m_j)}(\alpha,\vec{R})\ {}^{r}O^{m_j m_j}_{(n_1 l_j)(nl)_j}(\alpha,\beta;\vec{0}) \tag{102} $$

$$ {}^{p}O^{m_i m_j}_{(nl)_i(nl)_j}(\alpha,\beta;\vec{P}) = \sum_{n_1=max(1,n_i-1)}^{n_i+1} R_{(nlm)_i(n_1 l_j m_j)}(\alpha,\beta,\vec{P}) O^{m_j m_j}_{(n_1 l_j)(nl)_j} \tag{103} $$

Then, in terms of Q, the form factor becomes

$$ {}^{Q}F_{(nlm)_1(nlm)_2}(\alpha_1,\alpha_2;\vec{R};\vec{P}) = \sum_{(nlm)_3} Q_{(nlm)_1(nlm)_3}(\alpha_1,\vec{R})\ {}^{p}O^{m_3 m_2}_{(nl)_3(nl)_2}(\alpha_1,\alpha_2;\vec{P}) \tag{104} $$

where a pre-superscript has been added to indicate that F has its internuclear dependence expressed in terms of the Q function. In terms of R, then

$$ {}^{R}F_{(nlm)_1(nlm)_2}(\alpha_1,\alpha_2;\vec{R};\vec{P}) = \sum_{(nlm)_3} {}^{r}O^{m_1 m_3}_{(nl)_1(nl)_3}(\alpha_1,\alpha_1;\vec{R}) R_{(nlm)_3(nlm)_2}(\alpha_1,\alpha_2,\vec{P}) \tag{105} $$

Using Eqs. (104) and (105) in (93) results in

$$ {}^{Q}E = \frac{1}{2\pi^2} \sum_{(nlm)_2} Q^{*}_{(nlm)_a(nlm)_2}(\alpha_a,\vec{R}_{AB}) \sum_{(nlm)_1} Q_{(nlm)_d(nlm)_1}(\alpha_d,\vec{R}_{DC}) \; {}^{Q}I^{m_1 m_c m_2 m_b}_{(nl)_1(nl)_c(nl)_2(nl)_b}(\alpha_d,\alpha_c,\alpha_a,\alpha_b;\vec{R}_{CB}) \tag{106} $$

$$ {}^{R}E = \frac{1}{2\pi^2} \sum_{(nlm)_2} {}^{r}O^{*m_a m_2}_{(nl)_a(nl)_2}(\alpha_a,\alpha_a,\vec{R}_{AB}) \sum_{(nlm)_1} {}^{r}O^{m_d m_1}_{(nl)_d(nl)_1}(\alpha_d,\alpha_d,\vec{R}_{DC}) \; {}^{R}I^{m_1 m_c m_2 m_b}_{(nl)_1(nl)_c(nl)_2(nl)_b}(\alpha_d,\alpha_c,\alpha_a,\alpha_b;\vec{R}_{CB}) \tag{107} $$

where

$$ {}^{Q}I^{m_1 m_c m_2 m_b}_{(nl)_1(nl)_c(nl)_2(nl)_b}(\alpha_d,\alpha_c,\alpha_a,\alpha_b;\vec{R}_{CB}) = $$
$$ \int d\vec{P}\ \frac{1}{P^2} e^{+i\vec{P}\cdot\vec{R}_{CB}}\ {}^{P}O^{*m_2 m_b}_{(nl)_2(nl)_b}(\alpha_a,\alpha_b;\vec{P})\ {}^{P}O^{m_1 m_c}_{(nl)_1(nl)_c}(\alpha_d,\alpha_c;\vec{P}) \tag{108} $$

$$ {}^{R}I^{m_1 m_c m_2 m_b}_{(nl)_1(nl)_c(nl)_2(nl)_b}(\alpha_d,\alpha_c,\alpha_a,\alpha_b;\vec{R}_{CB}) = $$
$$ \int d\vec{P}\ \frac{1}{P^2} e^{+i\vec{P}\cdot\vec{R}_{CB}} R^{*}_{(nlm)_2(nlm)_b}(\alpha_a,\alpha_b;\vec{P}) R_{(nlm)_1(nlm)_c}(\alpha_d,\alpha_c;\vec{P}) \tag{109} $$

It is then easy to see that

$$ {}^{Q}I^{m_1 m_c m_2 m_b}_{(nl)_1(nl)_c(nl)_2(nl)_b} = \sum_{n_4=max(1,n_2-1)}^{n_2+1} \sum_{n_3=max(1,n_1-1)}^{n_1+1} {}^{R}I^{m_1 m_c m_2 m_b}_{(nl)_1(n_3 l_c)(nl)_2(n_4 l_b)} \times O^{m_b m_b}_{(n_4 l_b)(nl)_b} O^{m_c m_c}_{(n_3 l_c)(nl)_c} \tag{110} $$

and thus only ${}^{R}I$ needs to be considered at this point in the development. Thus, using Eq. (75) in Eq. (109) produces

$$ {}^{R}I^{m_1 m_c m_2 m_b}_{(nl)_1(nl)_c(nl)_2(nl)_b}(\alpha_d,\alpha_c,\alpha_a,\alpha_b;\vec{R}_{CB}) = $$
$$ \sum_{n_4=max(|n_2-n_b|,1)}^{n_2+n_b} \sum_{l_4=|l_2-l_b|,2}^{min(n_4-1,l_2+l_b)} G^{*(nlm)_2(nlm)_b}_{(nl)_4}(\alpha_a,\alpha_b) $$
$$ \sum_{n_3=max(|n_1-n_c|,1)}^{n_1+n_c} \sum_{l_3=|l_1-l_c|,2}^{min(n_3-1,l_1+l_c)} G^{(nlm)_1(nlm)_c}_{(nl)_3}(\alpha_d,\alpha_c) $$
$$ \times J^{(m_1-m_c)(m_2-m_d)}_{(nl)_3(nl)_4}(\alpha_d+\alpha_c,\alpha_a+\alpha_b;\vec{R}_{CB}) \tag{111} $$

where

$$ J^{m_1 m_2}_{(nl)_1(nl)_2}(\alpha_1,\alpha_2;\vec{R}) \equiv \int d\vec{P} \frac{1}{P^2} e^{+i\vec{P}\cdot\vec{R}}\ \overline{\Psi}^{*\,m_2}_{(nl)_2}(\alpha_2,\vec{P}\,)\overline{\Psi}^{m_1}_{(nl)_1}(\alpha_1,\vec{P}\,) \tag{112} $$

In order to perform the integral in Eq. (112), the modified CSFT ($\overline{\Psi}$) must be explicitly given. This can be done by first relating the CS to the B-function of Steinborn[8] via

$$S_{nl}^{m}(\alpha,\vec{r}) = \alpha^{3/2}\sum_{t=1}^{n-l} a_t^{nl} B_{tl}^{m}(\alpha,\vec{r}) \tag{113}$$

where

$$a_t^{nl} = \frac{(-1)^{n+l-1}2^{l+5/2}}{(2l+1)!!}\left[\frac{n(n+l)!}{2(n-l-1)!}\right]^{1/2}\frac{(-n+l+1)_{t-1}(n+l+1)_{t-1}}{(t-1)!(l+3/2)_{t-1}} \tag{114}$$

where the Pochmanner symbol is defined by

$$(b)_n \equiv \frac{\Lambda(b+n)}{\Lambda(b)} = \prod_{j=1}^{n}(b+j-1) \tag{115}$$

Then taking the Fourier transform of Eq. (113) and using Eq. (53), the Fourier transform of $\overline{\Psi}$ is obtained as

$$\overline{\Psi}_{nl}^{m}(\alpha,\vec{P}) = (-i)^l\frac{2}{\pi}^{1/2}\sum_{t=1}^{n-l} a_t^{nl}\alpha^{2t+l+1/2}\frac{P^l}{[\alpha^2+P^2]^{t+l}}Y_l^m(\hat{P}) \tag{116}$$

Then, J can be evaluated as

$$\begin{aligned} J_{(nl)_1(nl)_2}^{m_1m_2}(\alpha_1,\alpha_2;\vec{R}) = 4\pi &\sum_{t_2=1}^{n_2-l_2} a_{t_2}^{(nl)_2}\alpha_2^{2t_2+l_2+1/2}\sum_{t_1=1}^{n_1-l_1} a_{t_1}^{(nl)_1}\alpha_1^{2t_1+l_1+1/2} \\ &\times \sum_{l_3=|l_1-l_2|}^{l_1+l_2}\delta_{l_1+l_2+l_3=even}[(-1)^{l_1}i^{l_1+l_2+l_3}]\langle l_2m_2|l_1m_1|l_3,m_2-m_1\rangle \\ &\times W_{(t_1+l_1),(t_2+l_2)}^{l_3,\left[\frac{l_1+l_2-l_3}{2}\right]}(\alpha_1,\alpha_2;R)\,Y_{l_3}^{*m_2-m_1}(\hat{R}) \end{aligned} \tag{117}$$

where

$$W_{m,n}^{l,j}(\alpha_1,\alpha_2;R) \equiv \frac{2}{\pi}\int dP\,\frac{P^{l+2j}}{\left[\alpha_1^2+P^2\right]^m\left[\alpha_2^2+P^2\right]^n}\,j_l(RP) \tag{118}$$

The W integral may be evaluated by the methods developed by Harris and Michels.[29]

Thus, the evaluation of E, the 4-center electron repulsion integral, has been described. The programming of these results is underway.

This work was supported by the Air Force Office of Scientific Research under Contract No. F49620-89-C-007.

References

1. *Proceedings of the First International Conference on ETO Multicenter Molecular Integrals* , edited by C.A. Weatherford and H.W. Jones, (D. Reidel, Holland, 1982).
2. P.O. Löwdin, Adv. Phys. **5**, 1 (1956).
3. M.P. Barnett and C.A. Coulson, Philos. Trans. R. Soc. London Ser. A **243**, 221 (1951); M.P. Barnett, in *Methods in Computational Physics*, V. 3, edited by B. Alder, S. Fernbach, and M. Rotenberg, (Academic Press, New York, 1963), p. 95; and references therein.
4. F.E. Harris and H.H. Michels, J. Chem. Phys. **43**, S165 (1965).
5. H.W. Jones and C.A. Weatherford, Int. J. Quant. Chem. **S12**, 483 (1978).
6. H.J. Silverstone, J. Chem. Phys. **48**, 4098 (1986); and references therein.
7. E. J. Weniger, J. Math. Phys. **26**, 276 (1985).
8. E.J. Weniger, J. Grotendorst, and E.O. Steinborn, Phys. Rev. A**33**, 3688 (1986).
9. V. Fock, Z. Phys. **98**, 145 (1935).
10. T-I. Shibuya and C. Wulfman, Proc. R. Soc. London Ser. A **286**, 376 (1965).
11. J.S. Alper, J. Chem. Phys. 55, 3770 (1971); **55**, 3780 (1971).
12. B.K. Novosadov, Int. J. Quant. Chem. **24**, 1 (1983).
13. M. Rotenberg, Ann. Phys. (NY) **19**, 262 (1962).
14. T. Koga and T. Matsuhashi, J. Chem. Phys. **88**, 1110 (1988).
15. G. Arfken, *Mathematical Methods For Physicists*, Third Edition, (Academic Press, New York, 1985).
16. I.N. Sneddon, *Special Functions of Mathematical Physics and Chemistry*, (Oliver and Boyd, Edinburgh, 1966).

17. C.A. Weatherford, Ref. 1, p. 29.

18. C.A. Weatherford, unpublished.

19. R. Shakeshaft, Phys. Rev. A**34**, 244 (1986).

20. E. Filter and E.O. Steinborn, J. Math. Phys. **21**, 2725 (1980).

21. H.H. Kranz and E.O. Steinborn, Phys. Rev. A**25**, 66 (1982).

22. L.C. Biedenharn, J. Math. Phys. **2**, 433 (1961).

23. B.R. Judd, *Angular Momentum Theory For Diatomic Molecules*, (Academic Press, Inc., New York, 1975).

24. A.R. Edmunds, *Angular Momentum in Quantum Mechanics*, (Princeton U.P., Princeton, New Jersey, 1957).

25. R.N. Zare, *Angular Momentum*, (Wiley, Princeton, New York, 1988).

26. J. Schwinger, J. Math. Phys. **5**, 1606 (1964).

27. T. Koga, J. Chem. Phys. **83**, 2328 (1985).

28. T. Koga and T. Matsuhashi, J. Chem. Phys. **87**, 4696 (1987).

29. F.E. Harris and H.H. Michels, Adv. Chem. Phys. **13**, 205 (1967).

SCHRÖDINGER EQUATION MESH REQUIREMENTS IN THE FINITE DIFFERENCE DISCRETIZATION FOR NON-SPHERICAL POTENTIALS

by

Charles A. Weatherford[†]

Physics Department

and

Center for Nonlinear & Nonequilibrium Aeroscience

Florida A&M University

Tallahassee, FL 32307

U.S.A.

ABSTRACT

The Schrödinger equation for the scattering of an electron by a hydrogen molecule is solved by converting it to a block-tri-diagonal matrix equation. The discrete mesh of points in the angular variable must be made more dense as the potential energy deviates from spherical symmetry to maintain a desirable level of accuracy. The present paper investigates the nature of this dependence, and the relative effect of third-order and fifth-order differentiation rules. It is found that the existence of one large element in the K-matrix sets a lower bound on the accuracy of all elements. This bound, and therefore the overall accuracy of the numerical approximation, can be substantially improved by the use of the higher-order rules.

[†]This work was supported by NASA contract NAGW-2930 and NCC 2-492, and an Air Force contract 27256-PH-SAH. A grant of computer time from Florida State University is gratefully acknowledged.

1. INTRODUCTION

Traditional electron scattering theory is concerned with the results of collisions between an electron and a target under the assumption that their interaction depends only on their separation, and is independent of their angular orientation. When the target is an atom, this asumption is justified, but when the target atoms are bound into molecules, the great simplification afforded by the conservation of angular momentum are no longer available. A numerical analysis must therefore be introduced at an earlier stage in the solution of the problem.

The K-matrix is a concise and computationally simple means of presenting the results of a scattering calculation using the method of partial differential equations. This work will investigate the relationship between the mesh size required in a finite-difference approximation to the K-matrix and the deviation of the scattering potential from spherical symmetry for various levels of accuracy. 'Accuracy' is defined as the difference between the numerical approximation and a hypothetical continuum-limit K-matrix, which must be inferred from the behavior of the approximation.

The angular accuracy is roughly independent of the radial properties of the potential, so the numerical requirements of the polar-angle dependence can be investigated without a detailed model of the physical potential. The angular momentum quantum number l provides a convenient basis for calculating the K-matrix, but one which is not a basis of eigenvectors. In an eigenvector basis, the K-matrix would be diagonal, and the numerical convergence of the various elements would be unrelated, with the states of higher rotational energy requiring a finer mesh. Here, by contrast, the error in the numerical approximation is spread over all coupled states. In particular, if one element dominates the others, a small relative error in that element will imply a large relative error in the other elements. The convergence of the largest element is found to be excellent, with accuracy of about 10^{-3} using 29 points in the angular mesh. The convergence of the smaller elements is limited by this effectively constant bound. Convergence beyond this limit requires vastly larger meshes, though a great improvement can be gained by the use of higher-order differentiation rules. It is found that adding rules of fifth order in the mesh spacing

requires little additional programming, and virtually no extra computer time for the models considered.

2. THE METHOD

The homonuclear diatomic molecule is the simplest system for which non-spherical terms contribute to the scattering potential, so it will serve as the physical anchor for an otherwise computational study. When the energy of the incident electron is between 1 and 10 electron volts, the non-spherical structure of the molecule is particularly important. In such a situation, we use the axial symmetry of the molecule to reduce the Schrödinger equation to a two-dimensional partial differential equation. We assume for simplicity that the collision does not excite vibrational states of the molecule. Rotational excitations may be dealt with at the cross-section stage of the calculation in the usual adiabatic-nuclei manner.[1]

The target molecule may be assumed to be oriented in a particular direction in space so we use the axis of symmetry of the molecule as the z-axis of our coordinate system (Fig. 1), and define a modified wavefunction u which is related to the true wavefunction Ψ for the projectile by

$$\Psi(r,\theta,\phi) = \frac{1}{r^l} u(r,\theta) e^{im\phi}. \tag{1}$$

The equation for u in atomic units is

$$\frac{\partial^2 u}{\partial r^2} + \frac{1}{r^2}\left\{ cot(\theta)\frac{\partial^2 u}{\partial \theta^2} + \frac{\partial u}{\partial \theta}\right\} + \left\{ p^2 - 2V(r,\theta) - \frac{m^2}{r^2 sin(\theta)}\right\} u = 0 \tag{2}$$

where $V(r,\theta)$ is the scattering potential, and p is the momentum of the projectile. A finite difference approximation to this equation is solved on the domain $0 \leq r \leq R_{max}$, $0 \leq \theta \leq \frac{\pi}{2}$. The outer limit R_{max} is chosen to be sufficiently large that the scattered particle is effectively free at that distance. The range of θ has been cut in half to take advantage of the symmetry of the molecule under reflections in the $x-y$ plane.

The boundary condition at $r = 0$ requires that $u = 0$. At $\theta = 0$, there are two

possibilities: if m, the z-component of the orbital angular momentum, is nonzero, then $u = 0$; otherwise $\partial u/\partial\theta = 0$. At $\theta = \pi/2$, the parity of the system dictates either that $u = 0$ or $\partial u/\partial\theta = 0$. At $r = R_{max}$, we impose the requirement that the incoming electron be in a state of well-defined orbital angular momentum, so

$$u(R_{max}, \theta) = P_{lm}(cos\theta) \tag{3}$$

The parity of the associated Legendre function, $(-1)^{l+m}$, determines the choice of boundary condition at $\theta = \pi/2$. Though this parity is conserved by the scattered wave function, the value of l for the incident wave is not. Outgoing waves therefore contain a superposition of $l, l \pm 2, l \pm 4$, and so forth.

Once the wave function has been found, information about the scattering is extracted by matching it to the known asymptotic form

$$\Psi = \sum_{l'} \Big[A_{ll'} j_{l'}(pr) + B_{ll'} y_{l'}(pr) \Big] P_{l'm}(cos\theta), \tag{4}$$

where l and m are the index and order of the Legendre function used in the boundary condition at large r, and j and y are spherical Bessel functions. The coefficients **A** and **B** form matrices on the space of allowed values of orbital angular momentum.

The orthogonality of the Legendre functions may be used to project out a particular value of l'. When this is done for two different large values of r, the linear independence of the Bessel functions allows extraction of the unknown coefficients **A** and **B**. This process must be done for each allowed value of l'; then, the whole solution process repeated, allowing l to take on each permitted value. The result is two matrices describing the transformation of a angular momentum eigenstate into a scattered wave. In principle, the dimension of the matrices is infinite, but in practice the finite range of the non-spherical potentials provides a cutoff. For an H_2 molecule, with a projectile energy below 10 eV, values of l less than 5 are all that are required. Hence, the matrices are at most 3×3. The K-matrix is defined by the equation

$$\Psi = \sum_{l'} \Big[j_{l'}(pr) + K_{ll'} y_{l'}(pr) \Big] P_{l'm}(cos\theta), \tag{5}$$

so $\mathbf{K} = \mathbf{A}^{-1}\mathbf{B}$, and the influence of the artificial imposition of an initial orbital state is removed. The diagonal elements of K are the tangents of the elastic phase shifts, and the off-diagonal elements describe the coupling of states of different orbital angular momentum by the potential.

3. THE POTENTIALS

The potential energy function V in Eq. (2) represents the electromagnetic interaction of the projectile with the target molecule, and is the source of the breaking of spherical symmetry. In principle, this interaction is highly complicated. A molecule is by no means a static, rigid body in the presence of an incoming electron, so a potential model is not strictly correct, but the practical usefulness of potentials in calculations is great enough to excuse the gross simplification of the scattering problem they imply. The potentials involved in scattering from hydrogen molecules are approximations to three effects: the static electric moments of the molecule; the polarization of the molecule by the electric field of the projectile; and the substitution of an electron from the molecule for the projectile in the outgoing state, known as 'exchange.' Toy models have been adopted which mimic to some extent the radial structure of the physical potentials, and have angular properties which are expandable in the low-order Legendre polynomials of even parity.

Because the hydrogen molecule is composed of identical atoms, the lowest-order multipole field seen by the projectile is the quadrupole term

$$V_Q(r,\theta) = \frac{Q}{r^3} P_2(cos\theta) \tag{6}$$

where $Q = 0.49$ in atomic units. This form is valid for values of r which are outside the molecule for all θ. At shorter ranges, the quadrupole potential is cut off by the usual exponential term $(1 - exp[-(r/a)^6])$ as a multiplier. The adjustable parameter a is set to 1, since no effort is made to fit experimental data. The static potential inside the molecule is represented by a Yukawa function of unit range and arbitrary strength, which is adjusted as necessary to give the correct order of magnitude for the K-matrix.

Polarization of the target is well known to include terms of both spherical and P_2 character.[1] The form used here is

$$V_P(r,\theta) = \frac{1}{2r^4}\left(1 - e^{(-r)^6}\right)\left[a_0 + a_2 P_2(cos\theta)\right] \tag{7}$$

with a_0 =5.5, and a_2 =1.4.

The exchange potential is a crude form of the free electron gas model. The basic idea here is that the electron in the target may be approximated by a degenerate Fermi gas whose density varies with position.[1] The exchange potential is proportional to the Fermi momentum at any point in space, giving

$$V_\chi(\vec{r}\,) = -(\frac{3}{2\pi})\left[3\pi^2\beta(\vec{r}\,)\right] \tag{8}$$

The electron density $\beta(\vec{r}\,)$ is approximated by a simple sum,

$$\beta(r,\theta) = \frac{1}{4\pi}e^{-r}\left[1 + 1.3P_2(cos\theta)\right], \tag{9}$$

which has contours of constant density which resemble those of the sum of two hydrogen atoms separated by .7 angstroms. The resulting potential can be approximated by a linear combination of Legendre polynomials, which is

$$V_\chi(r,\theta) = -0.8e^{-r/3}\left[0.97 + 0.43P_2(cos\theta) + 0.1P_4(cos\theta)\right]. \tag{10}$$

The 'realistic' potential is a sum of these three terms.

The long-range quadrupole potential is the most important term in real scattering problems, but it does not vanish until a distance of 14 Bohr radii from the molecule's center is reached. This was determined *a posteriori*, by searching for a region in which the K-matrix does depend on small changes in R_{max}.) Such a long range requires a large number of radial points, and consequently a long running time for the computer code. Although the convergence properties of the angular approximation are roughly independent of the quality of the radial approximation, this independence is only valid when the radial mesh is on the order of magnitude of the mesh which gives decent radial convergence. Therefore,

the quadrupole term is generally omitted from this work, in the interest of a more efficient use of computer time. The P_2 terms in the polarization and exchange potentials are, in any case, expected to yield the same requirements on the angular mesh.

4. NUMERICAL ANALYSIS

The usual discrete approximation to Eq. (2) is obtained by replacing the radial variable with a set of N_r points, and the angle with a set of N_o points. The wavefunction therefore becomes a set of (real) values which solve the equation[2]

$$\begin{aligned} &\frac{1}{h_r^2}\left[u_{i+1,j} - 2u_{i,j} + u_{i-1,j}\right] \\ &\qquad \frac{1}{r_i^2}\left[\frac{1}{h_o}cot(\theta_j)(u_{i,j+1} - u_{i,j}) + \frac{1}{h_o{}^2}(u_{i,j+1} - 2u_{i,j} + u_{i,j-1})\right] + \\ &\qquad\qquad \left[p^2 - 2V_{i,j} - \frac{m^2}{r_i^2 sin^2(\theta_j)}\right]u_{i,j} = 0 \end{aligned} \tag{11}$$

Here, $u_{ij} = u(r_i, \theta_j)$, with $0 < i \leq N_r$ and $0 < j \leq N_o$. The spacings between the radial and angular points are h_r and h_o, respectively. (The values of h_r and h_o may in principle depend on i and j.) Eq. (11), together with the boundary conditions, gives a system of $(N_r + 2)(N_o + 2)$ coupled linear equations for the u_{ij}, which may be solved by conventional matrix method.[3]

The choice of the points r_i and θ_j presents an unavoidable conflict of interest. There are ways to improve the accuracy of a numerical solution of a differential equation by judicious choice of abscissae, just as there are ways to improve the numerical quadrature by which the elements of the K-matrix are projected out of the wave function. Unfortunately, the ways are mutually inconsistent. Numerical quadrature is optimized by choosing points so that successive errors alternate in sign, which is the worst possible choice of points for differentiation. Therefore, a compromise of equally-spaced abscissae will be used, and optimization achieved through higher-order integration and differentiation rules.

When the Schrödinger equation is solved on a two-dimensional lattice, the resulting matrix is block tridiagonal. This property, which makes the matrix easier to decompose

into lower and upper triangular matrices, depends on one of the variables having a simple three-point derivative. The other may be as complicated as the problem demands. In this work, the radial accuracy is of secondary interest, so the θ-derivative part of Eq. (11), which is in braces, will be explored with rules of greater accuracy (Table 25.2 in Ref. 4). For a point in the interior of the domain of approximation of θ, labelled by 'j' , rules of order h_o^5 are

$$\frac{\partial f}{\partial \theta} = \frac{1}{D_1}\{2f_{j-2} - 16f_{j-1} + 16f_{j+1} - 2f_{j+2}\}, \tag{12}$$

$$\frac{\partial^2 f}{\partial \theta^2} = \frac{1}{D_2}\{ - f_{j-2} + 16f_{j-1} - 30f_j + 16f_{j+1} - 2f_{j+2}\}, \tag{13}$$

where $D_1 = 24h_o$ and $D_2 = 12h_o^2$. (To simplify the formulae, $u_{i,j}$ has been replaced by f_j.) For points next to the boundary, asymmetrical rules must be used:

$$\frac{\partial f}{\partial \theta} = \frac{1}{D_1}\{ - 6f_{j-1} - 20f_j + 36f_{j+1} - 12f_{j+2} + 2f_{j+3}\}, \tag{14}$$

$$\frac{\partial^2 f}{\partial \theta^2} = \frac{1}{D_2}\{11f_{j-1} - 20f_j + 6f_{j+1} + 4f_{j+2} - f_{j+3}\}, \tag{15}$$

These rules are used for points next to the boundary at $\theta = 0$. Next to $\theta = \pi/2$, the subscript '$j+3$' is replaced by '$j-3$' , '$j+2$' by '$j-2$' and so forth, and there is an overall minus sign in the first derivative.

At the boundary, if $u = 0$ is the boundary condition, then it goes directly into the matrix. If Neumann boundary conditions apply, the process is more involved. First, terms in the Schrödinger equation proportional to $\partial r/\partial \theta$ are dropped. Then, Eq. (14) is used with $j = 0$ to get the relation

$$-6f_{-1} - 20f_0 + 36f_1 - 12f_2 + 2f_3 = 0 \tag{16}$$

which is solved for f_{-1}. This value is then used in Eq. (15) (with $j = 0$ again), to derive an expression for $\partial^2 u/\partial \theta^2$ at $\theta = 0$ which is accurate to fifth order in h_o:

$$\frac{\partial^2 f}{\partial \theta^2} = \frac{1}{D_2}\{ -(\frac{170}{3})f_0 - 72f_1 - 18f_2 - \frac{8}{3}f_3\}, \tag{17}$$

When Eq. (17) is used in place of the second derivative term in Eq. (11), the result is an approximation which significantly improves the numerical accuracy, compared to the three-point rules. As a test, when a spherical potential is assumed, and the K-matrix calculated, the off-diagonal matrix elements should vanish. In fact, for a given number of θ points, they are at most one fourth of those calculated with three-point rules, and of order 10^{-3} when the largest diagonal element is about 1.

5. RESULTS

Convergence of the K-matrix is determined in two ways. The first takes advantage of the invariance of the K-matrix under time reversal to require that the K-matrix be symmetric. The second is that the value of an element of the of the K-matrix change with changes in the number of θ points in a manner which points clearly to an asymptotic limit.

The matrices are not strictly symmetrical. When the scattering potential is spherical, the wave function should have the angular properties of the large-R boundary condition, all the way to the origin. This is true only when the boundary condition is for $l = 0$. When higher waves are used, each contains a contaminant of lower l values. This contamination decreases with each step in r away from the origin, reaching an eventual limit of about .002 times the amplitude of the correct wave. Therefore, any number less than .002 in the K-matrix is indistinguishable from zero. This seems to a be an artifact of the solution algorithm, reducible only by improving the J-derivative rule. (When a three-point rule is used, the corresponding limit is .008.)

The second criterion makes an accurate graphical depiction of the convergence difficult. The convergence of almost all elements is monotonic, so the choice of a specific limit is arbitrary, yet it has a great impact on the perceived quality of the convergence. For this reason, the first derivative of $K_{ll'}$ with respect to N_o is plotted in Figures 2-7.

To best isolate the effects of various non-spherical potentials, the K-matrices used to

produce Figures 2-7 are derived from several potentials. First, a spherical Yukawa potential was used. Then the same Yukawa potential multiplied by the Legendre polynomial $P_2(cos\theta)$. Then half of each is used. The length scale of the potential was 3, and its strength was set to -0.4. The momentum of the incoming particle was 0.8, corresponding to a kinetic energy of 8.7 eV. All these parameters were chosen to give significant K-matrix elements up to $l = 2$. An exception is the P_2 potential in Fig. 5. The $l = 2$ element was very small, so its relative error was extremely large, and not indicative of the numerical properties of the algorithm. The fourth curve on the graphs is the 'realistic' potential described above, with Yukawa of unit range in place of the long-range quadrupole.

Figures 2 and 3 show the slope versus N_θ of the K-matrix element for transitions between spherical waves. Fig. 2 is for a three-point rule, and Fig. 3 is for the five-point rules. The advantage of the five-point rule is most obvious at small numbers of theta points. As the mesh becomes finer, the relative advantage of the five-point rule diminishes, but it is still a factor of two better. Figures 4 and 5 are the same, for the d-wave to d-wave reaction.

Figures 6 and 7 are different. They show the difference between the $l = 0$ to 2 matrix element and the 2 to 0 element–this provide a test of time-reversal. The difference is normalized to the value of K_{02}, usually the smaller of the two. In judging the size of the relative error, it should be borne in mind that there is always a diagonal element of the K-matrix which dominates this term by an order of magnitude. The uncertainty in this dominant element is the primary source of this error. In this place, the five-point rule shows its particular virtue. The five-point rule shows a more symmetrical K-matrix with 11 points in the mesh than the three-point rule with 30.

6. CONCLUSIONS

The addition of five-point approximations to the angular derivatives requires only minor changes in the computer code for solving partial differential equations. It preserves the block-tridiagonal character of the equivalent linear system, so it requires no extra running time, and it yields significant improvement in the accuracy of the numerical solution.

The chief drawback of the partial-differential-equation method for non-spherical scattering problems is that the coupling between states makes the relative error in the small elements of the K-matrix large, since it is a small fraction of a large number. The largest element of the K-matrix thus creates a 'floor', a lower bound on the possible error in the other elements.

The contamination of the wave function by lower partial waves than the input boundary condition is the largest single source of error. It is an artifact of the $u = 0$ boundary condition at the origin. The natural tendency of this algorithm is to assume the smoothest possible wave function near $r = 0$, and it takes several steps way from the boundary before the large-r boundary condition can assert its dominance. A more sophisticated treatment of the radial derivatives might well be rewarded by a reduction of this defect.

Though this work has confined itself to the angular behavior of the wave function, the great improvements afforded by the higher-order approximations to the derivatives might have counterparts in the radial direction. This would destroy the tridiagonality of the matrix, but in applications where the size of the computer's memory is less of a constraint than the cost of processor time, it may be worthwhile.

REFERENCES

1. N.F. Lane, Rev. Mod. Phys. **52**, 29 (1980).
2. A. Temkin, C.A. Weatherford, and E.C. Sullivan, *Proceedings of the Sixteenth International Conference on the Physics of Electronic and Atomic Collisions* (Invited Papers), New York, N.Y., ed. A. Herzenberg (1989).
3. B. Carnahan, H.A. Luther, and J.O. Wilkes, *Applied Numerical Methods*, New York, N.Y., Wiley, (1969).
4. M. Abramowitz and I. Stegun, *Handbook of Mathematical Functions*, New York, N.Y., Dover (1970).

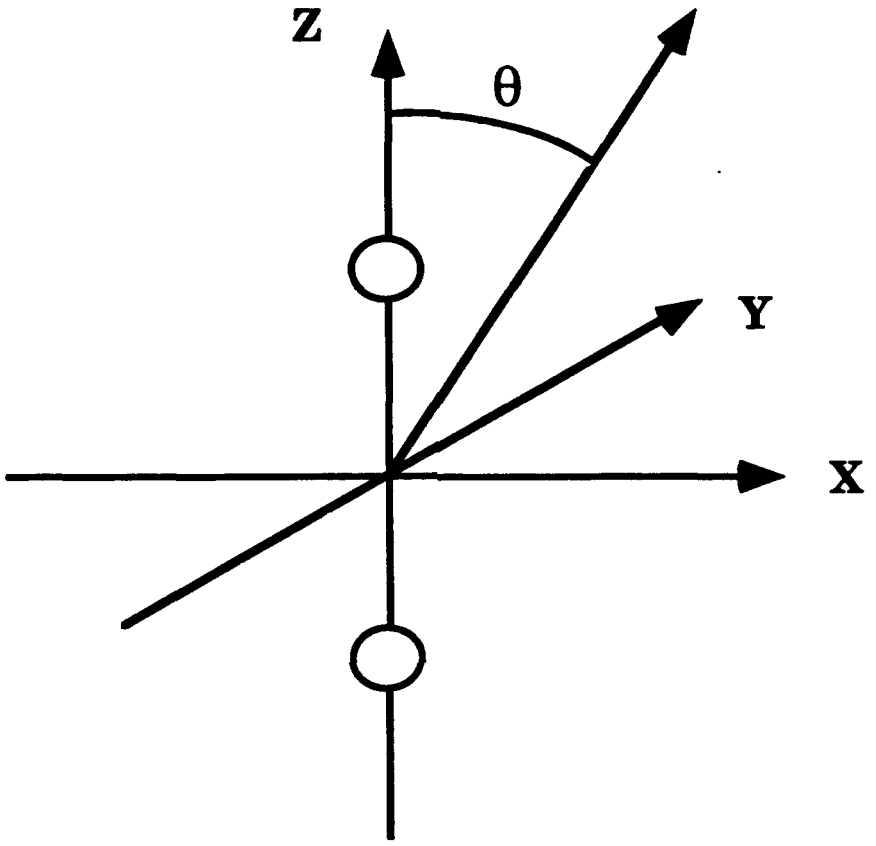

Figure 1. The coordinate system for scattering from a diatomic molecule.

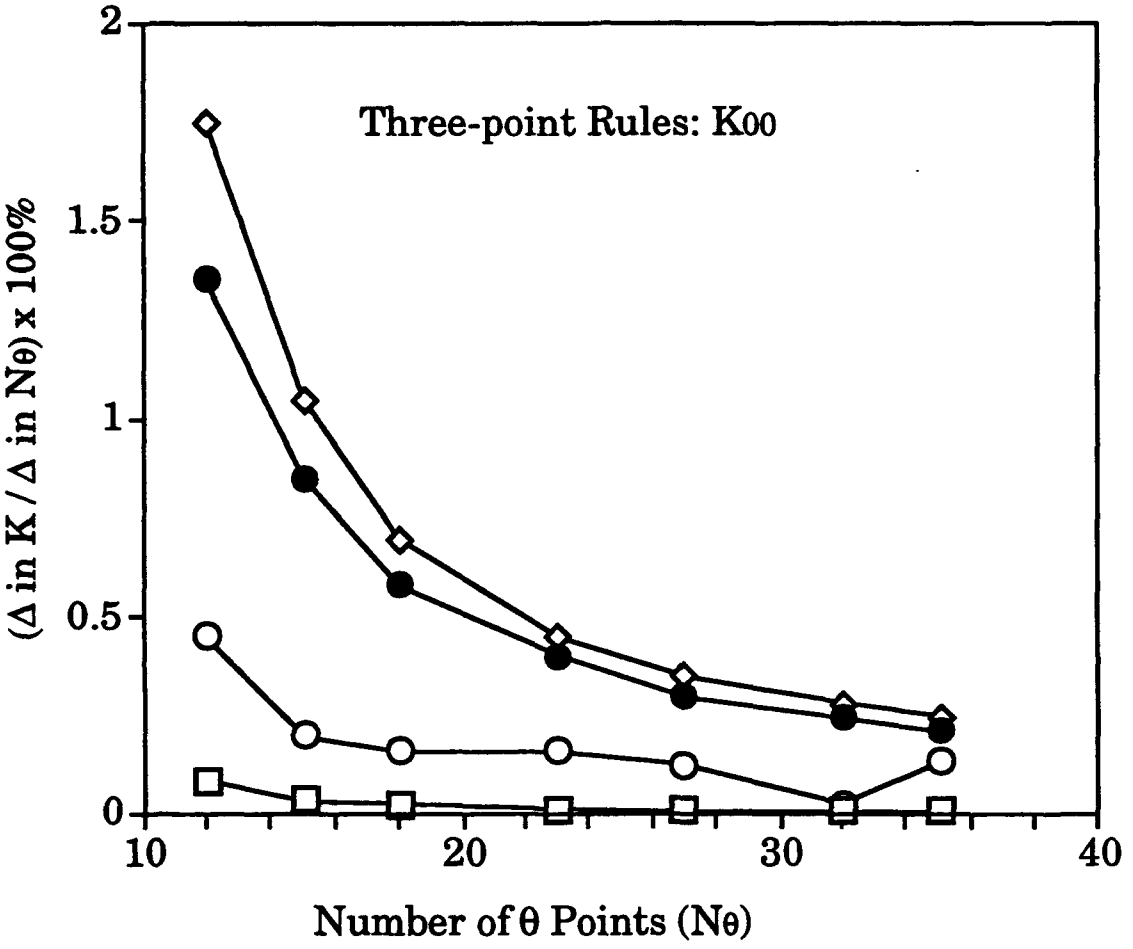

Figure 2. The relative change in the K-matrix element for s-wave→s-wave transitions, using three-point derivative rules: ▫, uses spherical potential, with a spherical angular term P_0; •, uses only term with P_2, the second Legendre polynomial; ○, uses the most realistic potential (see text); ◇, uses P_0 and P_2 terms.

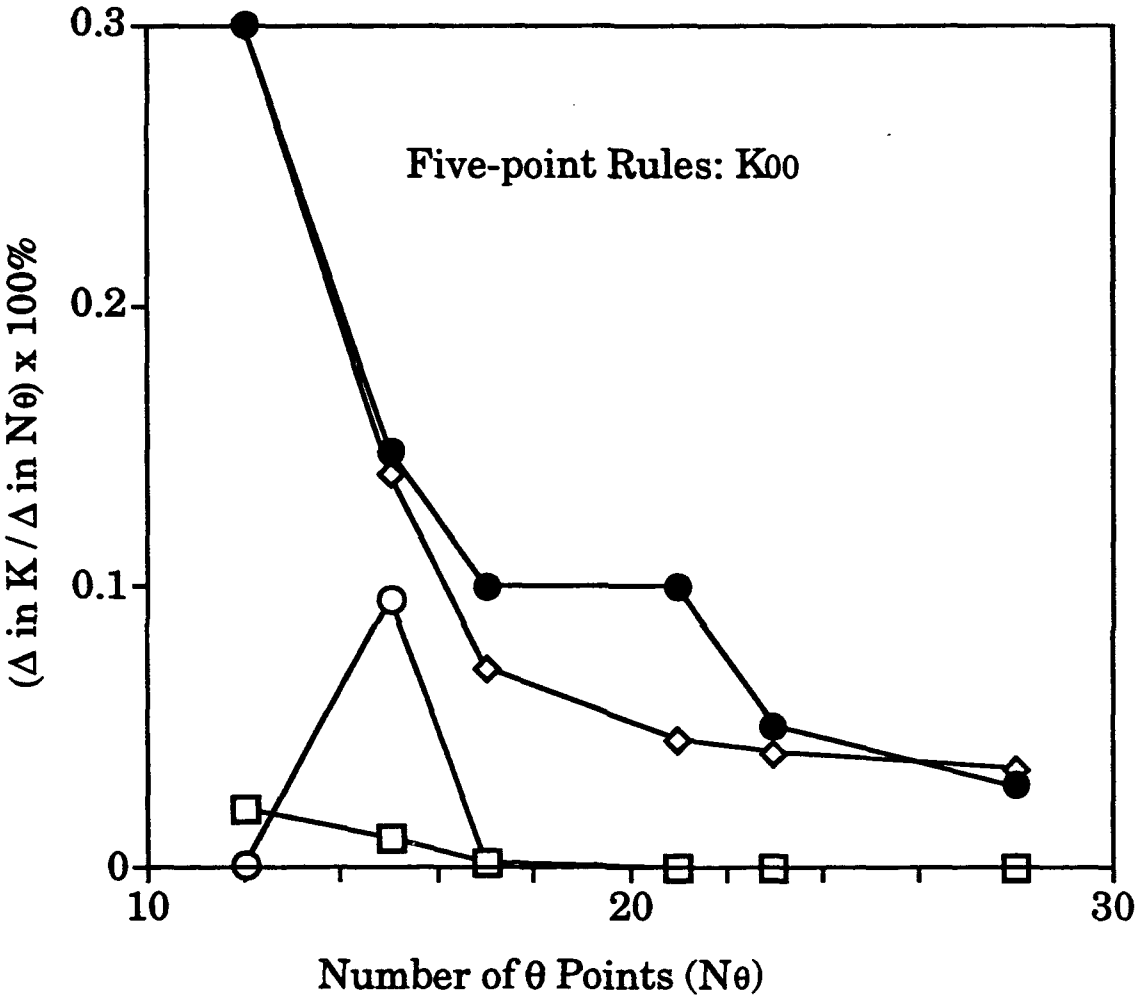

Figure 3. The relative change in the K-matrix element for s-wave→s-wave transitions, using five-point derivative rules: □, uses spherical potential, with a spherical angular term P_0; •, uses only term with P_2, the second Legendre polynomial; ○, uses the most realistic potential (see text); ◇, uses P_0 and P_2 terms.

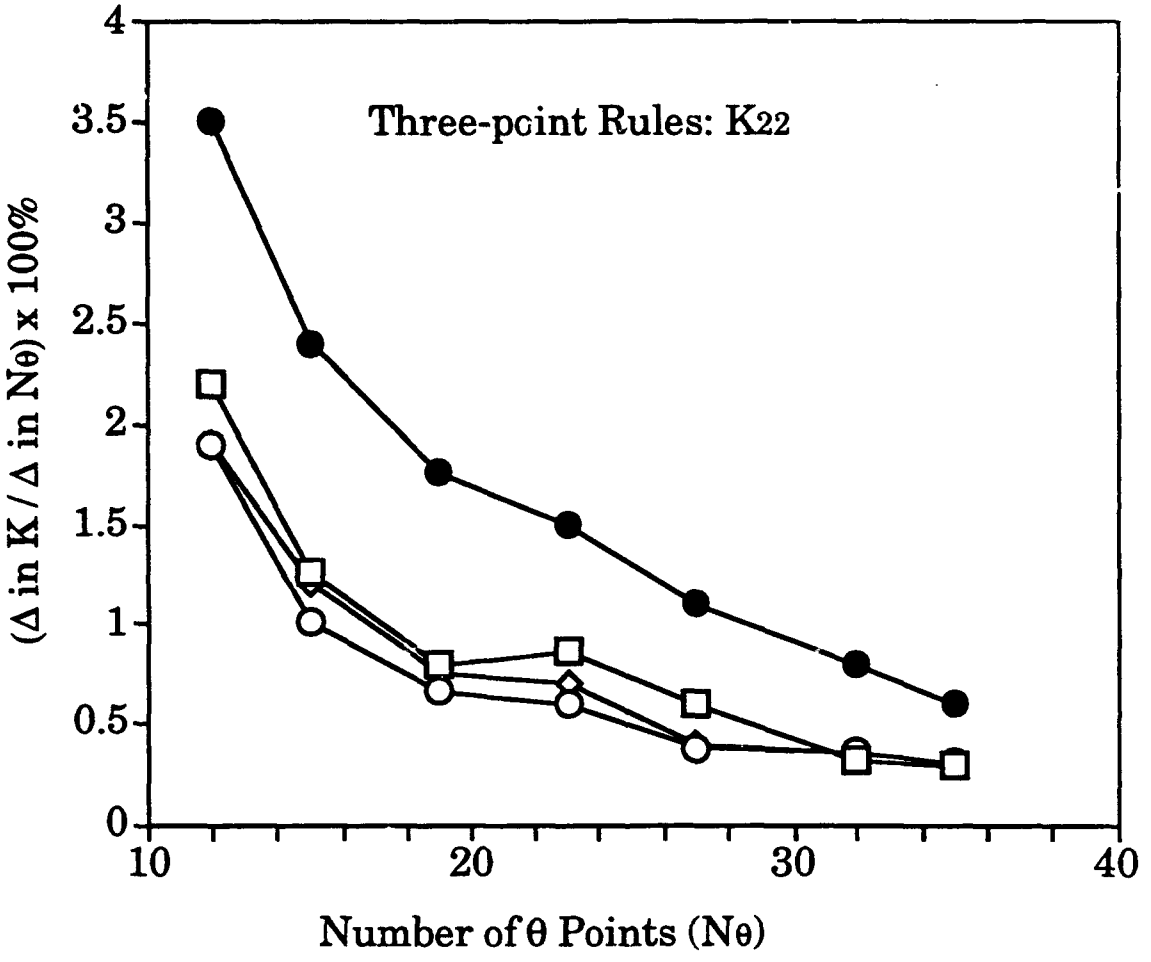

Figure 4. The relative change in the K-matrix element for d-wave→d-wave transitions, using three-point derivative rules: □, uses spherical potential, with a spherical angular term P_0; •, uses only term with P_2, the second Legendre polynomial; ○, uses the most realistic potential (see text); ◇, uses P_0 and P_2 terms.

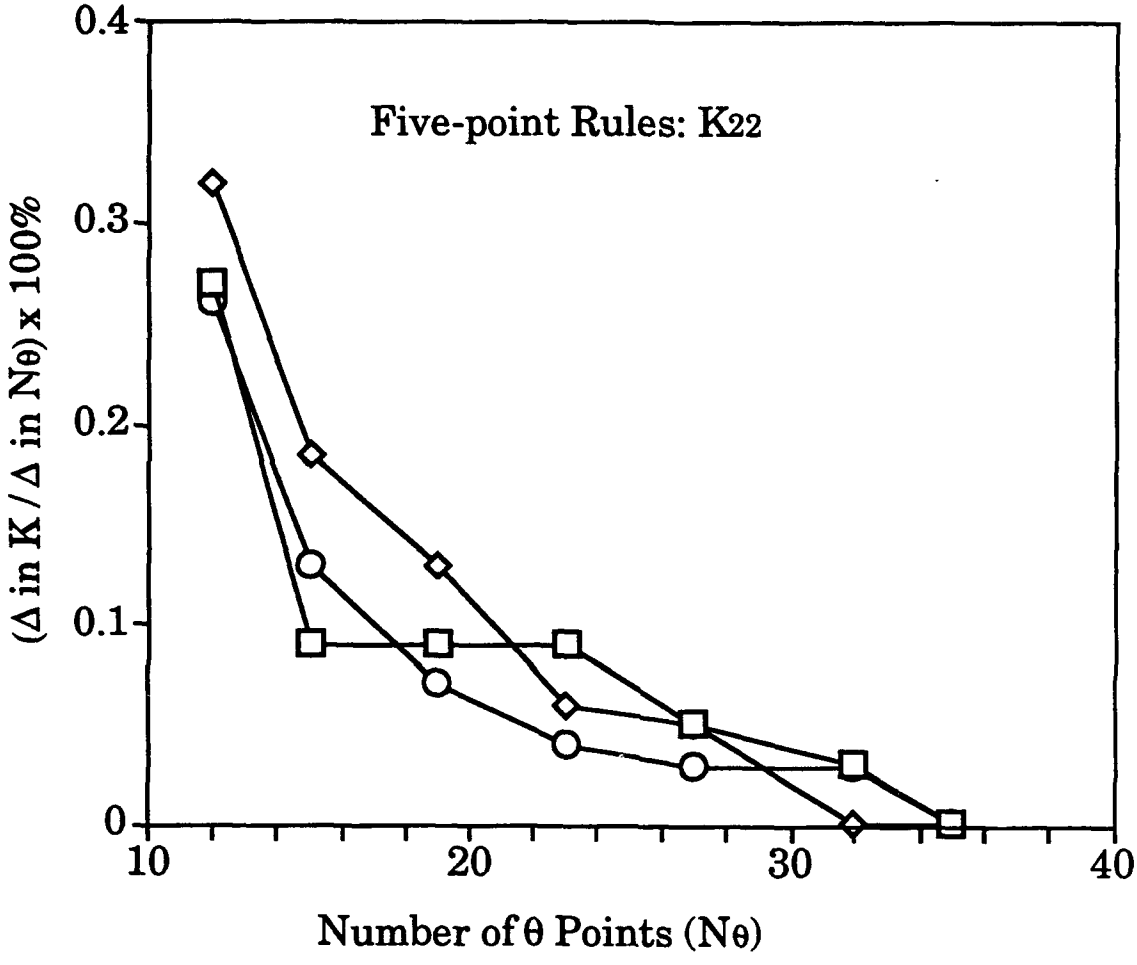

Figure 5. The relative change in the K-matrix element for d-wave→d-wave transitions, using five-point derivative rules: □, uses spherical potential, with a spherical angular term P_0; ○, uses the most realistic potential (see text); ◇, uses P_0 and P_2 terms.

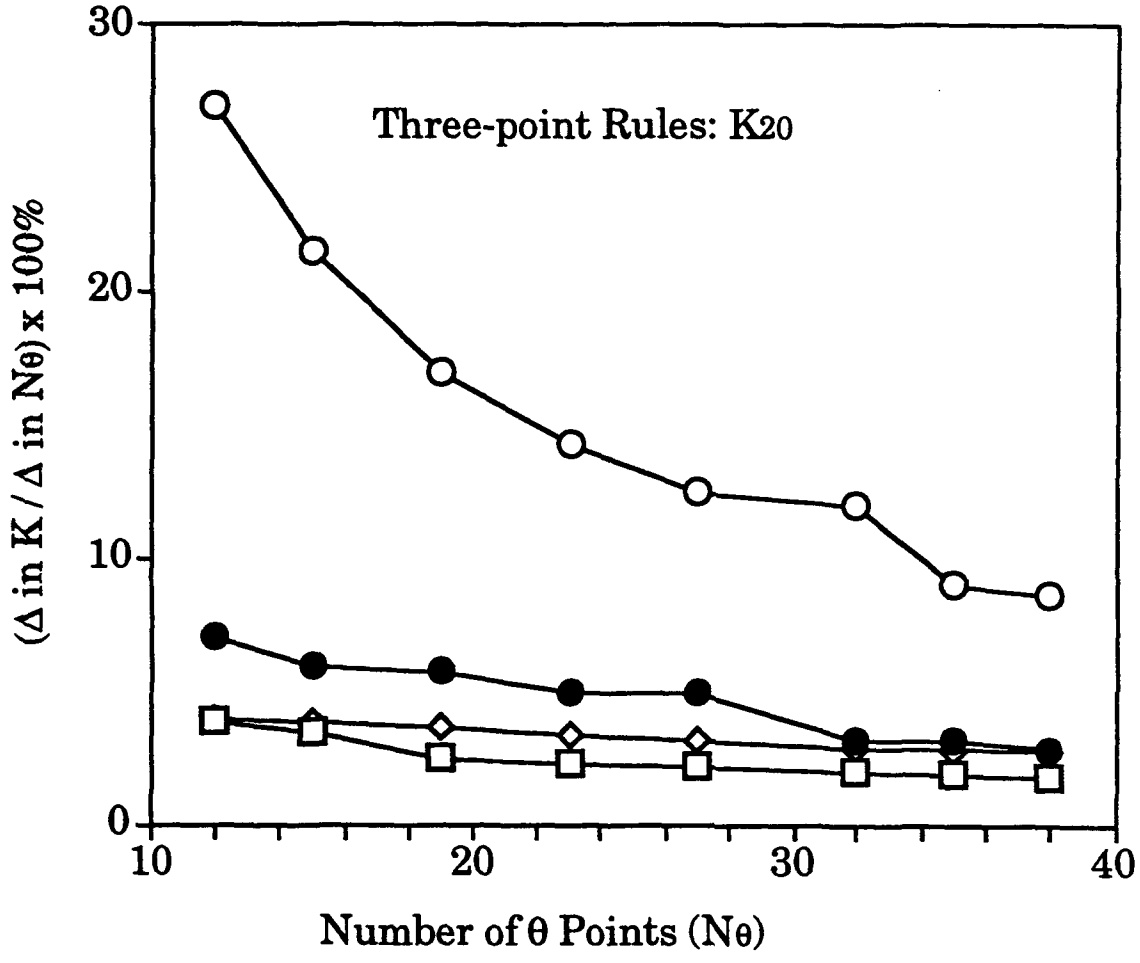

Figure 6. The relative change in the K-matrix element for s-wave→d-wave transitions, using three-point derivative rules: □, uses spherical potential, with a spherical angular term P_0; •, uses only term with P_2, the second Legendre polynomial; ○, uses the most realistic potential (see text); ◇, uses P_0 and P_2 terms.

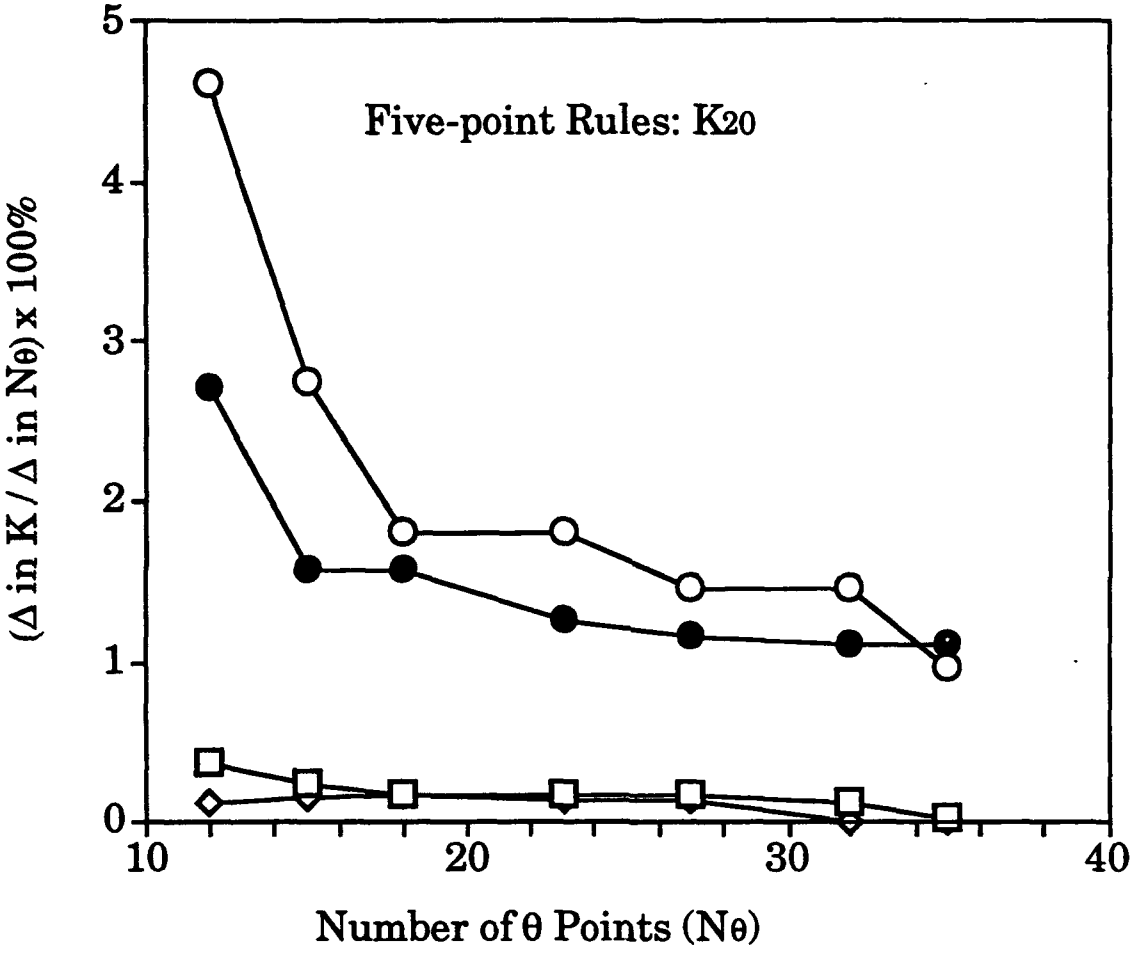

Figure 7. The relative change in the K-matrix element for s-wave→d-wave transitions, using five-point derivative rules: □, uses spherical potential, with a spherical angular term P_0; •, uses only term with P_2, the second Legendre polynomial; ○, uses the most realistic potential (see text); ◇, uses P_0 and P_2 terms.

Completion of hybrid theory calculation of the Π_g resonance in electron-N_2 scattering

C. A. Weatherford(*) and A. Temkin(+)

(*) Department of Physics
and
Center for Nonlinear & Nonequilibrium Aeroscience
Florida A&M University
Tallahassee, FL 32307

(+) Laboratory for Astronomy and Solar Physics
Goddard Space Flight Center
NASA, Greenbelt, MD 20771

Abstract

A calculation of e-N_2 scattering in the vicinity of the 2.4 eV (Π_g) resonance has been completed. The main element of the calculation is a 15 term vibrational close coupling expansion, reduced to coupled two-dimensional (2d) partial differential equations (pde's), and solved using the noniterative pde technique. The potential consists of static, exchange, and polarization parts; each part has been (previously) derived in a manner appropriate to its importance in the scattering equation. Results for the absolute total cross section, both in magnitude and shape of the substructure in the resonance region ($1.5< k^2<3.0$eV), are in excellent accord with experiment. Angular distributions are also calculated and found to vary significantly in shape in the immediate vicinity of the center of the resonance ($2.05<k^2<2.15$eV), indicating the need for differential measurements at a finer grid in energy, and therefore, requiring even better energy resolution. Comparison with other calculations and discussion of some theoretical aspects are also included.

PACS 34.80.Gs, 34.80.Bm
This paper was prepared for submittal to the Physical Review A.

1. INTRODUCTION

The purpose of this paper is to report a calculation of electron scattering from molecular nitrogen (e-N_2) using the noniterative partial differential equation technique.[1] This calculation is confined to the energy region around the 2.4 eV resonance; it consists of a 15-state vibrational close coupling expansion for the resonant (Π_g) partial wave combined with fixed-(plus adiabatic-)nuclei amplitudes for the other (contributing) partial waves. The underlying method is the hybrid theory.[2] We shall concentrate on the angular distributions for the lower vibrational states ($v = 0, 1, 2$), showing that their shapes change very rapidly from one energy to the next as one traverses the energy region in the center of the resonance. Thus, despite the fact that several differential scattering experiments have been reported (to be discussed below), they do not have the energy resolution, nor have they attempted to explore the variation in the angular distributions in this narrow energy region in detail. It is one of our aims to motivate such experimental investigations.

Several important developments in our calculations have been made since the introduction of the hybrid theory[2], which we have reported piecemeal since then. Briefly, the most salient of them are: the noniterative technique itself[1], the reduction of the scattering equation to 2d form, which was first outlined in Ref. 3, in addition to which—it turns out—the 2d technique could also be applied to the derivation of the polarization potential[4], as well as to a method for exactly including exchange in the static-exchange approximation.[5] And finally, the direct (i.e. non-exchange) static potential could be calculated[6] using a much better (MCSCF) approximation of the N_2 ground state than the SCF approximation, used originally.[2-5] Some interim results using a 10 state vibrational expansion were reported in Ref. 7.

2. THEORETICAL ASPECTS

We start with an antisymmetrized ansatz for the total wavefunction of the e-N_2 system [2,7]:

$$\Psi^{(m)} = \sum_{i=1}^{15} (-1)^{p_i} F^{(m)}(x_i; R) \Phi_{N_2}(x^{(i)}; R) \tag{2.1}$$

Here x_i are the coordinates (space and spin) of the i^{th} electron and $x^{(i)}$ is the collection of coordinates of the remaining (fourteen) electrons. The factor $(-1)^{p_i}$ is the parity of a cyclic permutation ($\hat{P}_i$) of the sequence $1, 2, ..., 15$, thus making $\Psi^{(m)}$ completely antisymmetric.

We first summarize the analysis, mostly of Ref. 5, whereby the basic integro-pde is

derived. (Note, however that we are here using Rydberg units as opposed to atomic units, used in Refs. [5,6]). Insertion of Eq. 2.1 into the Schrödinger equation, and premultiplication by the target ground state, Φ_{N_2}, yields the static exchange approximation. We first consider the ground state (Σ_g^+) to be represented by a single determinant (i.e. SCF approximation):

$$\Phi_{N_2} = det(1\sigma_g^2 2\sigma_g^2 1\sigma_u^2 2\sigma_u^2 3\sigma_u^2 1\pi_{xu}^2 1\pi_{yu}^2; \Sigma_g^+) \tag{2.2}$$

Labelling the different orbitals ϕ_α $[\alpha : 1\sigma_g, \cdots, 1\pi_{yu}]$, we recognize that each ϕ_α is an explicit function of the coordinates of a single electron and an implicit function of the internuclear separation R:

$$\phi_\alpha = \phi_\alpha(\vec{r}_1, \cdots; R)\zeta_\alpha(spin) \tag{2.3}$$

When one includes the R dependence of ϕ_α and $F^{(m)}$, one derives[7] a 3d pde for $F^{(m)}$:

$$\left[-\nabla^2 + H_{vib}(R) + V(\vec{r}; R) - E_{sc}\right] F^{(m)}(\vec{r}; R) = 2\sum_{\alpha=1}^{7} W_\alpha^{(m)}(\vec{r}; R)\phi_\alpha(\vec{r}; R), \tag{2.4}$$

where $V(\vec{r}; R)$ is (to begin with) the static potential between the scattered electron and the target (N_2):

$$V_{static}(\vec{r}; R) = \langle \Phi_{N_2} | V_{e-mol} | \Phi_{N_2} \rangle \tag{2.5}$$

and W_α are the (static) exchange kernels

$$W_\alpha^{(m)}(\vec{r}; R) = \int d^3r' \; \phi_\alpha^*(\vec{r}\,'; R)\frac{2}{|\vec{r} - \vec{r}\,'|}F^{(m)}(\vec{r}\,'; R) \tag{2.6}$$

The energy appearing in Eqs. 2.4 and 2.5 is

$$E_{sc} = k_v^2 + \epsilon_v, \tag{2.7}$$

and $H_{vib}(R)$ is the vibrational part of the target Hamiltonian from whose internuclear potential, vibrational wave functions (χ_v) and energies (ϵ_v) are evaluated. (In this calculation, the latter are obtained numerically from the MCSCF potential energy curve reported in Ref. 6.

For the static potential (2.5), we use an MCSCF approximation[6] of Φ_{N_2}. An MCSCF wave function is a sum of determinants, whereas the right hand side (i.e. the exchange part) of the scattering Eq. 2.4 *assumes* that Φ_{N_2} is a single determinant (i.e. SCF approximation). Thus (2.4) constitutes an admittedly unbalanced approximation, which

nevertheless seemed well justified[6,7] because (a) the exchange terms usually have a quantitatively smaller effect than the direct terms, and (b) when written as in (2.4), the exchange terms can be rigorously reduced to a coupled set of ordinary (i.e. non-integral) pde's.[6] This comes about by expanding $F^{(m)}$ and $W_\alpha^{(m)}$ in vibrational states χ_v of N_2

$$\begin{aligned} F^{(m)}(\vec{r};R) &= \sum_{v=0}^{N_v} F_v^{(m)}(\vec{r})\chi_v(R) \\ W_\alpha^{(m)}(\vec{r};R) &= \sum_{v=0}^{N_v} W_v^{(m,\alpha)}(\vec{r})\chi_v(R) \end{aligned} \tag{2.8}$$

and, using the well known property of the Coulomb potential as the Green's function of the kinetic energy,

$$\nabla^2\left(\frac{1}{|\vec{r}-\vec{r}\,'|}\right) = -4\pi\delta(\vec{r}\,'-\vec{r}), \tag{2.9}$$

allows the scattering equation (2.4) to be reduced to coupled, but nonintegral pde's[7]:

$$\begin{aligned} \left[\nabla^2 + k_v^2\right] F_v^{(m)}(\vec{r}) &= \sum_{v'=0}^{N_v}\left[V_{vv'}(\vec{r})F_{v'}^{(m)}(\vec{r}) - \sum_{\alpha=1}^{7}\phi_{vv'}^{(\alpha)}(\vec{r})W_{v'}^{(m,\alpha)})(\vec{r})\right], \\ \nabla^2 W_v^{(m,\alpha)}(\vec{r}) &= -4\pi\sum_{v'=0}^{N_v}\phi_{vv'}^{(\alpha)}(\vec{r})F_{v'}^{(m)}(\vec{r}). \end{aligned} \tag{2.10}$$

The double indexed quantities in (2.10) are vibrational matrix elements of the unsubscripted quantities. Thus the matrix elements in Eqs. 2.10 are given by the following expressions:

$$\begin{aligned} V_{vv'}(\vec{r}) &= \langle\chi_v(R)|V(\vec{r};R)|\chi_{v'}(R)\rangle, \\ \phi_{vv'}^{(\alpha)}(\vec{r}) &= \langle\chi_v(R)|\phi_\alpha(\vec{r};R)|\chi_{v'}(R)\rangle, \\ W_v^{(m,\alpha)}(\vec{r}) &= \sum_{v'=0}^{N_v}\langle\phi_{vv'}^{(\alpha)}(\vec{r}\,')|\frac{2}{|\vec{r}-\vec{r}\,'|}|F_{v'}^{(m)}(\vec{r}\,')\rangle. \end{aligned} \tag{2.11}$$

Eqs. 2.10 can be further reduced to 2d pde's by exploiting the cylindrical symmetry of the various functions. As derived in Ref. 5, they take the form

$$\begin{aligned} \left[\Delta(m) + k_v^2\right] f_v^{(m)}(\underline{z}) &= \sum_{v'=0}^{N_v}\left[V_{vv'}(\underline{z}\,')f_{v'}^{(m)}(\underline{z}) - \frac{1}{r}\sum_{\alpha=1}^{7}\phi_{vv'}^{(\alpha)}(\underline{z})w_{v'}^{(m,\alpha)}(\underline{z})\right], \\ \Delta(m-m_\alpha)w_v^{(m,\alpha)}(\underline{z}) &= -\frac{2}{r}\sum_{v'=0}^{N_v}\phi_{vv'}^{(\alpha)}(\underline{z})f_{v'}^{(m)}(\underline{z}). \end{aligned} \tag{2.12}$$

here $z = (r, \theta)$ and $\Delta(m)$ is the 2d Laplacian

$$\Delta(m) \equiv \frac{\partial^2}{\partial r^2} + \frac{1}{r^2}\left[\frac{\partial^2}{\partial \theta^2} + \frac{1}{sin\theta}\frac{\partial}{\partial \theta} sin\theta \frac{\partial}{\partial \theta} - \frac{m^2}{sin^2\theta}\right] \tag{2.13}$$

As stated above $V_{vv'}$ should be derived from the static potential seen by the scattered electron, given by Eq. 2.5. We have shown[6] that the use of an MCSCF Φ_{N_2} in (2.14) leads to a slightly less attractive potential than one obtained from an SCF approximation. That result is in qualitative accord with that found by Rumble et al.[8] Very recently, however, Meyer et al.[9] have carefully examined the Π_g resonance in the static *exchange* approximation and have found that the resonance, using an MCSCF ground state, when the consistent exchange terms are included, corresponds to a slightly *more* attractive effect than the corresponding consistent exchange approximation with an SCF ground state. Their conclusion (which we find quite surprising, but do not question) is that the use of SCF orbitals for exchange in Eqs. 2.10 and 2.11 is sufficiently inconsistent with the use of an MCSCF wave function in calculating the direct term, that it gives the opposite effect from what is obtained by using the MCSCF wavefunction.[9]

Nevertheless, with regard to our present calculation, we believe this effect is included by the way polarization has been incorporated. To our static potential, we add a polarization potential, as described in Ref. 6:

$$V(\vec{r}; R) \rightarrow V_{static}(\vec{r}; R) + V_{pol}(\vec{r}; R) \tag{2.14}$$

where

$$V_{pol}(\vec{r}; R) = \left(1 - e^{-(r/r_0)^2}\right) V_{pol}^{(OT)}(\vec{r}; R) \tag{2.15}$$

$V_{pol}^{(OT)}$ is calculated from a quasi-*ab initio* polarized orbital derivation of the polarization potential[4], but, as seen in (2.15), the latter is diminished in magnitude by a tuning factor, $(1 - exp[(r/r_0)]^2)$, in which r_0 was adjusted to give the Π_g resonance at the correct (i.e. experimental) energy.

We found specifically in Ref. 6 that a value of $r_0 = 2.430$ was required when using $V_{static}(MCSCF)$, whereas $r_0 = 2.934$ was required for an SCF wavefunction. (There is an unfortunate typographical error in Ref. 6, which read $r_0 = 2.394$.) What this implies, in agreement with Meyer et al.[9], is that although (symbolically)

$$(V_{static} + V_{exch})_{MCSCF} < (V_{static} + V_{exch})_{SCF} < 0, \tag{2.16}$$

because

$$(V_{pol})_{MCSCF} \geq (V_{pol})_{SCF}\,, \tag{2.17}$$

it is perfectly possible that

$$(V_{static} + V_{exch} + V_{pol})_{MCSCF} \approx (V_{static} + V_{exch} + V_{pol})_{SCF}\,, \tag{2.18}$$

[To repeat, the above equations culminating in Eq. 2.18 are intended as a measure of "size" in an average sense; in detail, both the r and R dependence of each side will be noticeably different from the other. We expect therefore that the left hand side, which derives from the better (MCSCF) wave function, does represent a considerable improvement, and that is what is used here.]

Thus, from the pragmatic point of view of this calculation, we consider the criticism of Ref. 9 to have been overcome; in fact, we believe that the results we shall present are, in the region of the center of the resonance ($1.6 < k^2 < 3eV$ *and* $v \leq 2$), the most accurate that have thus far been calculated.

Moreover, the conclusion of Ref. 9 notwithstanding, it is completely possible that if one had included the effect of static polarization, exchange, and correlation simultaneously, (part of such effects would be described by the exchange-polarization terms in a full polarized orbital treatment[10], for example), and if one had then isolated the piece labelled $V_{static} + V_{exch}$ separately, then it might have led to the result of Weatherford et al.[6], that the MCSCF result would be less attractive than the corresponding SCF result [i.e. the reverse of (2.16)].

3. RESULTS AND COMPARISONS

To the one resonant partial wave (Π_g), we add the four most important non-resonant partial waves ($^1\Sigma_g$,$^1\,\Sigma_u$,$^1\,\Pi_u$,$^1\,\Delta_g$), calculated in the fixed-plus adiabatic-nuclei approximations, as discussed in Ref. 6. Let us first show and discuss the total cross section σ_T (the sum of all energetically allowed vibrational channels, summed and averaged over rotational states in the usual way). The resonance with its famous substructure[11], is usually compared, as it is here, with the experimental result of Kennerly.[12] The theoretical curves shown are our previous 10 state result[7] (dashed curve), our present 15 state result (solid curve), compared to experiment and the Schwinger multichannel calculation of Huo et al.[13,14]

With reference to our calculations, the comparison of the 10 and 15 state results gives a good idea of the convergence of the close coupling expansions: we would say that our calculations are well converged to just beyond the first resonance ($k^2 < 1.95eV$), reasonbly well converged to just beyond the second ($\approx 2.2eV$), and approximately converged to $\approx 2.5eV$. Of particular note, therefore, is the fact that ours is the only calculation which describes the magnitude of the first peak ($\sigma_T \approx 27\mathring{A}^2$ at $k^2 = 1.95eV$) and gives the ratio of

the first two peaks accurately. The calculation of Huo et al.[14] is almost as satisfactory, while their adjoining paper[13] gives the whole sequence of vibrational excitation cross sections in remarkable accord with experiment.[15]

The ability of such theories as in Refs. 13 and 14 to achieve such an elaborate overview of the entire resonance substructure goes back to the physical ideas underlying the boomerang model (cf. Ref. 17), which have been given their most rigorous justification in the R-matrix theory and calculations of Schneider, LeDourneuf, and VoKyLan.[18] More discussion of these theories will be included in the latter parts of this paper.

In this paper, we shall concentrate on angular distributions. In Fig. 2, we show the elastic differential cross section at 1.50 eV, just below the onset of the Π_g resonance. Also shown are various other theoretical[2,14,19] and experimental[20-22] results. Both similarities and differences are evident. The results continue into the heart of the resonance region ($k^2 \approx 2.1eV$), in Figs. 3 and 4. We have divided those results into two parts: in Fig. 3, we show our present results at three energies surrounding 2.10 eV; one sees how significantly the shape varies over 0.1 eV. This is particularly relevant to the fact that the latest experiment[22] only claims an energy uncertainty of just that amount. Nevertheless, the discrepancy between all these results and the original hybrid theory calculation[2] is clear. In Fig. 4, the same experimental information is compared to the present calculation and that of Huo et al.[14] at 2.10 eV. Here the similarity of the calculated results, both of which provide absolute values, is the most striking feature. It should be noted that an SCF target representation was used in Ref. 14. The agreement between theories suggests that the recent experiment[22] is dominated by the particular energy in the composite beam which gives the dominant cross section at a particular angle.

The comparison of experiment and theoty at 3.0 eV is shown in Fig. 5. The similarity of the recently calculated results continues, but — referring back to Fig. 1 — we emphasize that at 3 eV, the energy is definitely pressing the outer edge of reliability of the present calculation. The other interesting feature of the latest experiment[22], noted there as well, is that the absolute magnitude in the directions $\theta < 110°$ favors the original hybrid result.[2]

In the next three figures (6,7,8), we show differential cross sections in the excitation transition to the first vibrational state. At the lowest energy (1.50 eV), our present calculation (Fig. 6) is definitely favored by the experiment of Brennan et al.[22], whereas, in the vicinity of the dominant peak (Fig. 7), that is only true in the middle of the angular range. Note that a different set of experimental results from an Australian group has also been included.[23] At the highest energy, 3 eV, the graph also includes results of an R-matrix calculation[24] and yet another experiment.[25] Here the similarity of the present results with those of the R-matrix calculation is the most notable feature, particulary at middle angles, where they agree best with the experimental results of Ref. 23.

Finally we show in Fig. 9, the angular distribution associated with the excitation of the

second vibrational state in the vicinity of the dominant peak. Here the two experimental results[22,23] are in agreement with each other to within their experimental errors, and they agree best with our present result at the experimental energy 2.10 eV, rather than at its fringes (2.05, 2.15 eV).

4. DISCUSSION

This completes the presentation of the results of this calculation. (More results are available upon request.) Although the method (the hybrid theory) is *ab initio* in principle, it contains here one phenomenological parameter, the polarization cut-off r_0 [cf. Eq. 2.15]. The main practical purpose for doing this is to provide the best cross sections for (several space) applications. It will be recalled that our (hybrid) theory was developed in the context of SAR arcs.[2] The numerical results of that calculation were collected as a NASA document.[26] The present (more accurate) cross sections are intended for the understanding of secondary electron flux in the lower F region of the ionosphere. The specific question concerns whether or not there is a dip in the electron distribution function.[27] Relevant ionospheric calculations are now ongoing at Goddard Space Flight Center[28], using our cross sections and those of others, principally Huo et al.[13,14]

From a more fundamental point of view, the present results are intended to be a more definitive comparison with experiment in the resonance region, particularly with angular distributions. As we have seen from the comparisons in the previous section, there is still insufficient agreement among experiments themselves to provide a definitive check at this time. In addition, future experiments will require an even finer energy resolution, at a finer energy grid, to be compelling in this regard. This having been said, it is important to acknowledge that great progress in experimental angular distributions, culminating in the recent work of the Australian group[22,23], has already been made.

With regard to calculational methodology, specifically hybrid vs. R-matrix and/or other L^2 basis set theories, in addition to what was said above and elsewhere[29], it is clear that the latter are capable of giving the greater overall accuracy at the present time, as is exemplified by the results of Refs. (13,14,18). (In further detail, for example, the R-matrix theory shows that the Π_g resonance is dominated by short range correlations rather than the long range polarizability.) However, if insufficient correlation is included, the R-matrix method and L^2 methods in general, can yield noticeable inaccuracy (cf. Ref. 30, for example).

Furthermore, the basic tenet of the hybrid theory is common to both approaches;[2,29] it is the fact that if the interaction time of the resonance is comparable to vibrational time scales of the target molecule, but short compared to rotation time scales, then in one way

or another, a dynamical treatment of the $N+1$ electron system is required. That treatment can be either a dynamical coupling of the incident particle with the vibrational motion of the target, or a recalculation of the Born-Oppenheimer problem of the $(N+1)$-electron system, followed by a calculation of the vibrational spectrum in the (necessarily complex) potential energy well of the compound system.

The drawback of the present methodology is due to the slow convergence of the vibrational close coupling expansion. In principle, that can be overcome by going to a 3d approach in which the internuclear separation (R) becomes the third dynamical variable. Such a theory has already been outlined,[31] and the non-iterative pde method[1] has been generalized to three and higher dimensional equations and applied to a solvable model.[32] The implementation of this program is already in progress, however, its completion will not be easy: in particular, the detailed substructure that such calculations reveal, will depend critically on the range and mesh size with which the R variable can be covered.

Perhaps the most exciting potential application of the 3d pde technique, also discussed in Ref. 32, is the fact that it can be applied to scattering (in principle) from arbitrary polyatomics in the fixed-nuclei approximation.[33] Augmented by the adiabatic-nuclei approximation,[33] such a method would be an invaluable tool in studying scattering processes in galactic environments, such as the Orion nebula, where it is known that exotic molecules can form (cf. Ref. 34, for example) which may not be amenable to laboratory experimentation, so that theoretical calculation provides the only reasonable alternative.

ACKNOWLEGEMENTS

Work of A.T. was done under NASA RTOP 432-36-58-01. C.A.W. was partially supported by NASA grant NAG-5307 and NASA contract NAGW-2930; he would also like to acknowledge a grant of computer time by Florida State University on a CRAY-YMP.

REFERENCES

1. E.C. Sullivan and A. Temkin, Comp. Phys. Comm. **25**, 97 (1982).
2. N. Chandra and A. Temkin, Phys. Rev. A**13**, 188 (1976).
3. A. Temkin in *Symposium on Electron – Molecule Collisions*, ed. by I. Shimamura and M. Matsuzawa.
4. K. Onda and A. Temkin, Phys. Rev. A**28**, 621 (1983).
5. C.A. Weatherford, K. Onda, and A. Temkin, Phys. Rev.A**31**, 3620 (1985).
6. C.A. Weatherford, F.B. Brown, and A. Temkin, Phys. Rev.A**35**, 4561 (1987).

7. C.A. Weatherford and A. Temkin in *Electron – Molecule Scattering and Photoionization*, ed. by P.G. Burke and J.B. West (Plenum Press, N.Y. and London, 1988), p. 229.
8. J.R. Rumble, W. J. Stevens, and D.G. Truhlar, J. Phys. **B17**, 3151 (1984).
9. H.-D. Meyer, S. Pal, and U. Riss, Phys. Rev. **A46**, 186 (1992).
10. A. Temkin, Phys. Rev. **107**, 1004 (1957).
11. D.E. Golden, Phys. Rev. Lett. **17**, 847 (1966).
12. R.E. Kennerly, Phys. Rev. **A21**, 1876 (1980).
13. W.H. Huo, T.L. Gibson, M.A.P. Lima, and V. McKoy, Phys. Rev. **A36**, 1632 (1987).
14. W.H. Huo, M.A.P. Lima, T.L. Gibson, and V. McKoy, Phys. Rev. **A36**, 1642 (1987).
15. M. Allan, J. Phys. **B18**, 4511 (1985).
16. L.A. Morgan, J. Phys. **B19** L439 (1986).
17. L. Dube and A. Herzenberg, Phys. Rev. **A20**, 194 (1979).
18. B.I. Schneider, M. LeDourneuf, and VoKyLan, Phys. Rev. Lett. **43**, 1926 (1979).
19. M.A. Morrison, B.C. Saha, T.L. Gibson, Phys. Rev. **A76** 3682 (1987).
20. T.W. Shyn and G.R. Carignan, Phys. Rev. **A22**, 923 (1980).
21. W. Sohn, K.-H. Kochem, K.-M. Scheuerlein, K. Jung, H. Ehrhardt, J. Phys. **B19**, 5017 (1986).
22. M.J. Brennan, D.J. Alle, P. Euripides, S. Buckman, and S.J. Brunger, J. Phys. **B25**, 2669 (1992).
23. M.J. Brunger, P.J.O. Teubner, A.M. Wiegold, and S.J. Buckman, J. Phys. **B22**, 1443 (1989).
24. C.J. Gillan, O. Nagy, P.G. Burke, L.A. Morgan, and C.J. Noble, J. Phys. **B20**, 4585 (1987).
25. H. Tanaka, T. Yamamoto, and T. Okada, J. Phys. **B14**, 2081 (1981).
26. N. Chandra and A. Temkin, NASA Technical Note TN D-8347, 1976.
27. P.G. Richards, D.G. Torr, and W.A. Abdou, J. Geophys. Res. **91**, 304 (1986).
28. W.R. Hoegy (work in progress; we thank Dr. Hoegy for valuable discussions on the space physics aspects of this problem).
29. A. Temkin in *Electronic and Atomic Collisions*, ed. by N. Oda and K. Takayanagi, (North Holland Publ. Co., 1980) p. 95.
30. L.A. Morgan, J. Phys. **B19**, L439 (1986).
31. A. Temkin, C.A. Weatherford, and E.C. Sullivan, AIP Conf. Proc. 204, A. Herzenberg ed. (AIP, N.Y., 1990), p. 133.
32. E.C. Sullivan and A. Temkin, Comp. Phys. Comm. **71**, 319 (1992).
33. A. Temkin, K.V. Vasavada, E.S. Chang, and A. Silver, Phys. Rev. **182**, 57 (1969).
34. *Molecules in the Galactic Environment*, M.A. Gordon and L.E. Snyder eds. (John Wiley & Sons, N.Y., 1973).

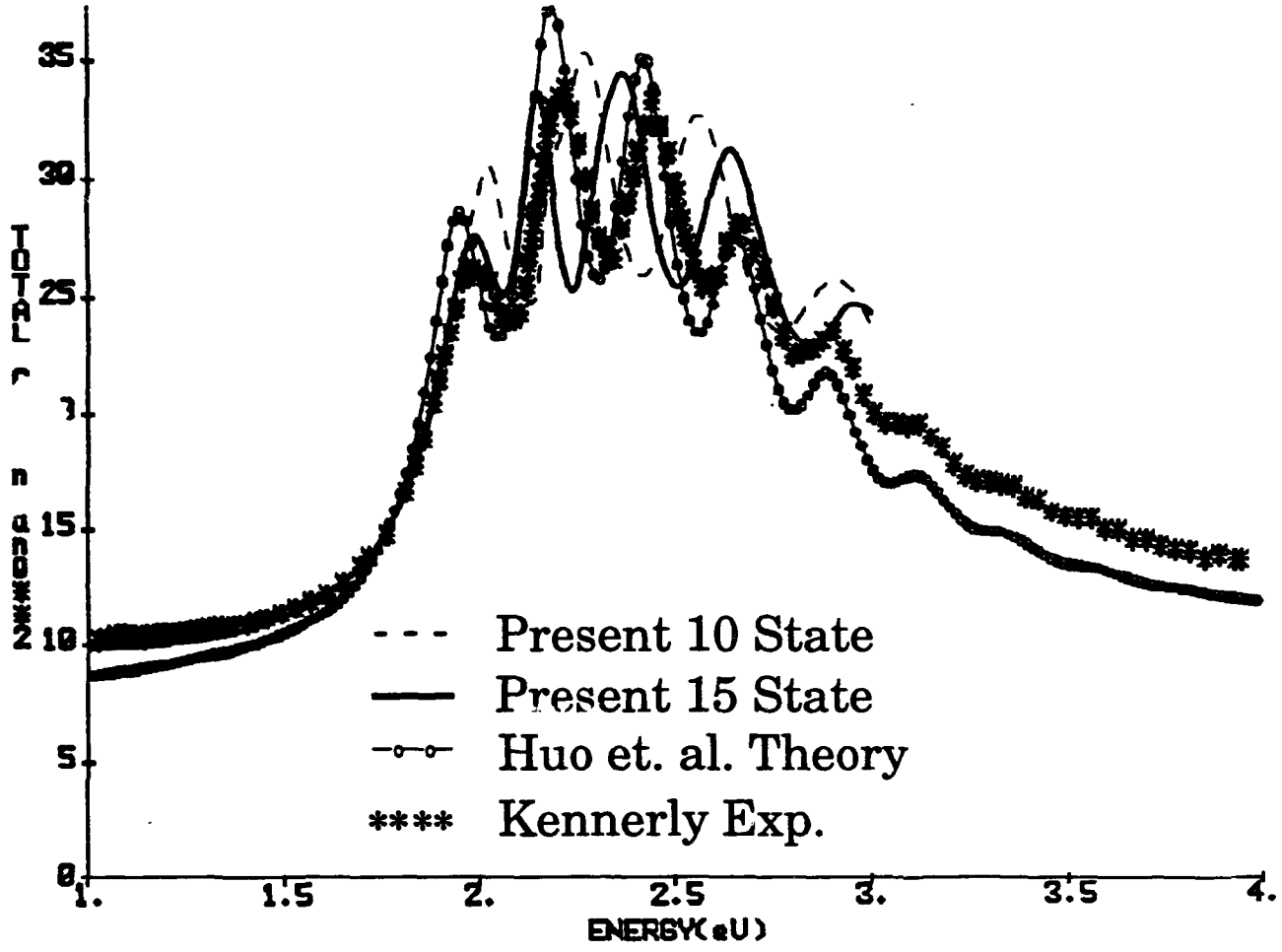

Fig. 1. Total integrated cross section in square Angstroms (A^2): Experiment: (* * *) Ref. 12. Theory: (———) present [15 state results]; (- - -) our 10 state results (Ref. 7); (-o-o-o-) Ref. 14.

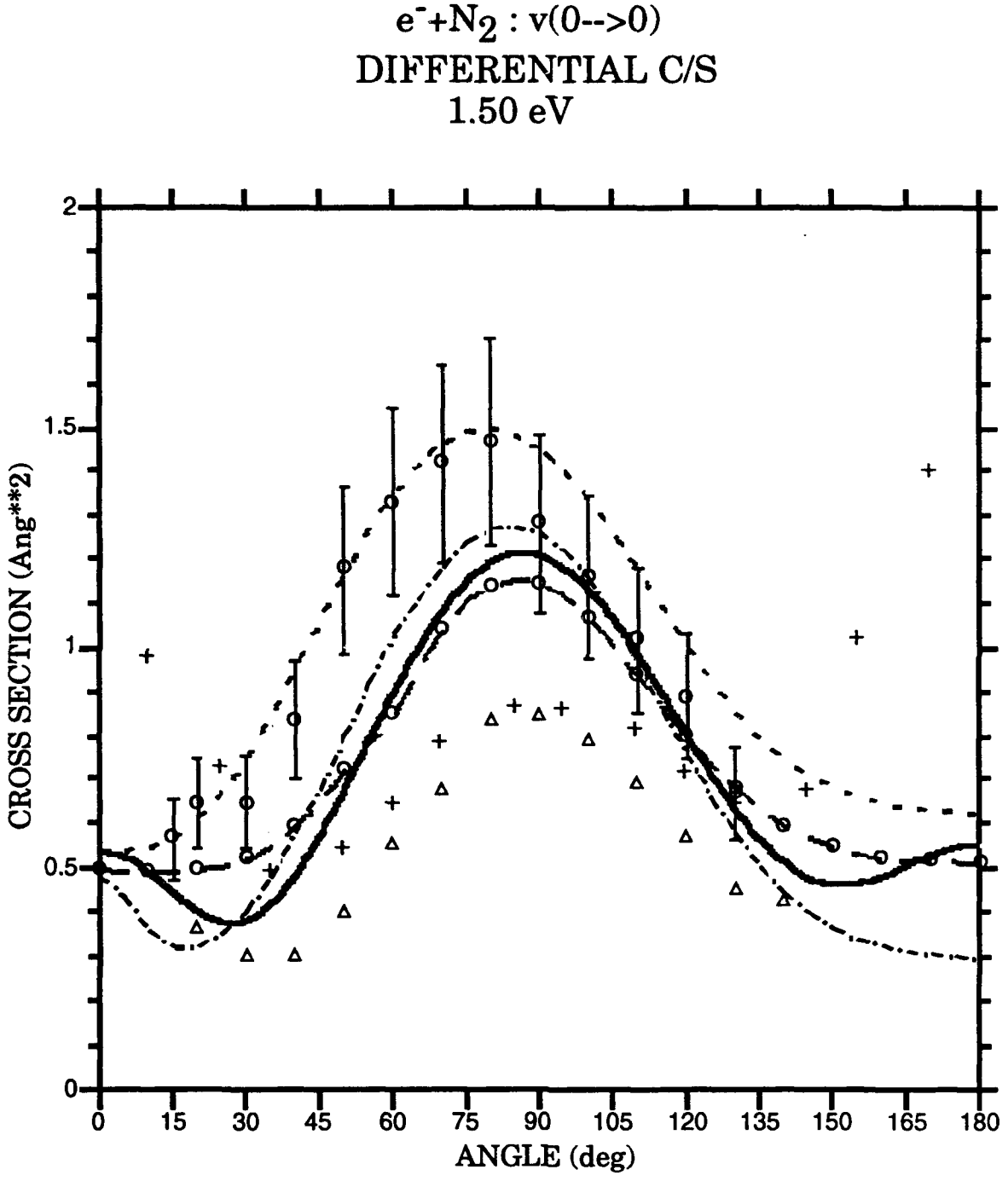

Fig. 2. $d\sigma_{00}/d\Omega$ at 1.50 eV: Theory: (———) present; (-o-o-o-) Ref. 14; (- - -) Ref. 2; (— - — -) Ref. 19. Experiment: ($\Phi\Phi\Phi$) Ref. 22; (+++) Ref. 20; ($\Delta\Delta\Delta$) Ref. 21.

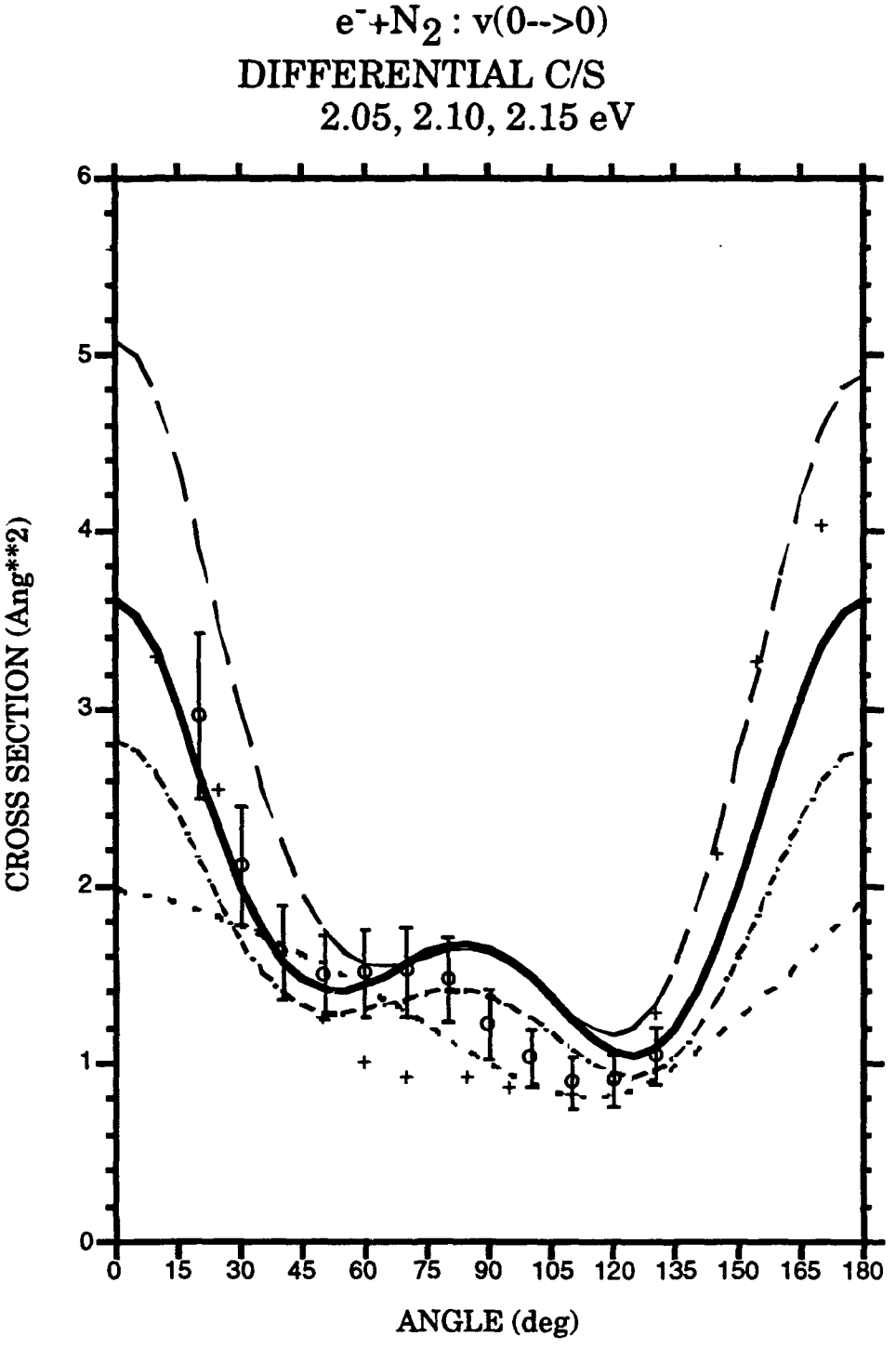

Fig. 3. $d\sigma_{00}/d\Omega$. Theory: (— - - —) present at 2.05 eV; (———) present at 2.10 eV; (— — — —) present at 2.15 eV; (- - -) Ref. 2. Experiment: ($\Phi\Phi\Phi$) Ref. 22; (+++) Ref. 20.

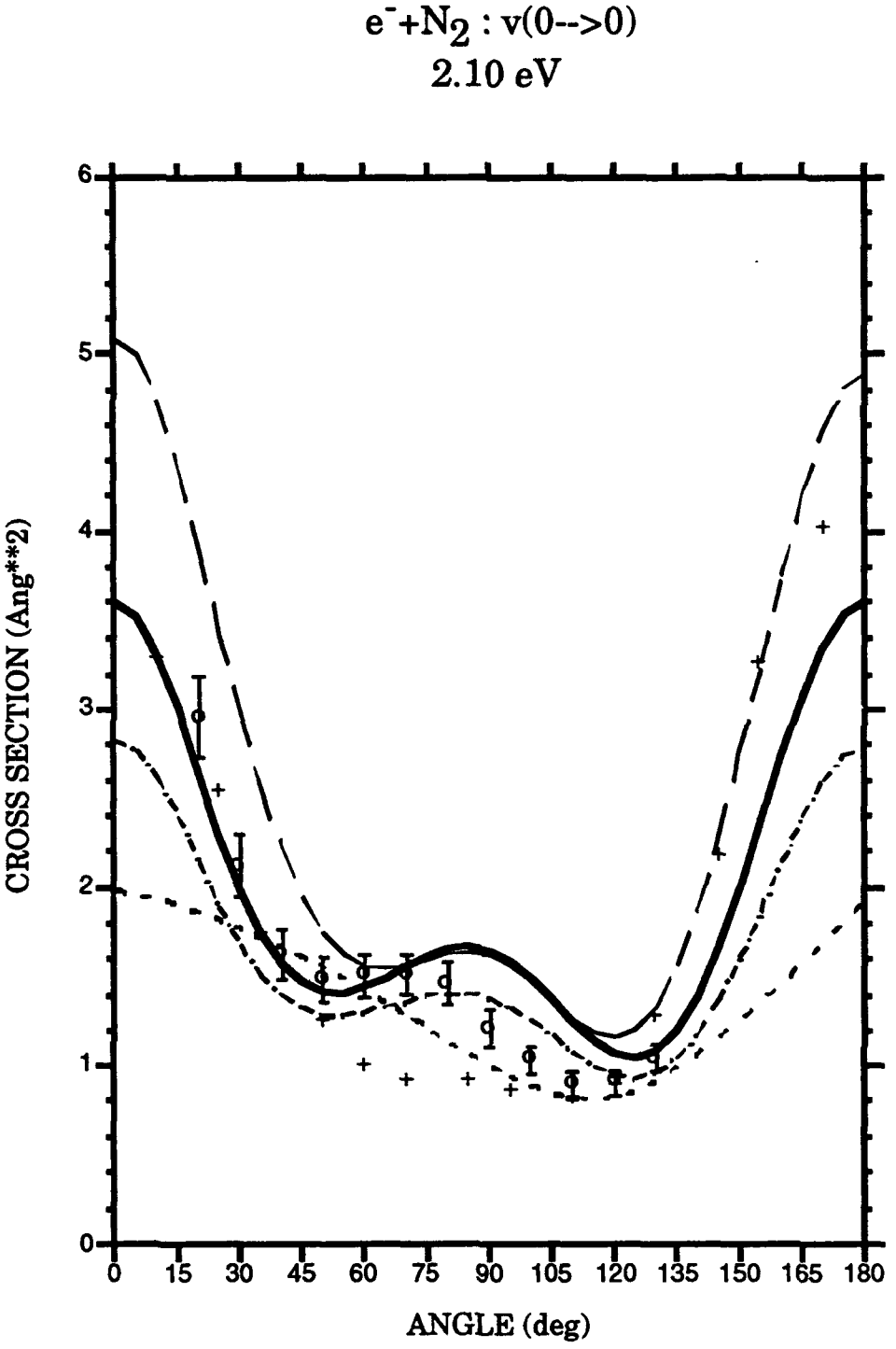

Fig. 4. $d\sigma_{00}/d\Omega$ at 2.10 eV. Theory: (———) present; (-o-o-o-) Ref. 14. Experiment: ($\Phi\Phi\Phi$) Ref. 22; (+++) Ref. 20.

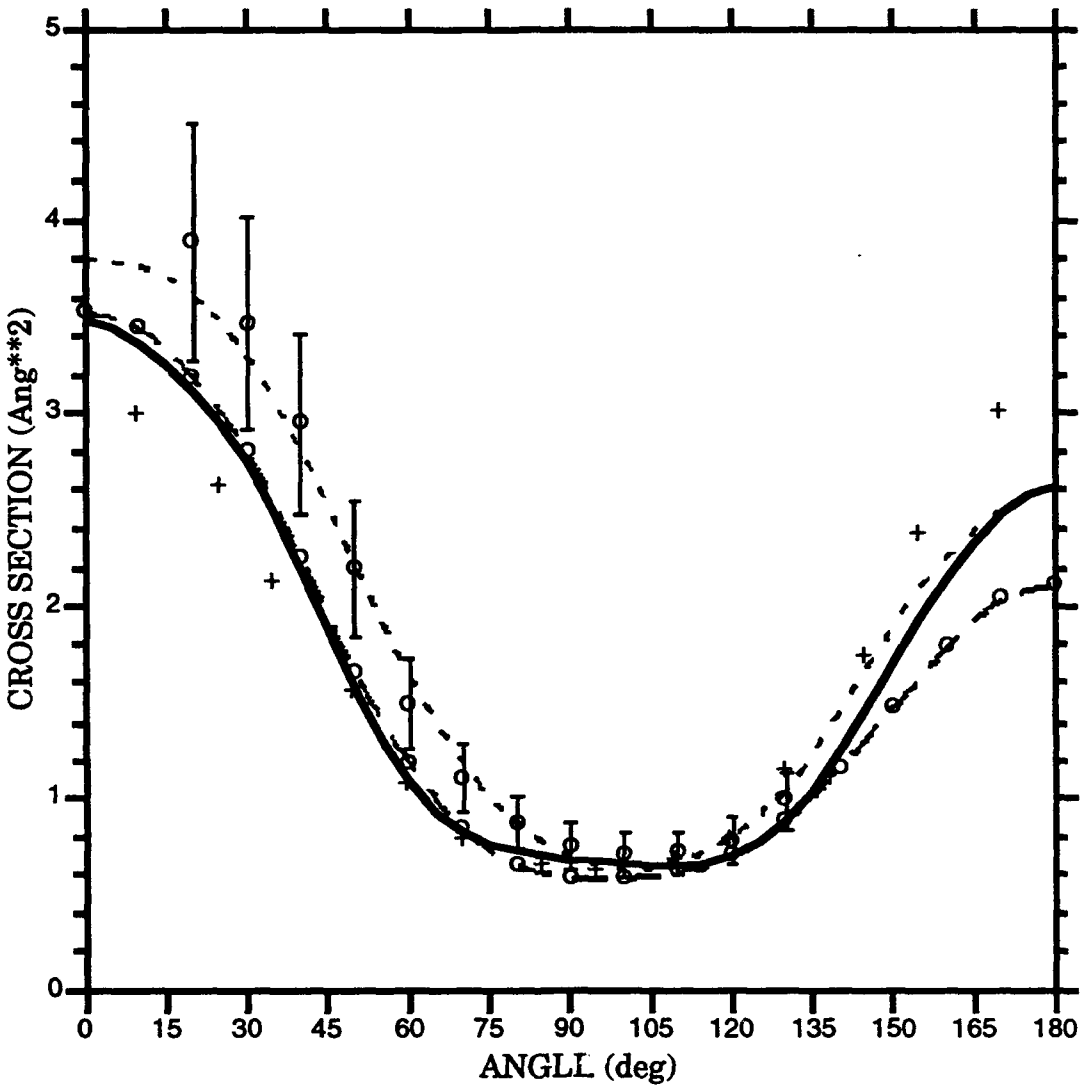

Fig. 5. $d\sigma_{00}/d\Omega$ at 3.00 eV. Theory: (———) present; (- - -) Ref. 2. Experiment: ($\Phi\Phi\Phi$) Ref. 22; (+++) Ref. 20.

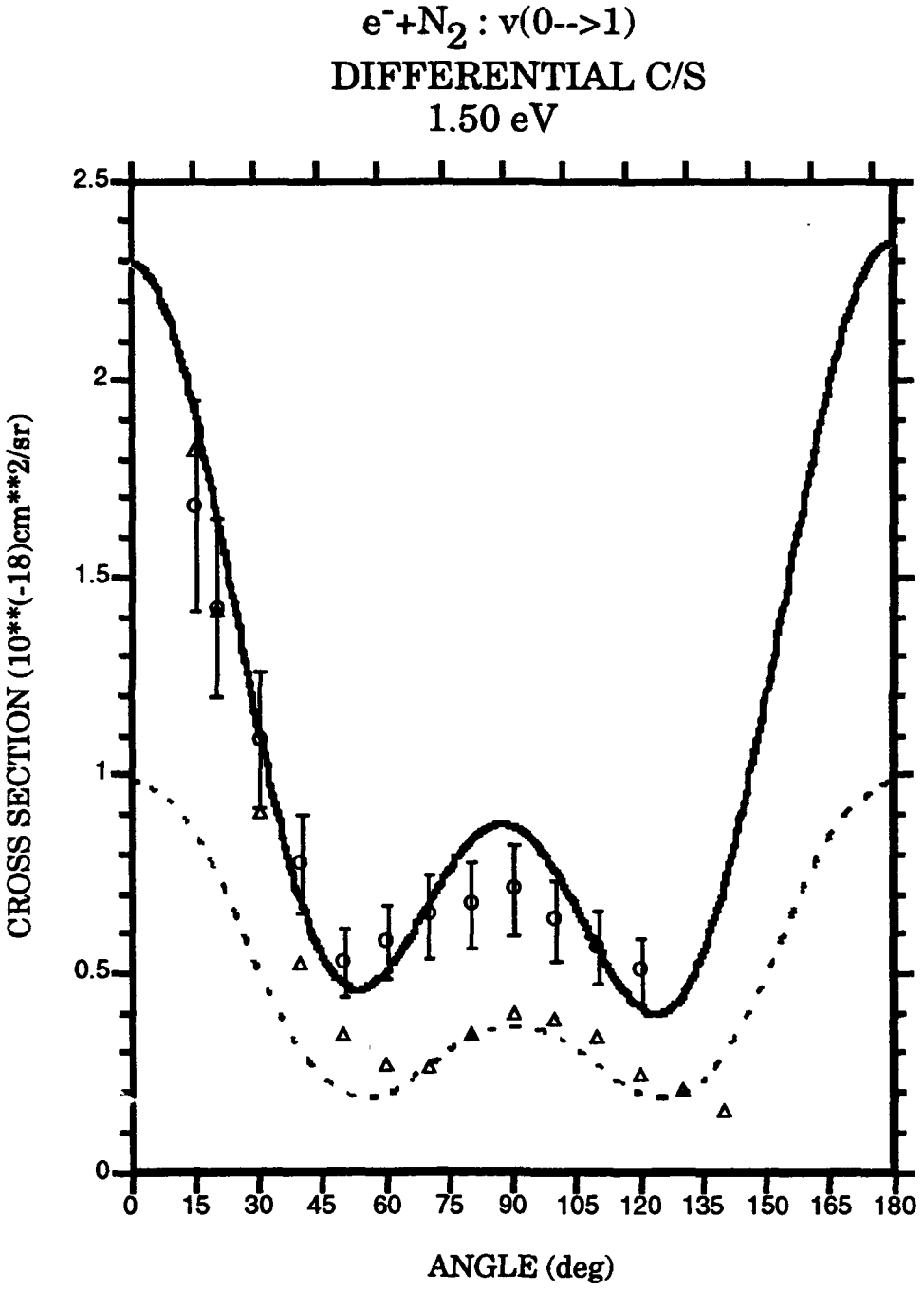

Fig. 6. $d\sigma_{01}/d\Omega$ at 1.50 eV. Theory: (———) present; (- - -) Ref. 2. Experiment: ($\Phi\Phi\Phi$) Ref. 22; ($\Delta\Delta\Delta$) Ref. 21.

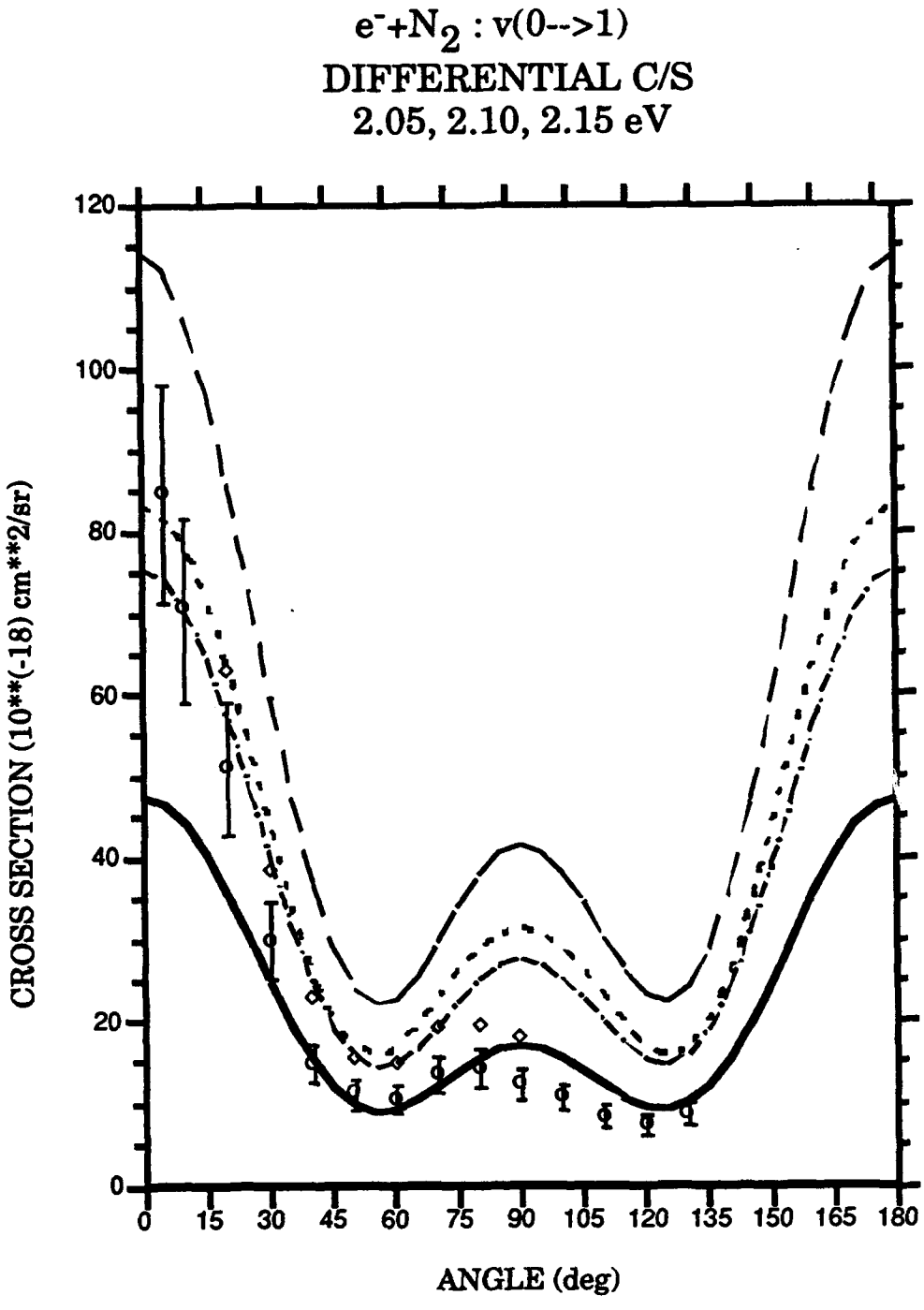

Fig. 7. $d\sigma_{01}/d\Omega$: Theory: (— - - —) present at 2.05 eV; (————) present at 2.10 eV; (—— —) present at 2.15 eV; (- - -) Ref. 2. Experiment: ($\Phi\Phi\Phi$) Ref. 22; ($\diamond\diamond\diamond$) Ref. 23.

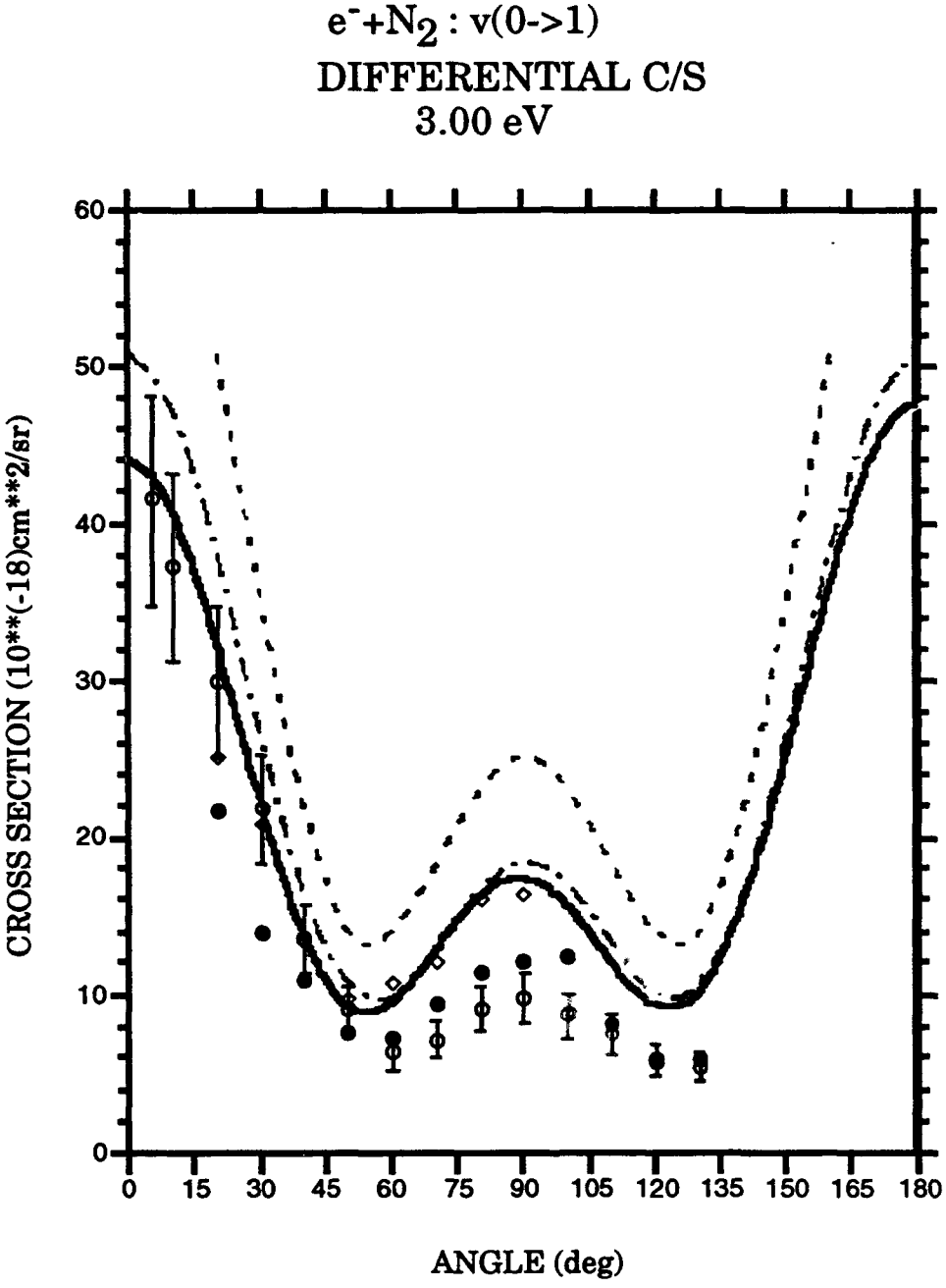

Fig. 8. $d\sigma_{01}/d\Omega$ at 3.00 eV. Theory: (———) present; (- - -) Ref. 2; (— - — -) Ref. 24. Experiment: ($\Phi\Phi\Phi$) Ref. 22; ($\diamond\diamond\diamond$) Ref. 23; (●●●) Ref. 25.

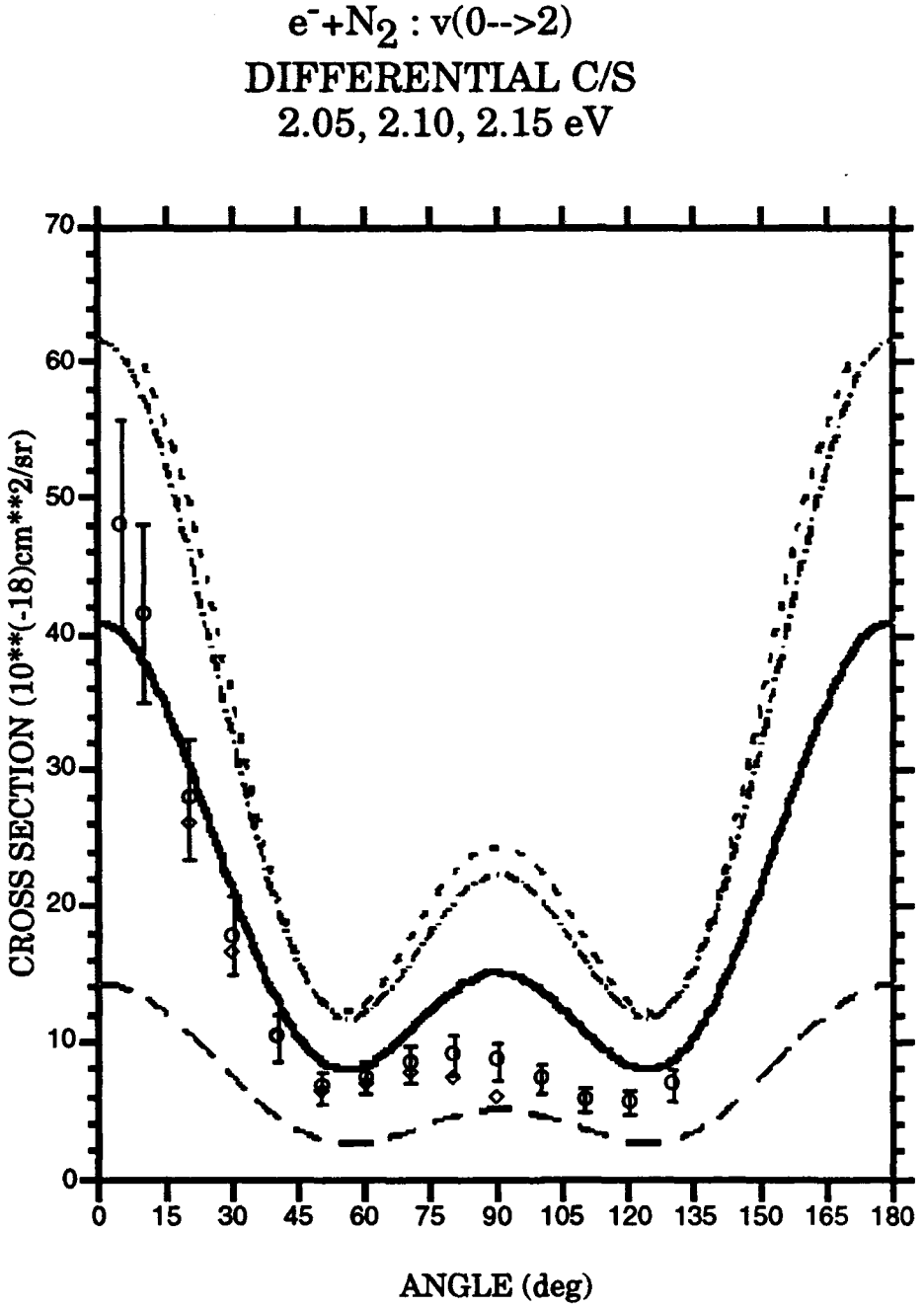

Fig. 9. $d\sigma_{02}/d\Omega$: Theory: (— - - —) present at 2.05 eV; (————) present at 2.10 eV; (—— —) present at 2.15 eV; (- - -) Ref. 2. Experiment: ($\Phi\Phi\Phi$) Ref. 22; ($\diamond\diamond\diamond$) Ref. 23.